

BULGARIAN CHEMICAL COMMUNICATIONS

2018 Volume 50 / Special Issue I

Selection of papers presented on the 4th International Conference
on the New Trends in Chemistry, May 10-12, 2018
St. Petersburg, Russia

*Journal of the Chemical Institutes
of the Bulgarian Academy of Sciences
and of the Union of Chemists in Bulgaria*

Selected papers presented on the 4th International Conference on the New Trends in Chemistry, St.Petersburg, Russia, May 10-12, 2018

Preface

This special issue of the Bulgarian Chemical Communications is dedicated to the new trends in chemistry and contains papers based on oral and posters presentations from the 4th International Conference on New Trends in Chemistry organized in St. Petersburg, Russia, May 10-12, 2018. The topics are Polymer Chemistry and Applications, Pharmaceutical Chemistry, Computational Chemistry, Environmental Chemistry, Bio Chemistry, Physical Chemistry, Analytical Chemistry, Organic Chemistry, Material Chemistry and Inorganic Chemistry. In this issue, 8 manuscripts are selected for publication.

This conference has provided a common platform for scientists and experts from various institutions to share knowledge, ideas, and achievements, to discuss impedance data analysis in a friendly environment. The symposium was dedicated to recent developments in the field of chemistry.

We would like to express our sincere gratitude to all the authors and reviewers of the manuscripts, and to the editorial team of the Bulgarian Chemical Communications, all of whom have critically evaluated and improved the content.

Visiting Editors:

PhD. Dr. Habil. Agata Bartyzel

Maria Curie-Sklodowska University in Lublin

Department of General and Coordination Chemistry, Poland

E-mail: agata.bartyzel@poczta.umcs.lublin.pl

Assoc. Prof. Dr. Dolunay SAKAR DASDAN

Department of Chemistry, Yildiz Technical University

Istanbul, TURKEY

E-mail: dsakar@yildiz.edu.tr

An investigation of the pH effect on the particle size and zeta potentials of poly(ethylene glycol) and poly ethylene-block-poly(ethylene glycol) with various molecular weights

D. Sakar Dasdan*, G. Tosun, Y. Karahan

Yildiz Technical University, Faculty of Arts and Sciences, Department of Chemistry, 34220 Esenler, Istanbul, Turkey

Received July 1, 2018; Accepted October 1, 2018

The aim of this study is to investigate the effect of the polyethylene (PE) segments on the charge and particle size of poly(ethylene glycol). For this purpose, in this current work, to compare the charge and particle size of poly(ethylene glycol) and PEG co-polymerized with PE segments polyethylene-block-poly(ethylene glycol) (PE-b-PEG) which is surfactant, emulsifier for coatings, ceramics, mold release agent and thickening with different molecular weights have been examined by Zeta Potential Analyzer. Zeta potential, mobility, and particle size of PEG and PE-b-PEG systems were determined by using the Zeta Potential Analyzer in water as a function of pHs.

Keywords: PEG, PE-block-PEG, Stability, Particle size, Zeta potential, pH effect

INTRODUCTION

Poly(ethylene glycol) is a polyether having strongly hydrogen bonds with water and is one of the most studied polymers in current materials science and biotechnology because of not only its unique behaviors in solution but also its wide applications. Poly(ethylene glycol) (PEG), otherwise known as poly(oxyethylene) or poly(ethylene oxide) (PEO), is a synthetic polyether that is readily available in a range of molecular weights. These polymers are amphiphilic and soluble in water as well as in many organic solvents (e.g., methylene chloride, ethanol, toluene, acetone, and chloroform). Low molecular weight ($M_w < 1,000$) PEGs are viscous and colorless liquids, while higher molecular weight PEGs are waxy, white solids with melting points proportional to their molecular weights to an upper limit of about 67 °C. [1]

PEG has been found to be nontoxic and is approved by the FDA for use as excipients or as a carrier in different pharmaceutical formulations, foods, and cosmetics. Most PEGs with $M_w < 1,000$ are rapidly removed from the body unaltered with clearance rates inversely proportional to polymer molecular weight. This property, combined with the availability of PEGs with a wide range of end-functions, contributes to the wide use of PEGs in biomedical research: drug delivery, tissue engineering scaffolds, surface functionalization, and many other applications. [2-5]

PEG was used as a nontoxic, water-soluble dispersant/stabilizer. Also known as Carboxwax®, it is present in health and beauty aids, including laxatives, toothpastes and eye drops, and is an

excipient in tablet formulations. [6] PEG stabilizes organ and blood donations. Several studies have shown that PEG molecular weight and loading have a significant effect on extending circulatory life. [7-11]

Polyethylene (PE) based materials are widely used in many fields due to the combination of excellent physical and chemical properties along with low cost. However, the lack of chemical functionality and structural diversity is the common barrier for broadening their applications. Hence, it is urgent to develop the PE-based materials functionalized by polar groups such as glycols or polymer segments with some improved or modified properties. [12]

Zetasizer measurements which are zeta potential, particle size and mobility provide valuable properties of particles or molecules in liquid medium. These characteristics directly affect bioavailability, stability, dissolution and immunotoxicity of the molecules. [13-19]

In this work, to investigate the charge and particle size of PEG and PE-b-PEG with various molecular weights were measured by the zetasizer measurements such as the particle size, mobility and zeta potential as a function of pH.

EXPERIMENTAL

Instrument and materials

The particle size of PEG and PE-b-PEG solutions in water were measured via Brookhaven 90 Plus/BI-MAS (Multi Angle Particle Sizing, 15 mW solid state laser) and electrophoretic mobility and zeta potential measurements of all solutions were also determined by Brookhaven Zeta Potential

* To whom all correspondence should be sent:
E-mail: dolunaykar@yahoo.com

D. Sakar Dasdan et al.: An investigation of the pH effect on the particle size and zeta potentials of poly (ethylene glycol)... Analyzer (35 mW solid state laser in red at 660 nm wavelength) in water as a function of pH. The polymers PEG and PE-b-PEG were purchased from Sigma Aldrich. The properties of PEG and PE-b-PEG are given in Tables 1 and 2, respectively.

Table 1. Properties of PEG

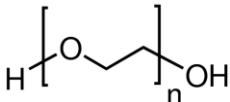
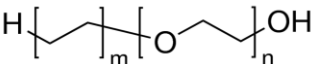
PEG			
			
Property (Mv)	PEG1:100.000g/mol	PEG2:400.000g/mol	PEG3:900.000g/mol
T _g (°C)	-67	-	-
T _m (°C)	65	65	65
d(g/ml)	1.13	1.18	1.21
Viscosity(cP)	12-50	2.25-4.5	8.8-17.6

Table 2. Properties of PE-b-PEG

PE-b-PEG			
			
Property (M _n)	PE-b-PEG1:575 g/mol	PE-B-PEG2:920g/mol	PE-b-PEG3:2250g/mol
Composition (EO, wt %)	20	50	80
T _m (°C) (DSC)	101	105	90
d (g/ml)	1.05	1.05	1.1
OH value (mg/KOH g)	85	55	-

Zetasizer measurements

Particle size. Particle size determination via dynamic light scattering (DLS) is a capable tool to determine the size of particles based on scattering of light [20]. DLS measures the (hydrodynamic) radius of a hypothetical solid particle scattering light with the same intensity as the particles under investigation while diffusing in the dispersion. DLS measures the (hydrodynamic) radius of a hypothetical solid particle scattering light with same intensity as the particles under investigation while diffusing in the dispersion.

DLS instrument calculates the particle size from the translational diffusion coefficient (D). The relationship is called Stokes-Einstein equation and is given by:

$$D = k_B T / 6\pi\eta R_H \quad (1)$$

where T is absolute temperature in degrees Kelvin, η is the liquid's viscosity, R_H is hydrodynamic radius, d_H is particle hydrodynamic diameter, $d_H = 2R_H$ and k_B is Boltzmann's constant.

Mobility and zeta-potential: The velocity (in m/sec) for a unit field strength (1 Volt/m) is called electrophoretic mobility, and is given the symbol μ_e . The electrophoretic mobility of a charged particle is defined as the ratio between its stationary velocity, v_c and the applied electric field, E:

$$\mu_e = v_c / E \quad (2)$$

It is related to the zeta potential. The electrostatic potential on that surface is called zeta potential and it is that potential which is measured, when one measures the velocity of the particles in a d.c. electric field. Zeta potential values provide an indirect measurement of the net charge on the particle surface. It is also an aid in predicting long-term stability. It is calculated from Marian Smoluchowski equation as follows:

$$\mu = \varepsilon\zeta / \eta \quad (3)$$

μ , is electrophoretic mobility, ε , is electric permittivity of the liquid, η is viscosity of liquid. [21]

RESULTS AND DISCUSSION

The particle size, mobility and zeta potential of PEG and PE-b-PEG solutions with different molecular weights in water were measured as a function of pH.

The pH effect on particle size, mobility and zeta Potential of PEG1, PEG2 and PEG3 solutions were given in Table 3, Table 4 and Table 5, respectively.

The pH effect on the particle size of PEG1, PEG2 and PEG3 solutions is given in Figure 1.

The particle size of PEGs is increasing up to pH 5, after pH 5, it sharply decreases up to pH 6 and after pH 6 it increases up to pH 8, after pH 8, it decreases with increasing pH. The particle size of PEGs is not stable between pH 5 and 8. The particle size of PEGs decreases with increasing molecular weight.

The pH effect on the zeta potential of PEG1, PEG2 and PEG3 solutions is shown in Figure 2.

The zeta potential of PEGs is slightly negative, i.e., -3 mV, at pH 2 for PEG1 and is gradually decreasing with increasing pH, reaching a minimum value of -1 mV for PEG1, -1,96 mV for PEG2 and -2.35 mV for PEG3 at pH 6. Zeta

potential values of PEG1 and PEG2 are not changing with increasing pH except for PEG3.

The pH effects on particle size, mobility and zeta potential of PE-b-PEG1, PE-b-PEG2 and PE-b-PEG3 solutions are given in Tables 6, 7 and 8, respectively.

Table 3. Effect of pH on particle size, mobility and zeta potential of PEG1 in water.

pH	Particle Size (nm)	Mobility	Zeta Potential (mV)
2	2800	-0.17	-1.5
3	3050	-0.15	-1.57
4	3480	-0.13	-1.6
5	3700	-0.1	-1.25
6	3560	-0.09	-0.99
7	4750	-0.32	-4.5
8	5600	-0.35	-4.93
9	4690	-0.45	-5.21
10	3950	-0.43	-5.04
11	3690	-0.4	-5.02
12	3390	-0.4	-5.01

Table 4. Effect of pH on particle size, mobility and zeta potential of PEG2 in water

pH	Particle Size (nm)	Mobility	Zeta Potential (mV)
2	1570	-0.18	-2.33
3	1830	-0.21	-2.34
4	1970	-0.32	-2.14
5	2180	-0.38	-2.06
6	1900	-0.23	-1.96
7	2360	-0.29	-3.7
8	3820	-0.59	-5.85
9	3590	-0.48	-5.68
10	3290	-0.52	-5.55
11	3220	-0.44	-5.35
12	3000	-0.45	-5.48

Table 5. Effect of pH on particle size, mobility and zeta potential of PEG3 in water

pH	Particle Size (nm)	Mobility	Zeta Potential (mV)
2	1200	-0.25	-3.23
3	1630	-0.20	-3.11
4	1730	-0.18	-3.01
5	1970	-0.15	-2.65
6	1300	-0.11	-2.35
7	1460	-0.49	-5.44
8	1920	-0.51	-6.24
9	1670	-0.55	-7.56
10	1230	-0.81	-8.21
11	1200	-0.85	-8.51
12	1140	-0.88	-8.45

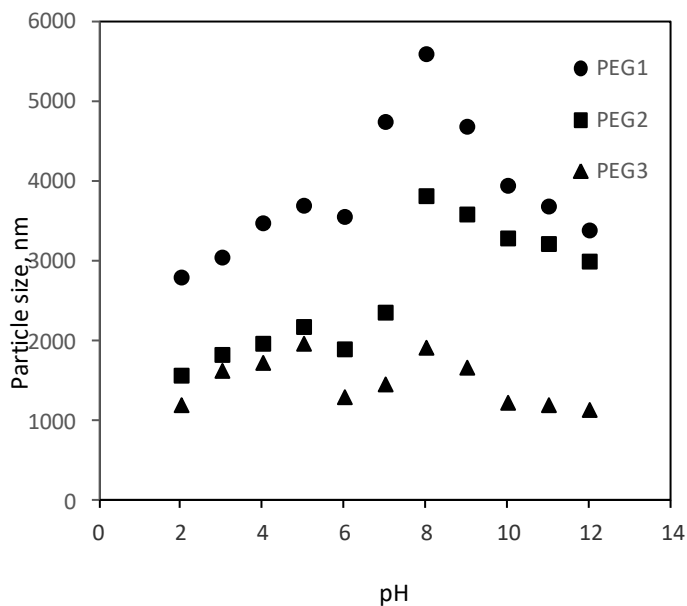


Fig.1. Effect of pH on the particle size of PEG1, PEG2 and PEG3 solutions

The pH effect on particle size of PE-b-PEG1, PE-b-PEG2 and PE-b-PEG3 solutions is shown in Figure 3.

The particle size of PE-b-PEGs increases up to pH 5, after pH 5, the particle size of PE-b-PEGs sharply decreases at pH 6. After this point, the

particle size of PE-b-PEGs increases with increasing pH, however, it decreases with increasing molecular weight.

The pH effect on the zeta potential of PE-b-PEG1, PE-b-PEG2 and PE-b-PEG3 solutions is shown in Figure 4.

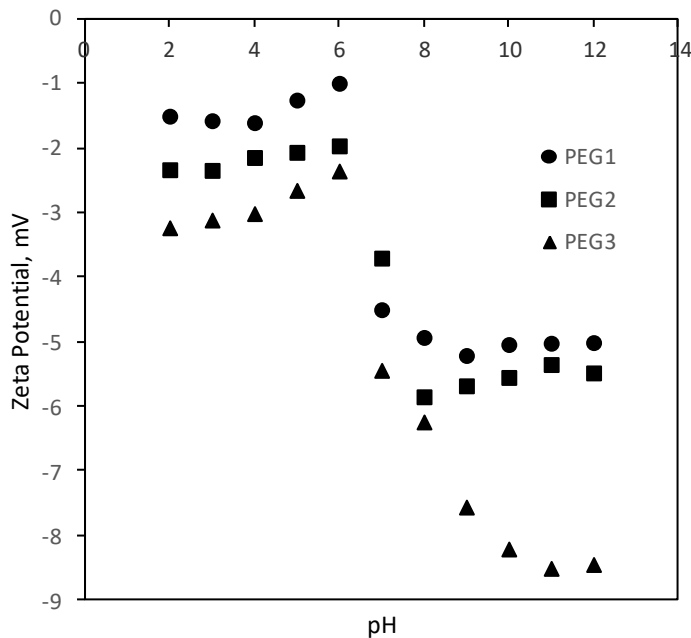


Fig.2. Effect of pH on zeta potential of PEG1, PEG2 and PEG3 solutions

Table 6. The pH effect on particle size, mobility and zeta potential of PE-b-PEG1 in water

pH	Particle Size (nm)	Mobility	Zeta Potential (mV)
2	2200	-1.64	-12,51
3	2300	-1.32	-11,44
4	2400	-1.27	-11,28
5	2600	-1.21	-11,02
6	2350	-1.79	-15,12
7	2700	-1.88	-16,56
8	3030	-1.78	-15,07
9	3080	-1.73	-13,79
10	3140	-1.68	-12,84
11	3090	-1.58	-12,05
12	3120	-1.19	-10,86

Table 7. Effect of pH on particle size, mobility and zeta potential of PE-b-PEG2 in water

pH	Particle size (nm)	Mobility	Zeta potential (mV)
2	1150	-0.24	-5.56
3	1180	-0.2	-4.51
4	1190	-0.27	-3.46
5	1290	-0.26	-3.30
6	960	-0.34	-4.37
7	1090	-0.55	-6.56
8	1070	-0.44	-5.57
9	1050	-0.26	-5.48
10	1150	-0.32	-4.65
11	1220	-0.29	-3.63
12	1240	-0.26	-3.33

Table 8. Effect of pH on particle size, mobility and zeta potential of PE-b-PEG3 in water

pH	Particle Size (nm)	Mobility	Zeta Potential (mV)
2	550	-0.38	-3.54
3	590	-0.28	-2.77
4	600	-0.25	-2.52
5	580	-0.1	-1.34
6	200	-0.31	-3.28
7	390	-0.34	-4.47
8	350	-0.44	-3.96
9	370	-0.44	-3.85
10	320	-0.26	-2.94
11	300	-0.18	-1.98
12	290	-0.15	-1.83

The zeta potential of PE-b-PEGs is negative, i.e., -12.51 mV, at pH 2 for PE-b-PEG1 and is gradually increasing with increasing pH up to pH 5, after this point, the zeta potential values of PE-b-PEGs are decreasing sharply up to pH7. After pH 7, the zeta potential of PE-b-PEGs is increasing with increasing pH. The zeta potential values are decreasing with increasing molecular weight. PE segments reduce the the particle size of PEG and increase the zeta potential of PEG.

CONCLUSIONS

According to the results, pH changes affect the particle size and zeta potential values of PEGs and PE-b-PEGs with increasing molecular weight. It means that It has to be considered that the charge and particle size of PEGs and PE-b-PEGs in different pHs when they are using as supporting material. PE segments reduce the particle size of PEG and increase the zeta potential of PEG.

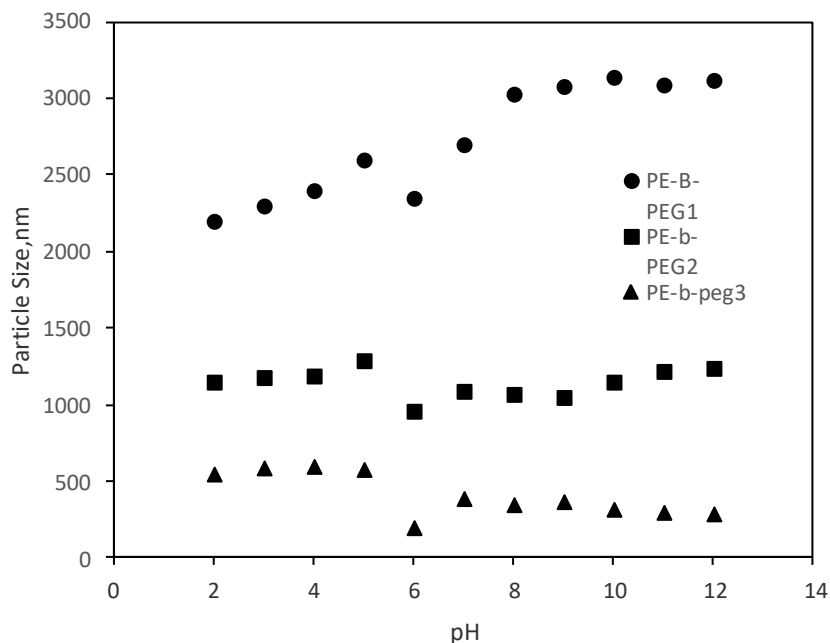


Fig. 3. Effect of pH on the particle size of PE-b-PEG1, PE-b-PEG2 and PE-b-PEG3 solutions

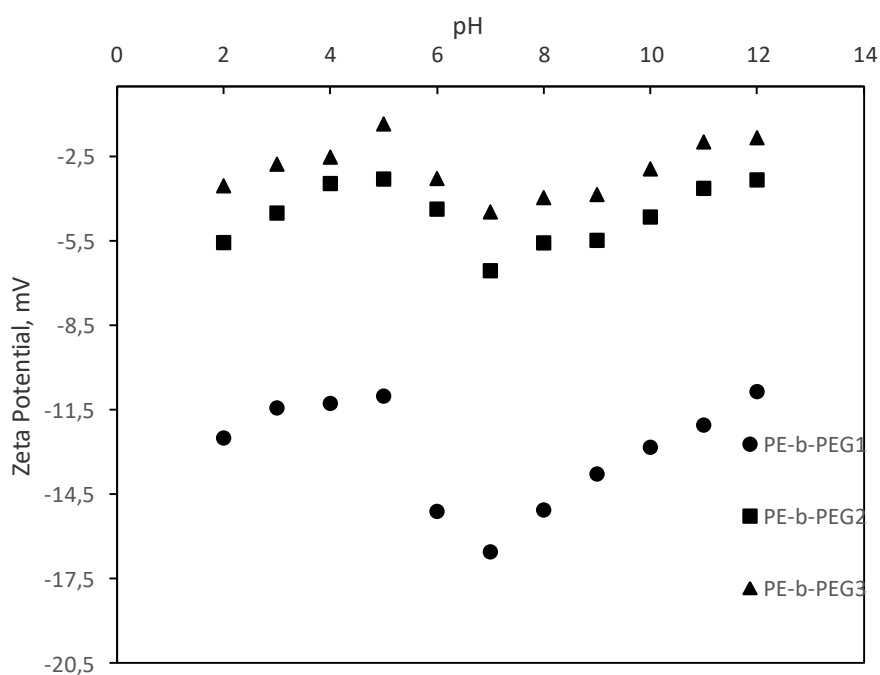


Fig. 4. Effect of pH on zeta potential of PE-b-PEG1, PE-b-PEG2 and PE-b-PEG3

Acknowledgement: This study was supported by the Scientific Research Project Coordination Center of Yıldız Technical University, Turkey (Project No: FYL-2018-3446).

REFERENCES

1. J. Chen, N. Li, Y. Gao, F. Sun, J. He, Y. Li, *Soft Matter*, **11**, 7835 (2015).
2. F.E. Bailey, J.V. Koleske, *Poly (ethylene oxide)*, Academic Press, New York, 1976.
3. F. Fuertges, A. Abuchowski, *J. Controlled Release*, **11**, 139 (1990).
4. P. K. Working, Safety of poly(ethylene glycol) and poly(ethylene glycol) derivatives, in: J.M. Harris, S. Zalipsky, (eds.), *Polyethylene Glycol Chemistry and Biological Applications*, American Chemical Society, Washington, DC, 1997.

- D. Sakar Dasdan et al.: An investigation of the pH effect on the particle size and zeta potentials of poly (ethylene glycol)...*
5. R. I. Mahato, *Biomaterials for delivery and targeting of proteins and nucleic acids*, CRC Press, 2005.
 6. R. G. Strickley, *Pharm. Res.*, **21**, 201 (2004).
 7. M. C. Woodle, K. K. Matthay, M. S. Newman, J. E. Hidayat, L. R. Collins, C. Redemann, F. J. Martin, D. Papahadjopoulos, *Biochim. Biophys. Acta*, **1105**, 193 (1992).
 8. T.M. Allen, C. Hansen, F. Martin, C. Redemann, A. YauYoung, *Biochim. Biophys. Acta*, **1066**, 29, (1991).
 9. A.L. Klibanov, K. Maruyama, A.M. Beckerleg, V.P. Torchilin, L. Huang, *Biochim. Biophys. Acta*, **1062**, 142 (1991).
 10. K. Maruyama, T. Yuda, A. Okamoto, S. Kojima, A. Suginata, M. Iwatsuru, *Biochim. Biophys. Acta*, **1128**, 44 (1992).
 11. A. Mori, A. L. Klibanov, V. P. Torchilin, L. Huang, *FEBS Lett.*, **284**, 263 (1991).
 12. D. D. Lasic, D. Needham, *Chem. Rev.*, **95**, 2601 (1995).
 13. <http://www.horiba.com/uk/scientific/products/particle-characterization/applications/drug-delivery/>
 14. V. G. Kadajji, G. V. Betageri, *Polymers*, **3**, 1972 (2011).
 15. K. Knop, R. Hoogenboom, D. Fischer, U.S. Schubert, *Angew. Chem. Int. Ed.* **49**, 6288 (2010)
 16. M. Wisniewska, *J. Dispers. Sci. Technol.*, **32**, 1605 (2011).
 17. H. L. Kutscher, P. Chao, M. Deshmukh, S. S. Rajan, Y. Singh, P. Hu, L. B. Joseph, S. Stein, D. L. Laskin, P. J. Sinko, *Int. J. Pharm.*, **402**, 64 (2010).
 18. D. Sakar Dasdan, A. Dizdar, G. Karakus, *Bul. Chem. Commun.*, **49**, Special Issue I, 43 (2017).
 19. F. Noyan Tekeli, *Bul. Chem. Commun.*, **49**, Special Issue I, 146 (2017).
 20. J. Ziegler, H. Wachtel, *J. Aerosol Med.*, **18**, 311 (2005).
 21. <http://zeta-potential.sourceforge.net/zeta-potential.shtml#SmoluchowskiEquation>

ИЗСЛЕДВАНЕ ВЛИЯНИЕТО НА pH ВЪРХУ РАЗМЕРА НА ЧАСТИЦИТЕ И ЗЕТА ПОТЕНЦИАЛА НА ПОЛИЕТИЛЕНГЛИКОЛ И ПОЛИЕТИЛЕН-БЛОК-ПОЛИЕТИЛЕНГЛИКОЛ С РАЗЛИЧНО МОЛЕКУЛНО ТЕГЛО

Д. Сакар Дашдан*, Г. Тосун, Я. Карахан

Йилдиз Технически университет, Факултет по науки и изкуства, Департамент по химия, 34220 Есенлер, Истанбул, Турция

Постъпила на 1 юли, 2018 г.; приета на 1 октомври, 2018 г.

(Резюме)

Полиетилен-блок-полиетиленгликол (PE-b-PEG) – повърхностно активно вещество, емулгатор за покрития и керамики, агент, спомагащ за освобождаване от леярната форма и сгъстяващ агент, е материал на основата на полиетилен. Той е модифициран с PEG сегменти за разширяване на областите на приложение. Целта на настоящата работа е да се изследва влиянието на PEG сегментите върху стабилността на PE-b-PEG във вода. За сравняване на товара и размера на частиците на полиетиленгликол и полиетилен-блок-полиетиленгликол с различно молекулно тегло е използван анализатор на зета потенциала. Зета потенциалът, мобилността и размерът на частиците на PEG и PE-b-PEG състемите са определени във вода в зависимост от pH.

Controlled release of donepezil hydrochloride from PEG-DA hydrogels

S. Senol, E. Akyol*

Department of Chemical Engineering, Yildiz Technical University, 34210 Istanbul, Turkey

Received July 1, 2018; Accepted October 1, 2018

Aim of the research work is to create a controlled-release system through the preparation and characterization of hydrogels based on polyethylene glycol diacrylate (PEG-DA). To determine the influence of photo-initiators on the drug release behavior of the resulting hydrogels, three different photo-initiators 2,2-dimethoxy-2-phenyl-acetophenone (Irgacure 651), 1-hydroxycyclohexyl phenyl ketone (Irgacure 184) and 2-hydroxy-4'-(2-hydroxyethoxy)-2-methylpropiophenone (Irgacure 2959) were used. In addition, hydroxyapatite (HAp) was employed to modify PEG-DA hydrogels. Fourier transform infrared (FT-IR) spectroscopy and digital microscopy were used for characterizing the prepared hydrogels. Swelling ratios and release behaviors of the prepared hydrogels under different conditions were investigated. Drug release studies were performed at pH 1.2, 6.8 and 7.4.

Keywords: PEG-DA based hydrogels, Controlled-release, Hydroxyapatite.

INTRODUCTION

Polyethylene glycol diacrylate (PEG-DA) hydrogels are very useful materials with a wide variety of applications such as controlled release, biomedical applications and pharmaceutical applications because of their low toxicity, biocompatibility, and increased mechanical stability [1-8].

Photo-crosslinking is a type of chemical crosslinking which is performed in the presence of UV radiation, crosslinking agents and chemical photo-initiator [9]. Hydrogels are prepared through photopolymerization on relevant time scales of seconds to several minutes. Photopolymerization has the ability to prepare hydrogels under mild and physiological conditions [10].

Hydroxyapatite (HAp) is a known calcium ion supply with a slow-release pattern, which has been gradually attracting significant attention due to its excellent bioactivity, biocompatibility and desirable biologic properties. Mixtures of hydroxyapatite and polymers show good biological properties and biocompatibility [11-16]. In order to improve the mechanical properties of the hydrogels, hydroxyapatite particles have been encapsulated in them to control drug release for drug delivery applications [17].

Alzheimer's disease (AD) is a type of dementia and irreversible brain disorder that affects patient's memory, thinking, and social life [18].

Donepezil is the most effective agent which is a potent and selective acetylcholinesterase inhibitor developed and used for the treatment of AD [19,20].

In this study, donepezil hydrochloride (DH) which was encapsulated in PEG-DA hydrogels was combined with HAp *via* photopolymerization. Fourier transform infrared (FT-IR) spectroscopy and digital microscopy were used to characterize the hydrogels.

EXPERIMENTAL

Materials

Polyethylene glycol diacrylate (PEG-DA, $M_n=700$) was purchased from Sigma Aldrich. Ethylene glycol dimethacrylate, 2,2-dimethoxy-2-phenyl-acetophenone (Irgacure 651, 99% purity), 1-hydroxycyclohexyl phenyl ketone (Irgacure 184, 99% purity), 2-hydroxy-4'-(2-hydroxyethoxy)-2-methylpropiophenone (Irgacure 2959, 98% purity), hydroxyapatite (powder, 5 μm , surface area $\geq 100\text{m}^2/\text{g}$), were purchased from Sigma-Aldrich. Donepezil HCl was generously gifted by Abdi İbrahim Company. Sodium chloride and hydrochloric acid were provided by Merck. Sodium hydroxide and monobasic potassium phosphate were supplied from J. T. Baker. All chemicals were used as received without further purification.

Preparation and Characterization of Hydrogels

PEG-DA based hydrogels were prepared in the presence of a photo-initiator (Irg 184, Irg 651, Irg 2959) and a crosslinking agent (ethylene glycol dimethacrylate), as shown in Table 1. The reactant mixtures were placed into glass molds (diameter of 15 mm, depth of 1 mm), and deaerated by bubbling with nitrogen gas during the reaction. Photopolymerization was performed at 365 nm under UV irradiation for 40 s.

* To whom all correspondence should be sent:
E-mail: eakyol@yildiz.edu.tr

Table 1. Experimental conditions for the synthesis of PEG-DA based composite hydrogels

Hydrogels	PEG-DA Mn=700	EGDMA	Irg 651	Irg 184	Irg 2959	HAp
Hydrogel 1 (H1)	50 %	3 %	0.5 %	-	-	-
Hydrogel 2 (H2)	50 %	3 %	-	0.5 %	-	-
Hydrogel 3 (H3)	50 %	3 %	-	-	0.5 %	-
Hydrogel 4 (H4)	50 %	3 %	0.5 %	-	-	0.05 %
Hydrogel 5 (H5)	50 %	3 %	-	0.5 %	-	0.05 %
Hydrogel 6 (H6)	50 %	3 %	-	-	0.5 %	0.05 %

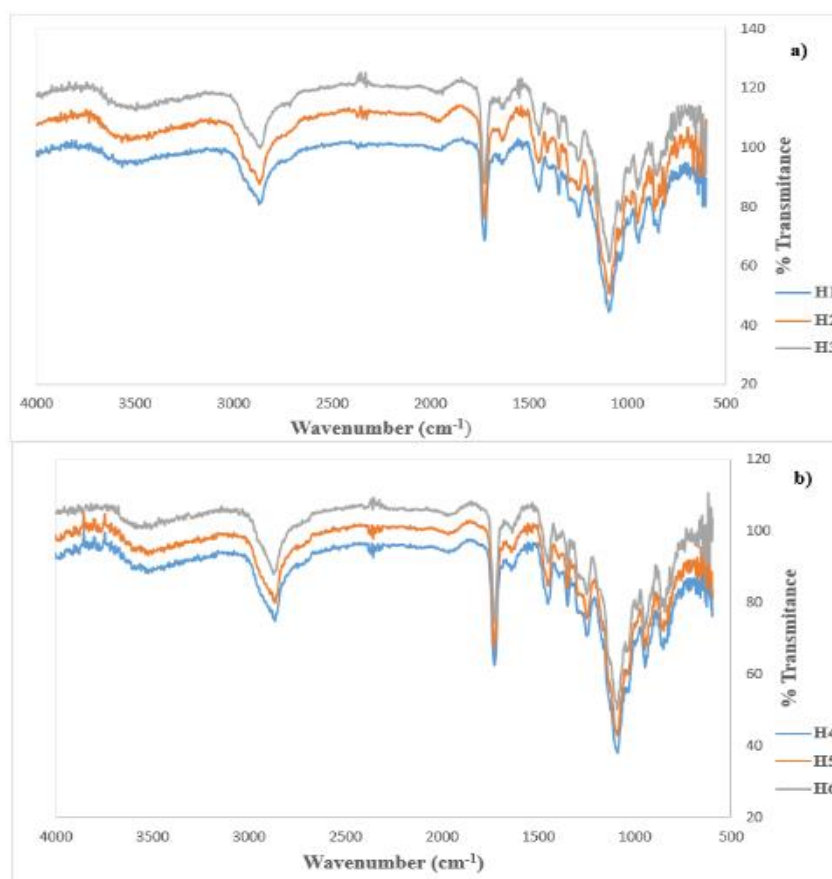


Figure 1. FT-IR analyses of PEG-DA hydrogels (a) and PEG-DA/HAp hydrogels (b)

Diameters of hydrogels were calculated by using micro photographs (Veho, VMS- 004 USB Microscope). Characterization of functional groups present in the hydrogels were performed by FT-IR spectroscopy (Perkin Elmer Spectrum 100). Swelling behavior was studied by a gravimetric method. Drug-loaded hydrogels were used for studying the swelling behavior at 37°C. At a predetermined time point, the hydrogels were taken out and weighed after removal of surface water. Swelling ratio was calculated as follows:

$$\text{Swelling ratio} = (W_s - W_i) / W_i \times 100$$

where W_i is the initial weight of the prepared hydrogel and W_s is the weight of the hydrogel in swollen state.

RESULTS AND DISCUSSION

Characterization of the Prepared Hydrogels

Characterization of hydrogels by FT-IR was carried out to determine the chemical structure and to confirm the combination.

The FT-IR spectrum of PEG-DA is shown in Figure 1 and Table 2. Absorption of the C=C bonds occurs at 1633 cm^{-1} and of the carbonyl groups at 1724 cm^{-1} . Absorption of the C=C bonds occurs at 1633 cm^{-1} and of the carbonyl groups at 1724 cm^{-1} .

The results demonstrated the existence of characteristic bands of HAp at 598 and 559 and at 1020 cm^{-1} attributed to P^{3-4} and PO_3^{4-} groups vibrations, respectively.

Table 2. Functional groups of hydrogels [21-23].

	Wavenumber (cm ⁻¹)	Functional group
PEG-DA	2700 - 3300	C-H
	3000 – 3700	O-H
	900 - 1300	C-O
	1600 - 1700	C=C
	1600 - 1900	C=O
HAp	561	ν ₄ vibrations normally associated with O-P-O modes
	600	
	631	
	832	CO ₃ ²⁻
	963	ν ₁ symmetric stretching vibrations normally associated with P-O mode
	1027	
	1091	PO ₄ ³⁻
	1374	CO ₃ ²⁻
	1644	CO ₃ ²⁻
	3215	water
	3570	OH ⁻

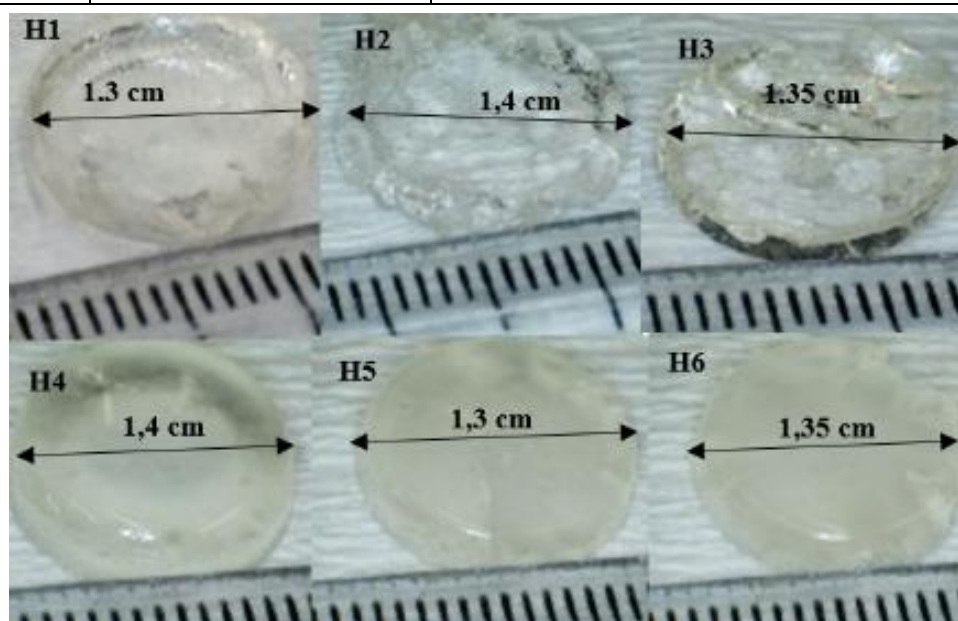


Figure 2. Samples of hydrogels

The sizes of hydrogels were between 1.3 and 1.4 mm, which were determined by digital microscopy.

Swelling properties of the hydrogels

The swelling properties of hydrogels were studied as functions of time and pH. Swelling ratios of hydrogels in deionized water and in solutions with pH 1.2, pH 6.8, pH 7.4 at 37°C are shown in Figure 3. An increase in the swelling degree was observed with the decrease in pH values for all synthesized formulations.

The percentage of swelling of H1 reached up 88 % within 24 h in deionized water, the percentage of swelling of H4 - 76 % within 24 h at pH 1.2, the

percentage of swelling of H4 - 80 % within 24 h at pH 6.8 and the percentage of swelling of H4 - 75 % within 24 h at pH 7.4.

Donepezil HCl release studies

The interaction of the hydrogels with donepezil hydrochloride was studied. pH 1.2, pH 6.8 and pH 7.4 were selected as media for the study of the hydrogels interaction with donepezil hydrochloride. Figures 4, 5 and 6 depict the percent cumulative release of donepezil hydrochloride from hydrogels at pH 1.2, pH 6.8 and pH 7.4, respectively, at 37°C.

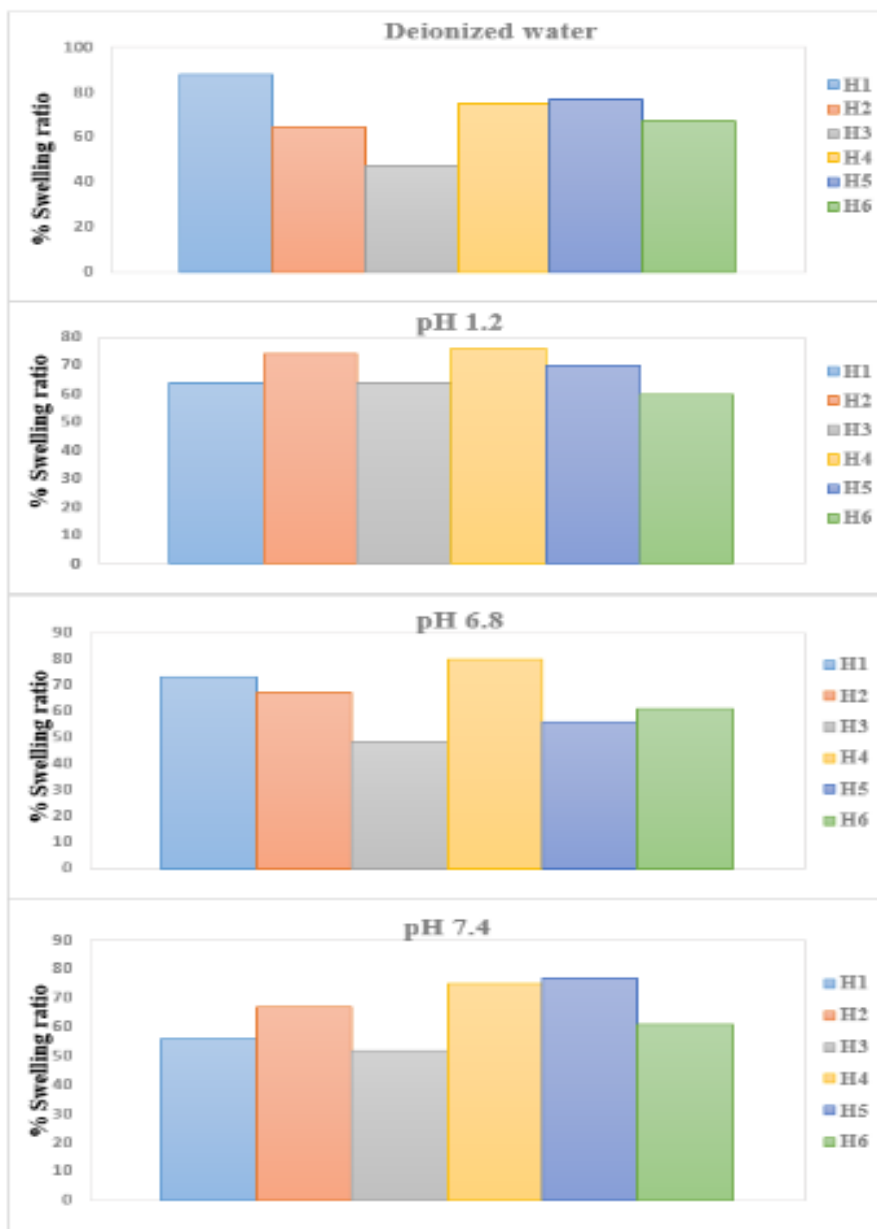


Figure 3. Swelling ratios of hydrogels

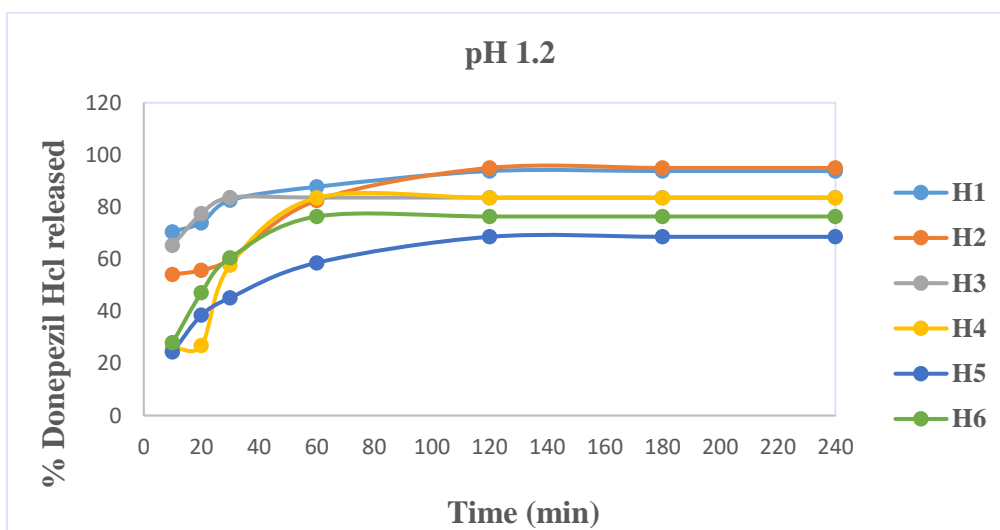


Figure 4. Donepezil HCl release of hydrogels in pH 1.2 media

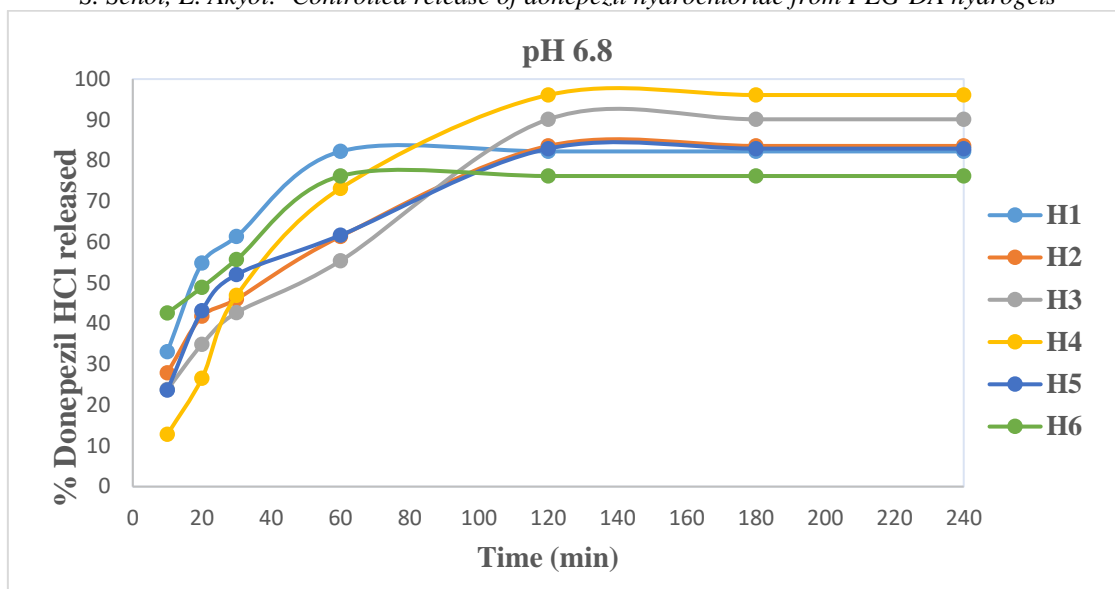


Figure 5. Donepezil HCl release of hydrogels in pH 6.8 media

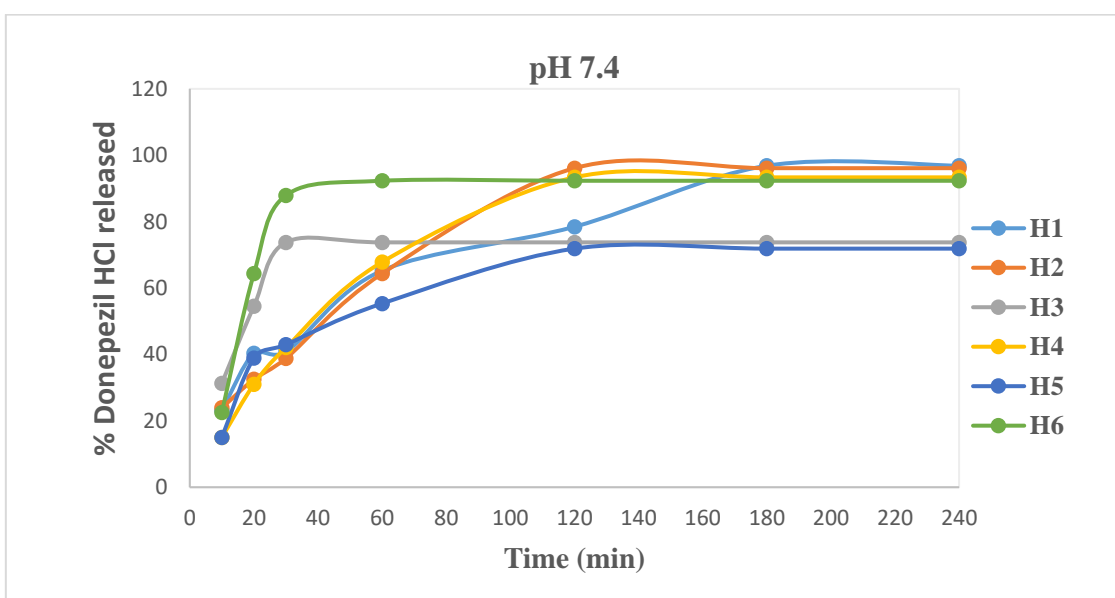


Figure 6. Donepezil HCl release of hydrogels in pH 7.4 media

It was found that in simulated gastric fluids (pH 1.2), the hydrogels showed a slower and steadier release rate. The drug release increased with the increase in pH of the medium. Also, the results indicated that the type and amount of photo-initiators changed the release behavior. The incorporation of hydroxyapatite into the hydrogel reduced donepezil hydrochloride release rate.

CONCLUSIONS

In summary, hydrogels containing various concentrations of HAp intended for oral administration were prepared and evaluated. Incorporation of HAp into the hydrogels improved the release behavior. These results indicated that PEG-DA-based hydrogels had a favorable behavior for drug delivery. The combination between PEG-

DA and HAp could delay the degradation rate of the hydrogels in simulated gastrointestinal fluid. The obtained results showed that the prepared hydrogels could be potentially beneficial for drug delivery applications.

Acknowledgements: This work was supported by the Research Fund of the Yildiz Technical University. Project Number: FDK-2017-3029.

REFERENCES

1. D. J. Munoz-Pinto, S. Samavedi, B. Grigoryan, M. S. Hahn, *Polymer*, **77**, 227 (2015).
2. F. Markus, F. Dreher, S. Laschat, S. Baudis, G. E.M. Tovar, A. Southan, *Polymer*, **108**, 21 (2017).
3. X. Dai, X. Chen, L. Yang, S. Foster, A. J. Coury, T. H. Jozefiak, *Acta Biomaterialia*, **7**, 1965 (2011).
4. P. N. Patel, C. K. Smith, C. W. Patrick, Jr, *J. Biomed. Mater. Res.*, **73A**, 313 (2005).

5. J. A. Beamish, J. Zhu, K. Kottke-Marchant, R. E. Marchant, *J. Biomed. Mater. Res.*, **92A**, 441 (2010).
6. R. P. Witte, A. J. Blake, C. Palmer, W. J. Kao, *J. Biomed. Mater. Res.*, **71A**, 508 (2004).
7. M. B. Mellott, K. Searcy, M. V. Pishko, *Biomaterials*, **22**, 929 (2001).
8. F. Sesigur, D. Sakar-Dasdan, O. Yazıcı, F. Cakar, O. Cankurtaran, F. Karaman, *Optoelectronics and Advanced Materials – Rapid Communications*, **10**, 97 (2016).
9. Z. A. Abdul Hamid, K.W. Lim, *Procedia Chemistry*, **19**, 410 (2016).
10. A. D. Lynn, T. R. Kyriakides, S. J. Bryant, *J. Biomed. Mater. Res.*, **93A**, 941 (2010).
11. M. Salehi, M. Naseri-Nosar, S. Ebrahimi-Barough, M. Nourani, A. Vaez, S. Farzamfar, J. Ai, *J. Physiol. Sci.*, **68**, 579 (2018).
12. N. M. Tatiana, V. Cornelia, R. Tatia, C. Aurica, *Colloid and Polymer Science*, **296**, 1555 (2018).
13. M. Shahmoradi, R. Rohanzadeh, F. Sonvico, M. Ghadiri, M. Swain, *Australian Dental Journal*, **63**, 356 (2018).
14. S. Senol, E. Akyol, *Journal of Materials Science*, **53**, 14953 (2018).
15. F. Branda, A. Costantini, G. Laudisio, A. Buri, *Journal of Materials Science*, **34**, 1319 (1999).
16. M. H. Kim, B. S. Kim, J. Lee, D. Cho, O. H. Kwon, W. H. Park, *Biomaterials Research*, **21**, 12 (2017).
17. G. Lin, B. Tarasevich, *Journal of Applied Polymer Science*, **128**, 3534 (2013).
18. E. Akyol, S. Senol, Ö. Doğan, *Bulgarian Chemical Communications*, **49**, 57 (2017).
19. J. Wang, Z-M. Wang, X-M. Li, F. Li, J-J. Wu, L-Y. Kong, X-B. Wang, *Bioorganic & Medicinal Chemistry*, **24**, 4324 (2016).
20. K. Makitani, S. Nakagawa, Y. Izumi, A Akaike, T. Kume, *Journal of Pharmacological Sciences*, **134**, 37 (2017).
21. G. E. J. Poinern, S. Brundavanam, S. K. Tripathy, M. Suar, D. Fawcett, *Physical Chemistry*, **6**, 11 (2016).
22. E.T. Mombeshora, R. Simoyi, V. O. Nyamori, P.G. Hdungu, *S. Afr. J. Chem.*, **68**, 153 (2015).
23. M. Imani, S. Sharifi, H. Mirzadeh, F. Ziaee, *Iranian Polymer Journal*, **16**, 13 (2007).

КОНТРОЛИРАНО ОСВОБОЖДАВАНЕ НА ДОНЕПЕЗИЛ ХИДРОХЛОРИД ОТ PEG-DA ХИДРОГЕЛОВЕ

С. СЕНОЛ, Е. АКЪОЛ*

Департамент по инженерна имия, Технически университет Йилдиз, 34210 Истанбул, Турция

Постъпила на 1 юли, 2018 г.; приета на 1 октомври, 2018 г.

(Резюме)

Целта на настоящата работа е да се създаде система за контролирано освобождаване на лекарства чрез получаване и охарактеризиране на хидрогелове на базата на полиетиленгликол диакрилат (PEG-DA). За определяне влиянието на фотоинициатори върху освобождаването на лекарства от получените хидрогелове са използвани три фотоинициатора: 2,2-диметокси-2-фенилацетофенон (Irgacure 651), 1-хидроксициклохексилфенил кетон (Irgacure 184) и 2-хидрокси-4'-(2-хидроксиетокси)-2-метилпропиофенон (Irgacure 2959). За модифициране на PEG-DA е използван хидроксиапатит. FT-IR спектроскопия и дигитална микроскопия са използвани за охарактеризиране на получените хидрогелове. Съотношенията на набъбване на хидрогеловите и поведението им при освобождаване са изследвани при различни условия. Освобождаването на лекарствата е изследвано при рН 1.2, 6.8 и 7.4.

Particle size prediction of copolymer-drug conjugate using partial least squares regression

F. Noyan Tekeli^{1*}, D. Sakar Dasdan², G. Karakus³

¹*Yildiz Technical University, Faculty of Arts and Sciences, Department of Statistics 34220 Esenler, Istanbul, Turkey*

²*Yildiz Technical University, Faculty of Arts and Sciences, Department of Chemistry, 34220 Esenler, Istanbul, Turkey*

³*Cumhuriyet University, Faculty of Pharmacy, Department of Pharmaceutical Chemistry, 58140, Sivas, Turkey*

Received July 1, 2018; Accepted October 1, 2018

Particle size of the copolymers and the associated polydispersity are among the most important factors affecting biopharmaceutical behavior in a wide variety of therapeutic applications. Particle size provides valuable properties of particles or molecules in liquid medium. This characteristic directly affects bioavailability, dissolution and immunotoxicity. Predicting particle size will often skip many preliminary studies that are necessary to optimize formulations. In this work, the particle size of copolymer-drug conjugates was tried to be predicted using partial least squares regression (PLSR). The aim of this article is to construct a mathematical model for predicting the particle size of the copolymer-drug conjugate produced by a preferred pharmaceutical polymer. PLSR is a method that involves a combination of principal component analysis and multiple regression analysis for building predictive models when the factors are many and highly collinear. In the present study, to calculate the particle size of the copolymer-drug conjugate, we used the zeta potential and the particle size of the copolymer and drug, and different pH values as inputs.

Keywords: Particle size, Copolymer-drug conjugate, Partial least squares regression, NIPALS algorithm

INTRODUCTION

Today, the use of synthetic polymers as controlled drug delivery systems or drug carrier biomaterials has increased the interest toward polymer conjugation with biologically active components. Generally, this type of conjugates accumulates in tumors and can reduce toxicity in the body. According to the desired location, the polymer conjugates can be synthesized as having degradable or non-degradable chemical bonds with the relevant drug. Polymer-drug conjugates are drug molecules that are held in polymer molecules. The drugs will stick to the polymer. The drugs are not activated until the enzyme associated with the diseased tissue is present. This process severely reduces the damage to healthy tissue. The results of polymer-drug conjugates are very promising [1-3].

Zetasizer measurements which include zeta potential, particle size and mobility, throw light on valuable properties of particles or molecules in liquid medium. These characteristics directly affect bioavailability, dissolution and immunotoxicity. Zeta potential provides an understanding of many important properties of the colloidal systems and allows them to be controlled and to determine the electrical charge or potential on the particles [4].

Measuring these characteristics for a copolymer-drug conjugate is an expensive, difficult and time-

consuming procedure, so it is beneficial to predict these characteristics from other chemical measurements. Computational chemistry permits to calculate specific chemical properties such as size, lipophilicity, and polarity at various sites on the molecule without even making the compound [5]. In this work, the particle size of copolymer-drug conjugates was estimated using PLSR.

Partial Least Squares Regression

Partial least squares (PLS) regression is a multivariate statistical technique that can be used when the numbers of observations are less than the number of variables. PLSR can be efficiently used with a large number of variables that are highly correlated and involving substantial random noise. It was proposed by Herman Wold in 1977 and was first used in social sciences. After the first application by Kowalski, in the late seventies, S. Wold and H. Martens pioneered the chemical applications of PLS [6]. With modern measurement instrumentation including spectrometers, chromatographs and sensor batteries, the data tend to be strongly collinear, loud, and incomplete, so we can investigate these data with the PLSR. Today, PLSR is a widely used technique in chemometrics, especially when the number of independent variables is significantly larger than the number of observations.

* To whom all correspondence should be sent:
E-mail: fnoyan@yildiz.edu.tr

The purpose of PLSR is to construct components that capture a large part of the information in the X variables useful for estimating the Y variable and reduce the dimensionality of the regression problem. These new orthogonal variables obtained by PLS algorithms do not have collinearity [7]. PLSR takes the relation model between $(N \times K)$ dimensional X and $(N \times M)$ dimensional Y variables.

Let X and Y be the centered and scaled matrix of the predictors and response values, respectively, for ease of interpretation and numerical stability [8]. PLSR uses singular value decomposition of $S = X'Y$ cross product matrix. The PLSR, where T is a score vector and W is its weight vector, begins with a linear combination of X:

$$T = XW^* \quad (1)$$

X-scores, which are estimated as linear combinations of the original variables, are few and orthogonal. The PLSR predicts both X and Y by regression on T and U:

$$X = TP' + E \quad (2)$$

$$Y = UC' + F \quad (3)$$

The P and C vectors are called the X and Y loadings, respectively, and E and F are the associated residual vectors. The X-scores are good summaries of X so the X-residuals, (e), are small. The Y-residuals, f, are the deviations between the observed and modelled responses, and comprise the elements of the Y residual matrix, F.

We replaced equation 1 in Eq. 3:

$$Y = XW^*C' + F = XB + F \quad (4)$$

The PLS regression coefficients B can be written as in equation (5) and B is not independent unless the number of the PLSR components (A) equals the number of X-variables (K).

$$B = W^*C' \quad (5)$$

The X-matrix is deflated by subtracting $t_a p_a'$ from X, a is the index of components ($a=1, 2, \dots, A$)

$$t_a = E_{a-1} W_a \quad (6)$$

$$E_{a-1} = E_{a-1} - t_a p_a' \quad (7)$$

$$E_0 = X \quad (8)$$

The relationship between w and w* is given as:

$$W^* = W(P'W)^{-1} \quad (9)$$

Regression coefficients for PLSR are obtained from:

$$B = W(P'W)^{-1}C' \quad (10)$$

The Y-matrix is deflated by subtracting $t_a c_a'$. It is not necessary, because the results are equivalent whether Y is deflated or not.

NIPALS (Non-Linear Iterative Partial Least Squares)

The PLS algorithm used in the study is NIPALS. Developed by H. Wold in the 1960s, the NIPALS is also known as the classical algorithm. The starting point of NIPALS are X and Y data matrices that are optionally transformed, scaled and centered data. In the NIPALS algorithm which aims to obtain the components that maximize the covariance matrix, not all components are obtained at the same time. At each step, a single component and the weight and load values of this component are obtained [8]. PLS weights are iteratively estimated that is NIPALS based on deflating X and Y variables at each iteration.

- a) Get a starting vector of u, usually one of the Y columns. With a single y, $u = y$.
- b) w: PLS-weight for X, $w = X'u / u'u$
- c) t: PLS-score for X, $t = Xw$
- d) c: PLS-loading for Y, $c = Y't / t't$
- e) u: PLS-score for Y, $u = Yc / c'c$
- f) Convergence is tested on the change in t, $\|t_{old} - t_{new}\| / \|t_{new}\| < \epsilon$, where ϵ is small 10^{-6} or 10^{-8} . If there is no convergence, return to step (b),
- g) Deflate X and optionally Y before repeating the above steps for new components.
 $X = X - tp'$
 $Y = Y - tc'$
- h) The algorithm continues until the cross-validation shows that there is no more significant information in X about Y [8,9].

EXPERIMENTAL INSTRUMENT AND MATERIALS

We want to predict the particle size of the copolymer-drug conjugate. The independent variables consist of zeta potential and particle size of the copolymer poly(maleic anhydride-co-vinyl acetate) (MAVA) and the drug acriflavine (AF) and pH values whereas the response variable is the particle size of the copolymer-drug conjugate (MAVA-AF).

In this study, the particle size and zeta potential of the novel copolymer-drug conjugate, MAVA-AF including the nontoxic drug carrier MAVA were measured as a function of pH in water and as a function of time in simulated body fluids. Experimental values were published in Ref. [3].

Zeta potential, ζ was automatically calculated by the analyzer using the following Smoluchowski equation:

$$\mu_e = \frac{\varepsilon\zeta}{\eta} \quad (11)$$

where μ_e is electrophoretic mobility, ε is the dielectric constant, ζ is the zeta potential and η is the electrolyte viscosity [10].

It was observed that there were high correlations between measured variables. PLSR is an efficient tool for developing a quantitative relationship between several collinear predictor variables \mathbf{X} - Zetasizer Measurements in this work and the independent variable \mathbf{Y} -drug size in this work.

RESULTS AND DISCUSSION

For this analysis, the PLSR algorithm written in SAS was used. The explanatory variables consist of zeta potential of the copolymer, particle size of the copolymer, zeta potential of the drug, particle size of the drug, and different pH values, whereas the

response variable is the particle size of the copolymer-drug conjugate. PLSR analysis results showed that 5 components explain most of the variability on both dependent (response) and independent (explanatory) variables. As shown in Table 1, the PLS model explains 100 % of the variation in predictors and about 98 % of the variation in responses [5]. This is a strong indication that the five PLS components are suitable for modeling.

The correlation loadings plot (Fig. 1) is an intense brief of many properties of the PLS model. In the cross-validation, the data set is divided into two or more groups. To create a model for all groups, one is left out to control the predicted capacity of the model. We can measure the overall capacity of the model by doing this for each group. The Predicted Residual Sum of Squares (PRESS) statistics is obtained from the result of this process. The number of components of the model with the minimum PRESS statistics gives the optimal number of PLS components [11]. The cross-validation results are shown in Table 2. The cross-validation analysis shows that the model with five PLS factors reaches the absolute minimum of predicted residual sum of squares.

Table 1. Percent variation accounted for by partial least squares factors

Number of Extracted Factors	Model Effects		Dependent Variables	
	Current	Total	Current	Total
1	40.7209	40.7209	78.6506	78.6506
2	42.9975	83.7184	14.2551	92.9057
3	13.6563	97.3747	1.0256	93.9314
4	2.3396	99.7143	1.5769	95.5083
5	0.2857	100.0000	3.1832	98.6915

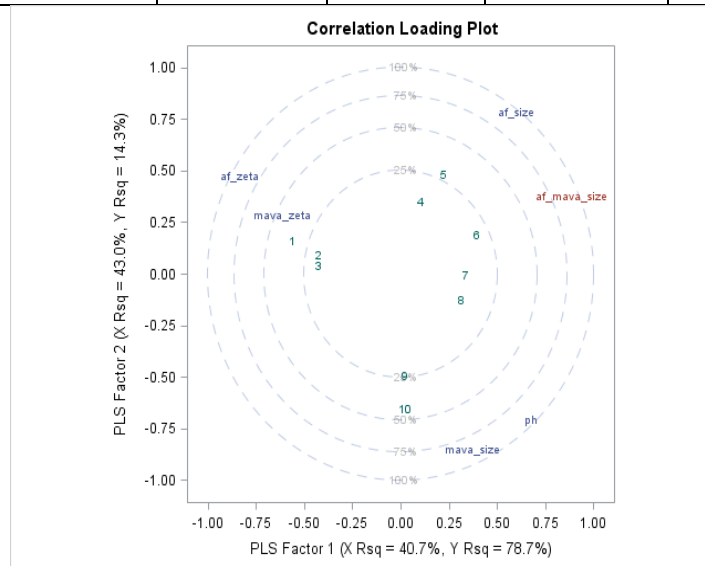


Figure 1. Correlation loadings plot

The cross-validation plot is shown in Fig. 2. From Figure 2, it is seen that five PLS factors are optimal for the PLS model.

In Table 3, the scores of 5 components obtained by the NIPALS algorithm are given.

The score matrix for \mathbf{X} , \mathbf{T} , consists of a linear combination of weight matrices \mathbf{W} and \mathbf{X} . The weights for score matrix of \mathbf{X} obtained by the NIPALS algorithm are given in Table 4.

Table 2. Cross-validation results

Number of Extracted Factors	Root Mean PRESS
0	1.111.111
1	0.805146
2	0.546011
3	0.418434
4	0.455074
5	0.267357
Minimum root mean PRESS	0.2674
Minimizing number of factors	5

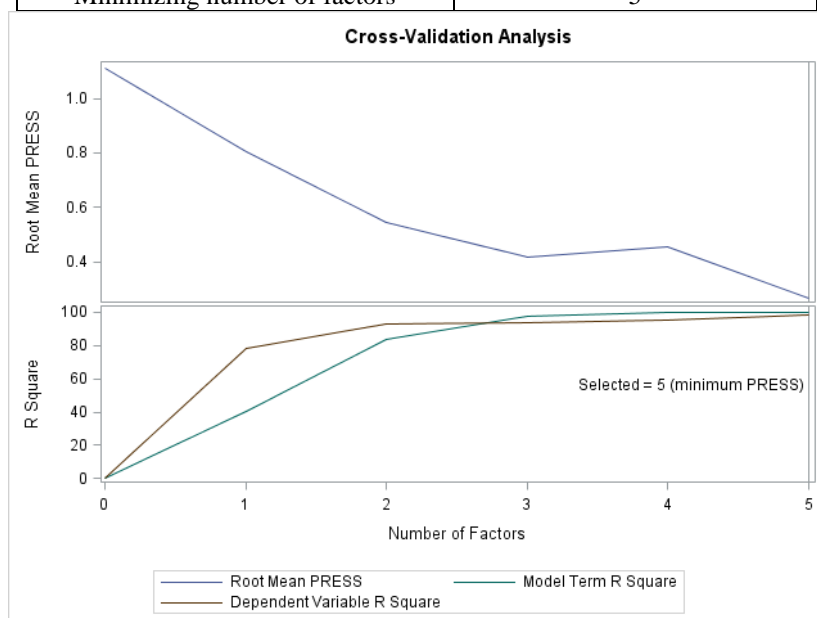


Figure 2. Cross-validation plot

Table 3. Scores for X by NIPALS algorithm

	Scores for X (T)				
	t ₁	t ₂	t ₃	t ₄	t ₅
1	-2.2893	0.657248	0.001768	-0.19824	-0.12443
2	-1.72851	0.368641	-0.41612	0.123511	-0.10848
3	-1.73328	0.163648	-0.29467	-0.18868	0.202632
4	0.411135	1.441116	-0.14654	0.773033	0.078009
5	0.899101	1.999483	1.821895	-0.25289	0.028022
6	1.608325	0.774276	-0.83651	0.118095	-0.09105
7	1.369919	-0.04711	-0.8099	-0.38613	-0.04425
8	1.278164	-0.55027	-0.34556	-0.26935	0.019102
9	0.093962	-2.07097	-0.00849	0.025979	0.165038
10	0.090485	-2.73606	1.034122	0.254671	-0.12459

Table 4. Weights for score matrix of X by NIPALS algorithms

	Weights for T				
	W1	W2	W3	W4	W5
pH	0.353	-0.44	0.439	0.407	0.655
MAVA-size	0.043	-0.527	0.536	0.095	-0.699
MAVA-zeta	-0.374	0.295	0.801	-0.574	0.197
AF-size	0.825	0.579	0.284	0.14	-0.198
AF-zeta	-0.533	0.354	0.212	0.896	-0.067

Table 5. Loading for X by NIPALS algorithms

	Loadings for X				
	p1	p2	p3	p4	p5
pH	0.476	-0.485	0.195	-0.018	0.655
MAVA-size	0.261	-0.582	0.393	0.418	-0.699
MAVA-zeta	-0.431	0.193	0.864	-0.53	0.197
AF-size	0.421	0.534	0.174	0.204	-0.198
AF-zeta	-0.585	0.322	-0.177	0.709	-0.067

Table 6. Regression coefficients and VIP values of explanatory variables

Label	Regression coefficients	VIP
pH	1.848599261	0.792799806
MAVA-size	-0.725061413	0.542219106
MAVA-zeta potential	0.026679280	0.753368178
AF-size	0.909555562	1.564985588
AF-zeta potential	0.752616534	1.02991427

The loadings for **X** obtained by the NIPALS algorithm are given in Table 5. As expressed in the equation $T = XW$, the components form a linear combination of the weight matrices **W** and **X**. Values of the weights show the contribution of explanatory variable to the component.

The loading matrix is used for modeling **X** according to the equation $X = TP$. Loading values show the amount of the explanation of the component to the explanatory variables. Regression analysis was performed after obtaining the 5 independent components. Table 6 gives the regression coefficients and VIP values of explanatory variables.

The regression coefficients represent the importance each predictor has in the prediction of the response. According to the regression coefficients, pH has the biggest influence on the dependent variable. The drug size (AF-size) has a great contribution in predicting particle size of the copolymer-drug conjugate (MAVA-AF size). The variable importance for projection (VIP) proposed

by Wold (1994) is a statistic parameter that shows which determinants are most useful for predicting dependent variables. An explanatory variable can be deleted from the model if it has a small VIP value and a relatively small coefficient (absolute value). Wold (1994) considered a value smaller than 0.8 for a small VIP value [12,13]. The copolymer particle size (MAVA-size) has a low VIP value for the PLS model. variable importance plot and regression parameter profile are given in Figs. 3 and 4, respectively.

The variable importance plot shows the contribution of each predictor in fitting the PLS model for both predictors and response. The particle size (MAVA-size) and zeta potential (MAVA-zeta potential) of copolymer are small absolute coefficients and small VIP's are seen in Figure 2 and Figure 3. As a result of the prediction results with five components, the residuals ranged from 0.000 to 0.051 and all of them are low. The PLSR model explains 98.6915 % of the variation in responses.

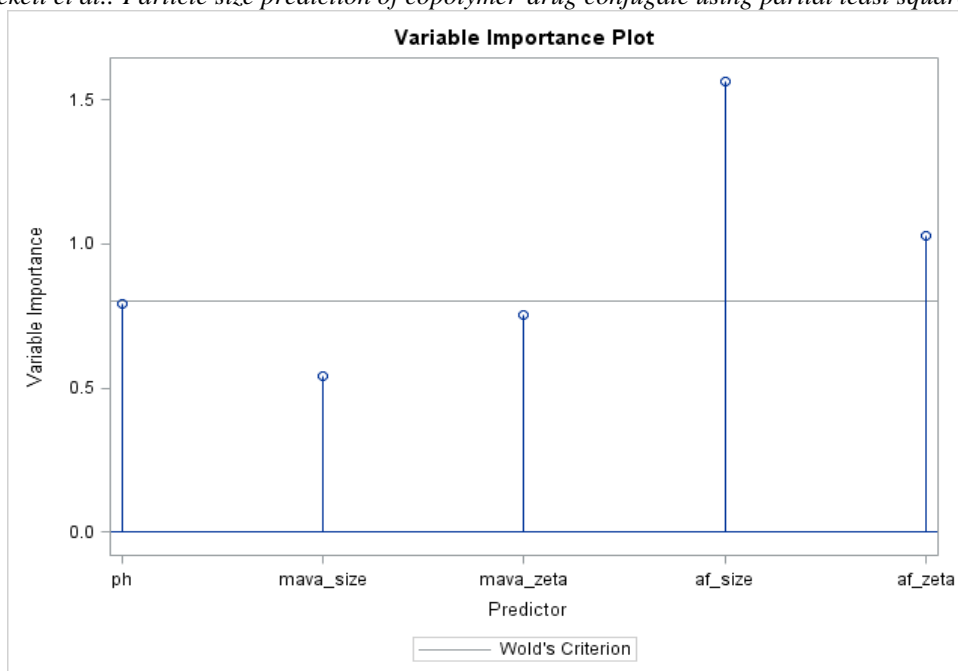


Figure 3. Variable importance plot

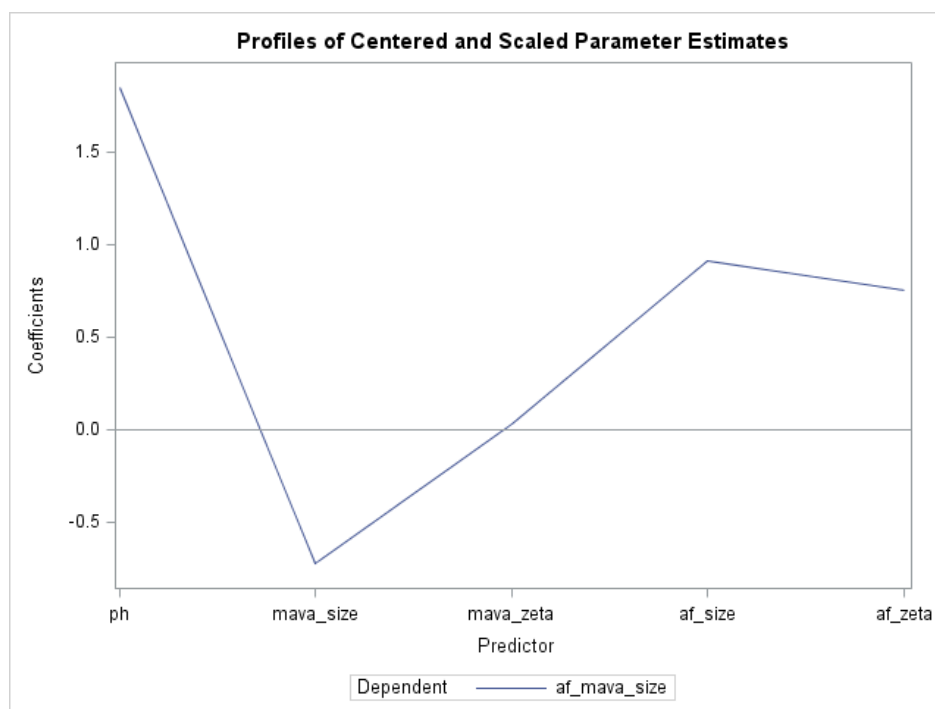


Figure 4. Regression parameter profile

CONCLUSIONS

In this work, a mathematical model was constructed using PLSR to estimate the particle size of the copolymer-drug conjugate produced by a preferred pharmaceutical polymer. The PLSR is a multivariate statistical method that can be used when there is a high correlation between variables. It consists of partial least squares and multiple linear regression analysis. First, explanatory variables, X, having multicollinearity were reduced

to components which explain the great amount of covariance between explanatory and response variable by using partial least squares. Then, a regression model was constructed by applying multiple linear regression analysis to the obtained independent new components. The NIPALS algorithm was used and it was found that the particle size of drug (AF) was the most effective in predicting particle size of the copolymer-drug conjugate (MAVA-AF).

F. Noyan Tekeli et al.: Particle size prediction of copolymer-drug conjugate using partial least squares regression

Acknowledgements: This work was supported by the Scientific Research Project Coordination Center of Yildiz Technical University, Turkey (Project No: 2016-01-02-YL06) and Sciences Research Projects Foundation of Cumhuriyet University, (CUBAP, Project No: F258)

REFERENCES

1. I.N. Larson, H. Ghandehari, *Chemistry of Materials*, **24**, 840 (2012).
2. A. N. Semenov, *Macromolecules*, **41**, 2243 (2008).
3. D. Sakar Dasdan, A. Dizdar, G. Karakus, *Bulg. Chem. Commun.*, **49**(I), 43(2017).
4. F. NoyanTekeli, *Bulg. Chem. Commun.*, **49**(I), 148 (2017).
5. SAS Institute Inc. 2008. SAS/STAT® 9.2 User's Guide. Cary, NC: SAS Institute Inc. <http://support.sas.com/documentation/cdl/en/statugpls/61818/PDF/default/statugpls.pdf>
6. E. Bulut, Ö. Gürünlü Alma, *Physical Sciences*, **6**(2), 36 (2011).
7. E. Bulut, U. Yolcu, M.Y. Tasmektepligil, E. Egrioglu, *World Applied Sciences Journal* , **21**(4), 572 (2013).
8. S.Wold , M. Sjostrom, L.Eriksson, *Chemometrics and Intelligent Laboratory Systems*, **58**, 109 (2001).
9. 9.G. Gergov, A. Alin, M. Doychinova, M. De Luca, V. Simeonov, Y. Al-Degs, *Bulg. Chem. Commun.*, **49**(2), 410 (2017).
10. Brookhaven Instruments Corporation, Instruction Manual for Zeta Potential Analyzer Instruction Book <https://support.sas.com/rnd/app/stat/papers/plsex.pdf>
11. T. Mehmood, K.Hovde Liland, L.Snipen, S.Sæbø, *Chemometrics and Intelligent Laboratory Systems*, **118**, 62, (2012).
12. E. Bulut, A.Alın, *Dokuz Eylül Üniversitesi İktisadi ve İdari Bilimler Fakültesi Dergisi*, **24** (2),127 (2009).

ПРЕДСКАЗВАНЕ НА РАЗМЕРА НА ЧАСТИЦИТЕ НА КОНЮГАТ ПОЛИМЕР-ЛЕКАРСТВО С ИЗПОЛЗВАНЕ НА РЕГРЕСИЯ НА ЧАСТИЧНИ НАЙ-МАЛКИ КВАДРАТИ

Ф. Ноян Текели^{1*}, Д. Сакар Дашдан², Г. Каракуш³

¹ *Технически университет Йилдиз, Факултет по науки и изкуства, Департамент по статистика, 34220 Есенлер, Истанбул, Турция*

² *Технически университет Йилдиз, Факултет по науки и изкуства, Департамент по химия, 34220 Есенлер, Истанбул, Турция*

³ *Университет Джумхуриет, Факултет по фармация, Департамент по фармацевтична химия, 58140, Сивас, Турция*

Постъпила на 1 юли, 2018 г.; приета на 1 октомври, 2018 г.

Размерът на частиците и свързаната с него полидисперсност са сред най-важните фактори, влияещи върху биофармацевтичното отнасяне при голям брой терапевтични приложения. Размерът на частиците или молекулите им придава ценни свойства във водна среда. Този фактор директно влияе върху биодостъпността, разтворимостта и имунотоксичността. Предсказването на размера на частиците често прави излишни много предварителни изследвания, необходими за оптимизиране на лекарствените препарати. В настоящата работа е направен опит за предсказване на размера на частиците на конюгата полимер-лекарство с помощта на регресия на частични най-малки квадрати (PLSR). Конструиран е математичен модел за предсказване на размера на частиците на конюгат полимер-лекарство, получен от предпочитан фармацевтичен полимер. PLSR е метод, който включва комбинация от анализ на основни компоненти и множествен регресионен анализ за изграждане на предсказуеми модели в случаите, когато има голям брой силно колинеарни фактори. За изчисляване на размера на частиците на конюгата полимер-лекарство ние използвахме зета-потенциала и размера на частиците на съполимера и на лекарството, както и различни рН стойности като входящи данни.

An entry to the synthesis of uleine-type alkaloids by Fischer indole synthesis reactions: FT-IR, NMR spectroscopy and computational study of the substituted carbazole compound

G. Serdaroglu¹, N. Uludag^{2*}

¹Sivas Cumhuriyet University, Department of Science Education, 58040, Sivas, Turkey

²Namık Kemal University, Department of Chemistry, 59030, Tekirdag, Turkey

Received July 1, 2018; Accepted October 1, 2018

An efficient and straightforward method for the synthesis of 2-(2,3,4,9-tetrahydro-1*H*-carbazole-2-yl)acetonitrile by Fischer reaction of phenylhydrazine hydrochloride acid and 2-(3-oxocyclohexyl)acetonitrile in presence of ethanol is reported. Mild reaction conditions, good yields of products, short reaction times, and operational simplicity are the advantages of this procedure. PES scan was performed to determine the stable conformers of the studied compound in the gas phase at B3LYP/6-31G(d,p) level of the theory. The ¹H and ¹³C NMR chemical shifts for each stable conformer of the studied compound were observed and simulated by the DFT method in both gas and water phases. Also, the recorded FT-IR spectrum of the studied compound was compared with the simulated vibrational modes for each stable conformer. NBO was employed to predict the important intra-molecular interactions contributing to the lowering of the molecular stabilization energy of each stable conformer. FMO analysis and MEP diagrams were performed to predict the physicochemical and quantum chemical parameters to estimate the chemical reactivity behavior and reactive sites of each stable conformer.

Keywords: *Strychnos* alkaloids, FT-IR, NMR, FMO, NBO

INTRODUCTION

The natural carbazole ring skeleton of indole alkaloids often serves as a key intermediate for the synthesis of pentacyclic *strychnos* alkaloids. It is found in over 300 natural products belonging to several biogenetic types, and including two of the best-known alkaloids, uleine, and dasycarpidone [1, 2]. It has been greatly used in the synthesis of natural products (NP_s), as well as in medicinal chemistry [3]. Among them, uleine-type NP_s exhibit remarkable biological activities such as anti-ulcer [4] and acetylcholinesterase inhibitory activities, and further research toward their potential bioactivities is of current interest [5]. Accordingly, significant efforts have been devoted to the efficient synthesis of this type of alkaloids [6-8]. Recently, we have described the synthesis of the uleine-type alkaloids (Fig. 1) [9-13]. Efficient and atom-economic total synthesis of a complex molecule is a great endeavor in organic synthesis.

Consequently, one step reactions have received much attention because they minimize the time and cost of the synthesis of highly functional molecules from simple building blocks. Moreover, this present method is advantageous with respect to the alternative synthetic approaches described for the synthesis of azocino [4,3-*b*] indole motif which is also found as a key feature in other *strychnos* alkaloids. It was decided to construct the 2-(2,3,4,9-tetrahydro-1*H*-carbazole-2-yl)acetonitrile of **3**. In this study, we present a new protocol for the enhanced construction of the skeleton toward the synthesis of uleine-type alkaloids.

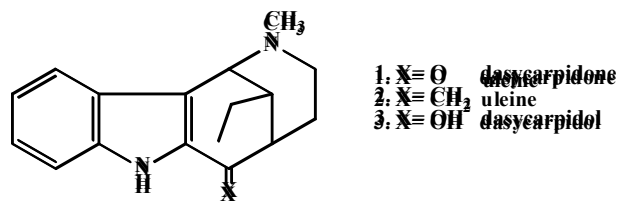
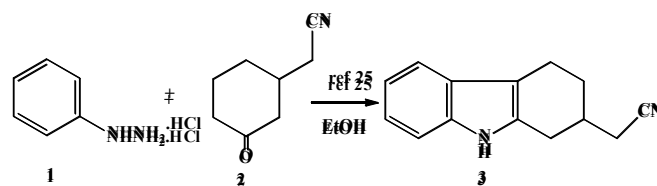


Fig. 1. Representatives of uleine-type alkaloids



Scheme 1. Synthesis of 2-(2,3,4,9-tetrahydro-1*H*-carbazol-2-yl)acetonitrile

* To whom all correspondence should be sent:
E-mail: nuludag@nku.edu.tr

EXPERIMENTAL AND COMPUTATIONAL
DETAILS

Computational details

¹H NMR (400 MHz) and ¹³C NMR (100 MHz) spectra were recorded with a Bruker instrument DPX-400 MHz high-performance digital FT-NMR spectrometer with CDCl₃ as the solvent and tetramethylsilane (TMS) as the internal standard at 25 °C. Chemical shifts are expressed in terms of parts per million (ppm) and the d coupling constants are given in Hz. IR spectra were obtained in KBr pellets using a Mattson 1000 FT-IR spectrometer. Elemental analyses were performed on a Costech ECS 4010 analyzer. Melting points were determined in a capillary tube on a Gallenkamp apparatus and were uncorrected. Reactions were monitored by thin layer chromatography (silica gel 60 F254). All reactions were carried out in an inert atmosphere of nitrogen. Purification of solvents was performed according to standard methods.

2-(2,3,4,9-tetrahydro-1H-carbazol-2-yl)acetonitrile (**3**)

Phenylhydrazine hydrochloride (**1**) (3.00 g, 20.74 mmol) and 2-(3-oxocyclohexyl)acetonitrile [**14**] (**2**) (5.69 g, 41.48 mmol) were added to 250 mL of ethanol. The reaction flask was evacuated for 10 min and back-filled with dry nitrogen. The mixture was refluxed for 14 h under stirring. TLC indicated the end of the reaction and formation of the product. The mixture was cooled and then the mixture was evaporated *in vacuo*. The crude product was dissolved in chloroform and washed first with water (2×50 mL) and then with 100 mL of 10% NaOH solution. Following drying of the organic layer over Na₂SO₄ the solvent was removed by evaporation and the residue was passed through a short silica gel column for further purification (1:1, ethyl acetate-*n*-hexane); R_f = 0.42) to give **3**. Yield 2.21 g (79%), as a pale yellow oil. IR (KBr, ν_{max}/cm⁻¹): 3267, 2925, 2165, 1607, 1455, 1319, 1241, 1010; ¹H NMR (400 MHz, CDCl₃, δ/ppm): 7.77 (s, 1H), 7.45 (d, *J* = 6.7 Hz, 1H), 7.34 (t, *J* = 8.0 Hz, 1H), 7.24 (td, *J* = 7.4 and 1.8 Hz, 1H), 2.94 (dd, *J* = 15.43 and 5.11 Hz, 1H), 2.77 (m, 2H), 2.62 (m, 1H), 2.54 (d, *J* = 7.4 and 3.8 Hz, 2H), 2.23 (m, 1H), 2.41 (m, 1H), 1.83 (m, 1H); ¹³C NMR (100 MHz, CDCl₃, δ/ppm): 135.9, 131.6, 127.4, 121.4, 119.3, 119.9, 118.1, 111.2, 108.9, 32.1, 28.9, 28.1, 22.8, 19.3; Anal. Calc. for C₁₄ H₁₄ N₂: C, 79.96; H, 6.71; N, 13.32. Found: C, 79.91; H, 6.67; N, 13.37.

The conformational analysis of the 2-(2,3,4,9-tetrahydro-1H-carbazol-2-yl)acetonitrile compound was employed to determine the stable conformer at B3LYP/6-31G(d,p) level of the theory [16-17]. Then, the three stable conformers predicted from the PES (potential energy surface) scan were re-optimized at 6-311++G(d,p) basis set in gas and water phase. The polarized continuum model (PCM) [18-19] was used to perform all analyses simulated in the water phase. NBO (natural bond orbital) analysis [20, 21] was conducted to elucidate the important intra-molecular interactions occurring in each stable conformer. The GIAO (Gauge-Independent Atomic Orbital) [22, 23] approach was used to predict the isotropic chemical shifts of each stable conformer. The simulated vibrational frequencies of each stable conformer were scaled down by using a scaling factor of 0.9668 [24] for B3LYP/6-311++G(d, p) and were assigned by VEDA package [25]. All calculations were carried out by G09W [26] and all schemes were prepared by using the ChemOffice 17 Suite [27]. GaussView 6.0 [28] was used to illustrate the HOMO, LUMO amplitudes and MEP diagrams, as well as to verify the vibrational modes of the stable conformers.

RESULTS AND DISCUSSION

In this study, our goal was to simplify the synthesis of compound **3** and we applied a new synthetic route for the synthesis of 2-(2,3,4,9-tetrahydro-1H-carbazol-2-yl)acetonitrile in high yields (up to 76%) through the indolization reaction between the starting phenylhydrazine hydrochloride and 2-(3-oxocyclohexyl)acetonitrile (**2**), which has been previously synthesized [14]. Reaction of compound **2** with phenylhydrazine hydrochloride by the Fischer indole reaction gave the carbazole derivative **3**. This compound is a versatile synthetic block and a subgroup of the uleine-type skeleton. 2-(2,3,4,9-tetrahydro-1H-carbazol-2-yl)acetonitrile moiety bearing a nitrile chain at the bridge carbon atom is the common key structure of the uleine alkaloids (Scheme 1) [15]. The basic skeletal features of these compounds, particularly pentacyclic ABCDE framework, can be seen in the namesake of the uleine family. In this study, new methodologies combining operational simplicity, high yields, readily available starting materials and low-cost reagents are desirable for the high throughput preparation of the target compounds.

Conformational analysis and structure descriptions

Fig.2 shows the structural skeleton with the original atomic numbers and ring descriptions of the 2-(2,3,4,9-tetrahydro-1*H*-carbazol-2-yl)acetonitrile compound. According to the acetonitrile group rotation around the ring part of the studied compound, one-dimensional PES scan (1D-PES) analysis was conducted by varying the dihedral angle τ (C27-C26-C13-C12) in the range of 0° - 360° in steps of 10° to predict the stable conformers in the gas phase by the B3LYP/6-31G(d,p) level of the theory. Fig.3 shows three stable conformers determined at -63° , 67° and 188° dihedral angles. All re-optimized conformers having no imaginary frequency were proved *via* conducting frequency calculations at 6-31G(d,p) and 6-311++G(d,p) basis sets in both gas and water phase. Table 1 shows the total and relative energy values for the three stable conformers, whose relative energies are close to each other and vary between 0-3.58 kcal mol⁻¹ for the 6-311++G(d,p) basis set (gas phase). It is clear that Conf3 is the most stable conformer except for the water phase by 6-311++G(d,p) basis set. On the other hand, Conf1 is predicted as the most stable conformer in the water phase by 6-311++G(d,p) basis set even though the energies of the Conf1 and Conf3 are very close to each other.

The selected optimized geometries of each stable conformer are given in Table 2 and are compared with the geometric parameters of the structurally related carbazole compound [29] because of lack of experimental and computational data. From Table 2, it can be seen that the bond lengths and angles for the three stable conformers are calculated to be very close to each other and the non-bonding angles for these conformers are different from each other. The C1-

C2 and C4-C5 bond lengths belonging to the aromatic ring (RA) for all conformers were determined in the range of 1.41-1.43 Å and were observed in the range of 1.39-1.41 Å [29]. Also, the C4-N23 bond length for the stable conformers is the same as each other, that is, this bond length has been predicted in 1.38 Å and was observed in 1.37 Å [29]. Similarly, the bond angles for each stable conformer are almost similar: the bond angles for all stable conformers were determined at C2-C1-C6=121°, C3-C4-C23=131°, C5-C4-C23=107° and C11-C12-C13=110°, and there is very good agreement with the corresponding experimental ones. On the other hand, the non-bonding angles have considerably varied from each other according to the acetonitrile group position around the ring part of the compound. The non-bonding angle C27-C26...C11 for the Conf1, Conf2 and Conf3 was calculated as 149°, 75°, 112° respectively. Here, it should be seen that the non-bonding angle for the Conf2 is smaller than that of the other conformers because the acetonitrile group for Conf2 is folded over the RC (ring C) more than the other conformers. Furthermore, the dihedral angles for the aromatic part of all stable conformers were computed as follows: C1-C2-C3-C4=0°, C4-C5-C6-C1=0°, N23-NC4-C3-C2=180°, N23C11-C16-C5=0° and agree with the corresponding observed ones. Moreover, the dihedral angle C27-C26-C13-C12 for the stable conformers was calculated as 177° (Conf1), -55° (Conf2), 66° (Conf3). From Table 2, it is clear that the acetonitrile group for Conf1 is a little deviated (3°) from C27-C26-C13-C12 backbone plane. The dihedral angle C12-C13-C14-C15 for the non-aromatic part of each stable conformer was predicted as 61° (Conf1), 57° (Conf2), 61° (Conf3) which are very close to the observed 62°.

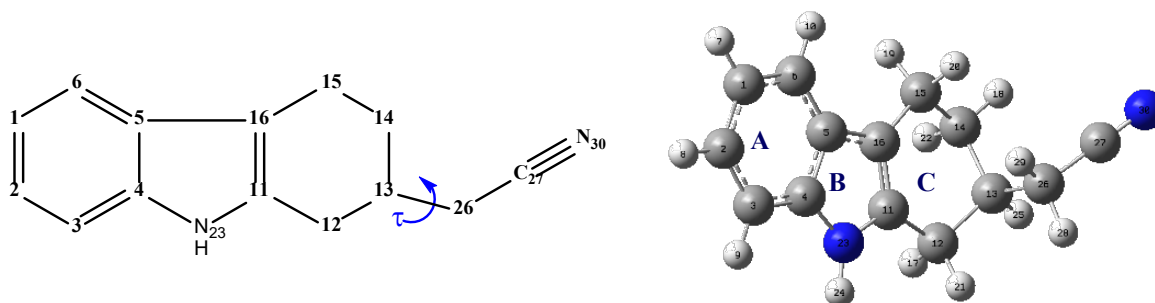


Fig. 2. The 2-(2,3,4,9-tetrahydro-1*H*-carbazol-2-yl)acetonitrile compound with the ring definition (right) and the skeleton of the compound with dihedral angle (left) τ (C27-C26-C13-C12)

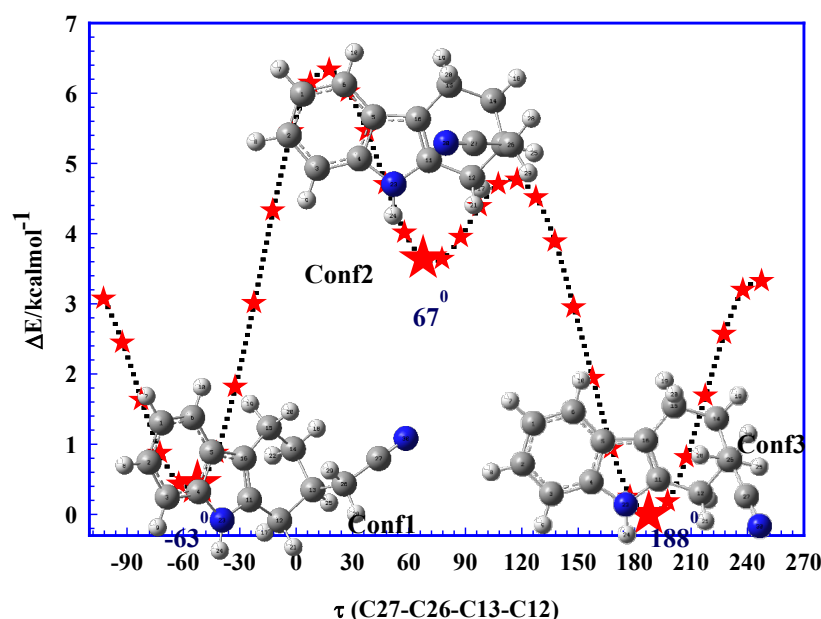


Fig. 3. PES scan of the studied compound at the B3LYP/6-31G(d,p) level of the theory in the gas phase.

Table 1. Total and relative energies for the three stable conformers of the studied compound.

Conf.	6-31G(d,p)				6-311++G(d,p)			
	Tot. energy/ hartree	ΔE/ kcalmol ⁻¹	Free energy / hartree	ΔG/ kcalmol ⁻¹	Tot. energy / hartree	ΔE / kcalmol ⁻¹	Free energy / hartree	ΔG / kcalmol ⁻¹
Gas Phase								
Conf1	-651.451845	0.366528	-651.241072	0.311245	-651.598189	0.384437	-651.388981	0.291792
Conf2	-651.446696	3.597769	-651.236057	3.458205	-651.592778	3.779973	-651.383752	3.573039
Conf3	-651.452430	0.000000	-651.241568	0.000000	-651.598802	0.000000	-651.389446	0.000000
Water phase								
Conf1	-651.464982	0.030980	-651.254216	0.020080	-651.612760	0.060856	-651.403627	0.000000
Conf2	-651.461789	2.034687	-651.250881	2.112824	-651.609383	2.180006	-651.399905	2.335590
Conf3	-651.465031	0.000000	-651.254248	0.000000	-651.612857	0.000000	-651.403603	0.015060

Table 2. Selected structural parameters for the three conformers of the studied compound at B3LYP/6-311++G(d,p) in the water phase

<u>Bond Length (Å)</u>	Exp.	Conf1	Conf2	Conf3	<u>Non-bonding angle (°)</u>	Exp.	Conf1	Conf2	Conf3
C1-C2	1.39 ^a	1.41	1.41	1.41	C27-C26....C11		149	75	112
C4-N23	1.37 ^a	1.38	1.38	1.38	C27-C26....C12		148	96	97
C4-C5	1.41 ^a	1.43	1.43	1.43	C27-C26....C14		94	105	147
C11-C16	1.36 ^a	1.37	1.37	1.37	C27-C26....C15		102	77	160
C11-N23	1.38 ^a	1.38	1.38	1.38	N30-C27....C11		159	103	132
N23-H24	0.86 ^a	1.00	1.00	1.00	N30-C27....C12		159	126	124
C27-N30		1.15	1.15	1.15	N30-C27....C14		123	133	158
C26-C27		1.46	1.46	1.46	N30-C27....C15		125	106	166
<u>Bond angle (°)</u>					<u>Dihedral angle (°)</u>				
C2-C1-C6	121 ^a	121	121	121	C1-C2-C3-C4	0.0 ^a	0	0	0
C3-C4-N23	131 ^a	131	131	131	C4-C5-C6-C1	0.6 ^a	-0	-0	-0
C5-C4-N23	107 ^a	107	107	107	N23-C4-C3-C2	180.0 ^a	180	180	180
C4-N23-H24	125 ^a	126	126	126	N23-C11-C16-C5	0.8 ^a	0	0	0
C12-C13-C14	113 ^a	110	111	111	N30-C27-C26-C13		-54	163	28
C26-C27-N30		179	177	179	C27-C26-C13-C12		177	-55	66
C14-C15-C16	110 ^a	111	110	111	C27-C26-C13-C14		-60	74	-171
C14-C13-C26		113	113	110	C12-C13-C14-C15	62.0 ⁰	61	57	61
C11-C12-C13	111 ^a	110	110	110	C12-C11-C16-C15	0.2 ⁰	-1	-2	-1

*experimental data are taken from ref.[29]

NBO analysis

NBO analysis [20,21] was used to elucidate the important intra-molecular interactions such as

resonance and hyper conjugative interactions contributing to the lowering of the stabilization

energy of a molecular system by using the results of the second order perturbative theory analysis.

Table 3 shows selected results obtained from the second order perturbative theory analysis for the three stable conformers at B3LYP/6-311++G(d,p) level in the water phase. Accordingly, the interaction energies occurred in the aromatic part of each stable conformers are very close to each other: the stabilization energy for the resonance interaction between the filled orbital π (C1-C2) and the unfilled orbital π^* (C3-C4) are calculated as Conf1=9.45, Conf2=9.47, Conf3=9.43 kcalmol⁻¹. In addition, the other resonance energies for the π (C3-C4) \rightarrow π^* (C1-C2) and π (C3-C4) \rightarrow π^* (C5-C6) interactions are computed as 5.35 and 8.21 kcal mol⁻¹ for Conf1; 4.65 and 8.76 kcalmol⁻¹ for Conf2; 5.76 and 8.18 kcalmol⁻¹ for Conf3. It should be noticed, however, that the stabilization energy of the interaction π (C11-C12) \rightarrow π^* (C5-C6) occurred in the RB of each stable conformer was computed as 9.91 kcalmol⁻¹ for Conf1, 12.01 kcal mol⁻¹ for Conf2, 9.93 kcalmol⁻¹ for Conf3. Here, it is clear from Table 3 that the stabilization energies occurring in the non-aromatic part of each stable conformer have begun to differ from each other according to the acetonitrile group orientation. In addition, there are also hyper-conjugative interactions being important for the stabilization energy, that is, the stabilization energies of the intra-molecular charge transfer for σ C12-H17 \rightarrow π^* (C11-C16) were calculated as 2.40 kcalmol⁻¹ for Conf1 and Conf3, 2.41 kcalmol⁻¹ for Conf2. On the other hand, the resonance energies of the interactions π (C27-N30) \rightarrow π^* (C1-C2) and π (C27-N30) \rightarrow π^* (C5-C6) occurring between the nitrile group and the aromatic ring were calculated as 0.37 kcalmol⁻¹ for Conf1 and 17.44 kcalmol⁻¹ for Conf2, but this kind of interaction was not determined for Conf3. It is clear that when the stabilization energies of LP (1) N23 and LP (1) N30 are compared with each other, the interaction energy between LP (1) N23 and the antibonding orbital is higher than that of LP (1) N30: the stabilization energies for the LP(1) N23 \rightarrow π^* (C3-C4) and LP(1) N30 \rightarrow π^* (C26-C27) interactions are calculated as 20.24 kcalmol⁻¹ and 4.90 kcalmol⁻¹ for Conf1, 19.78 kcalmol⁻¹ and 3.37 kcalmol⁻¹ for Conf2, 20.21 kcalmol⁻¹ and 5.22 kcalmol⁻¹ for Conf3, respectively. It can be said that the important contribution to the lowering of the molecular stabilization energy was provided by the intra-molecular charge transfer from the lone pair of the N23 atom to antibonding orbital(s), more than the lone pair of N30 atom.

Global reactivity parameters, FMO (Frontier Molecular Orbital) analysis and MEP (Molecular Electrostatic Potential)

FMO analysis is a very useful tool to explain/elucidate the kinetic stability, chemical reactivity behavior *via* the HOMO and LUMO orbitals showing the nucleophilic and electrophilic character of a sample molecular system. As it is well known, the ionization energy (I) and electron affinity (A) can be obtained from the HOMO and LUMO orbital energies according to the Koopman's theorem [30]. In addition, Parr and co-workers [31] have defined the DFT-based reactivity descriptors that are the electronic chemical potential (χ), global hardness (η), electrophilicity (ω) and the maximum charge transfer index (ΔN_{max}) as shown below:

$$I = -E_{HOMO} \quad (1)$$

$$A = -E_{LUMO} \quad (2)$$

$$\chi = -\frac{I+A}{2} \quad (3)$$

$$\eta = \frac{I-A}{2} \quad (4)$$

$$\omega = \frac{\mu^2}{2\eta} \quad (5)$$

$$\Delta N_{max} = \frac{I+A}{2(I-A)} \quad (6)$$

Table 4 presents the quantum chemical identifiers of each stable conformer of the studied compound obtained from the equations given above. The energy gap (ΔE) has changed in the following order: Conf2 < Conf1 < Conf3 in both the gas and water phases at two basis sets. It is clear that Conf2 has the lowest ΔE value which means the highest chemical reactivity and lowest kinetic stability. Moreover, the global hardness (η) has changed as Conf2 < Conf1 < Conf3 similar to the energy gap ordering of the stable conformers, in both the gas and water phases at two basis sets. Here, it can be noticed that Conf2 has the lowest hardness value which makes it the soft conformer of the studied compound. If it is looked at the chemical potential ordering of the three conformers, it can be seen that it has changed as Conf1 < Conf3 < Conf2. It can be also seen that Conf1 is the best electrophile because the electrophilicity index has changed as Conf2 < Conf3 < Conf1, in both the gas and water phases at two basis sets. But the maximum charge transfer capability (ΔN_{max}) calculated in the different ordering based on the basis set: (ΔN_{max}) has changed as Conf2 < Conf3 < Conf1 at 6-31G(d,p) basis set in both phases while it has changed as Conf3 < Conf1 < Conf2 at 6-311++G(d,p) basis set in both phases.

Table 3. Second-order perturbation theory analysis of the Fock matrix in NBO basis for the three stable conformers at B3LYP/6-311++G(d,p) level of the theory in the water phase

Donor(i)	Hybridization	ED _i /e	Acceptor (j)	Hybridization	ED _j /e	E(2)/ kcalmol ⁻¹	E(j)- E(i)/ a.u	F(i,j)/ a.u
<i>Conf1</i>								
π C1-C2 (2)	0.7099 p _(C1) + 0.7043 p _(C2)	0.82922	π^* C3-C4	p _(C3) - p _(C4)	0.21516	9.45	0.27	0.066
			π^* C5-C6	p _(C5) - p _(C6)	0.22349	9.83	0.28	0.069
π C3-C4 (2)	0.7117 p _(C3) + 0.7025 p _(C4)	0.81948	π^* C1-C2	p _(C1) - p _(C2)	0.21085	5.35	0.55	0.070
			π^* C5-C6	p _(C5) - p _(C6)	0.22349	8.21	0.29	0.063
π C5-C6 (2)	0.7182 p _(C5) + 0.6958 p _(C6)	0.81161	π^* C1-C2	p _(C1) - p _(C2)	0.21085	5.22	0.54	0.068
			π^* C3-C4	p _(C3) - p _(C4)	0.21516	9.98	0.27	0.067
			π^* C11-C16	p _(C11) - p _(C16)	0.15476	7.45	0.29	0.060
π C11-C16 (2)	0.6871 p _(C11) + 0.7266 p _(C16)	0.91108	π^* C5-C6	p _(C5) - p _(C6)	0.22349	9.91	0.30	0.073
			π^* C11-C16	p _(C11) - p _(C16)	0.15476	0.55	0.31	0.017
σ C12-H17 (1)	0.7831 sp ^{3.55} _(C12) + 0.6219 s _(H17)	0.98233	π^* C11-C16	p _(C11) - p _(C16)	0.15476	2.40	0.55	0.049
σ C12-H21 (1)	0.7817 sp ^{3.43} _(C12) + 0.6237 s _(H21)	0.98722	π^* C11-C16	p _(C11) - p _(C16)	0.15476	1.08	0.55	0.033
σ C15-H20 (1)	0.7767 sp ^{3.57} _(C15) + 0.6299 s _(H20)	0.98565	π^* C11-C16	p _(C11) - p _(C16)	0.15476	2.11	0.54	0.046
π C27-N30 (3)	0.6590 p _(C27) + 0.7521 p _(N30)	0.99423	π^* C1-C2	p _(C1) - p _(C2)	0.21085	0.37	0.66	0.022
LP (1) N23	p	0.81653	π^* C3-C4	p _(C3) - p _(C4)	0.21516	20.24	0.29	0.098
			π^* C11-C16	p _(C11) - p _(C16)	0.15476	18.26	0.31	0.096
LP (1) N30	sp ^{0.92}	0.98484	π^* C26-C27	sp ^{2.93} _(C26) - sp ^{0.86} _(C27)	0.01081	4.90	0.98	0.088
<i>Conf2</i>								
π C1-C2 (2)	0.7100 p _(C1) + 0.7042 p _(C2)	0.82977	π^* C3-C4	p _(C3) - p _(C4)	0.21596	9.47	0.28	0.066
			π^* C5-C6	p _(C5) - p _(C6)	0.21961	9.68	0.29	0.068
π C3-C4 (2)	0.7109 p _(C3) + 0.7033 p _(C4)	0.82060	π^* C1-C2	p _(C1) - p _(C2)	0.21099	4.65	0.65	0.071
			π^* C5-C6	p _(C5) - p _(C6)	0.21961	8.76	0.30	0.066
π C5-C6 (2)	0.7107 p _(C5) + 0.7035 p _(C6)	0.80662	π^* C1-C2	p _(C1) - p _(C2)	0.21099	4.45	0.64	0.068
			π^* C3-C4	p _(C3) - p _(C4)	0.21596	9.89	0.27	0.066
			π^* C11-C16	p _(C11) - p _(C16)	0.15494	7.32	0.29	0.059
π C11-C16 (2)	0.6864 p _(C11) + 0.7272 p _(C16)	0.91133	π^* C5-C6	p _(C5) - p _(C6)	0.21961	12.01	0.30	0.081
			π^* C11-C16	p _(C11) - p _(C16)	0.15494	0.52	0.30	0.016
σ C12-H17 (1)	0.7832 sp ^{3.56} _(C12) + 0.6218 s _(H17)	0.98260	π^* C11-C16	p _(C11) - p _(C16)	0.15494	2.41	0.55	0.049
σ C12-H21 (1)	0.7816 sp ^{3.44} _(C12) + 0.6238 s _(H21)	0.98679	π^* C5-C6	p _(C5) - p _(C6)	0.21961	0.50	0.54	0.023
			π^* C11-C16	p _(C11) - p _(C16)	0.15494	1.20	0.55	0.035
σ C15-H20 (1)	0.7773 sp ^{3.54} _(C15) + 0.6291 s _(H20)	0.98538	π^* C5-C6	p _(C5) - p _(C6)	0.21961	1.87	0.53	0.045
			π^* C11-C16	p _(C11) - p _(C16)	0.15494	2.17	0.54	0.046

G. Serdaroglu, N. Uludag: An entry to the synthesis of uleine-type alkaloids by Fischer indole synthesis reactions...

π C26-C27 (1)	0.7066 $sp^{2.89}_{(C26)+}$ 0.7076 $sp^{0.86}_{(C27)}$	0.99387	π^* C1-C2	$p_{(C1)-}$ $p_{(C2)}$	0.21099	0.33	1.12	0.027	
			π^* C5-C6	$p_{(C5)-}$ $p_{(C6)}$	0.21961	0.31	0.77	0.022	
σ C26-H28 (1)	0.7911 $sp^{3.46}_{(C26)+}$ 0.6117 $s_{(H28)}$	0.97813	π^* C5-C6	$p_{(C5)-}$ $p_{(C6)}$	0.21961	1.65	0.56	0.043	
π C27-N30 (1)	0.6481 $sp^{1.15}_{(C27)+}$ 0.7616 $sp^{1.07}_{(N30)}$	0.99818	π^* C1-C2	$p_{(C1)-}$ $p_{(C2)}$	0.21099	4.98	1.45	0.121	
π C27-N30 (2)	0.6569 $p_{(C27)+}$ 0.7540 $p_{(N30)}$	0.99434	π^* C5-C6	$p_{(C5)-}$ $p_{(C6)}$	0.21961	17.44	0.32	0.106	
π C27-N30 (3)	0.6609 $p_{(C27)+}$ 0.7505 $p_{(N30)}$	0.99377	π^* C5-C6	$p_{(C5)-}$ $p_{(C6)}$	0.21961	2.44	0.40	0.044	
LP (1) N23	p	0.81759	π^* C3-C4	$p_{(C3)-}$ $p_{(C4)}$	0.21596	19.78	0.29	0.098	
			π^* C11-C16	$p_{(C11)-}$ $p_{(C16)}$	0.15494	19.04	0.31	0.099	
LP (1) N30	$sp^{0.92}$	0.98441	σ^* C26-C27	$sp^{2.89}_{(C26)-}$ $sp^{0.86}_{(C27)}$	0.01272	3.37	0.92	0.070	
<i>Conf3</i>									
π C1-C2 (2)	0.7099 $p_{(C1)+}$ 0.7043 $p_{(C2)}$	0.82923	π^* C3-C4	$p_{(C3)-}$ $p_{(C4)}$	0.21517	9.43	0.28	0.066	
			π^* C5-C6	$p_{(C5)-}$ $p_{(C6)}$	0.22352	9.84	0.28	0.069	
π C3-C4 (2)	0.7117 $p_{(C3)+}$ 0.7025 $p_{(C4)}$	0.81943	π^* C1-C2	$p_{(C1)-}$ $p_{(C2)}$	0.21090	5.76	0.55	0.072	
			π^* C5-C6	$p_{(C5)-}$ $p_{(C6)}$	0.22352	8.18	0.29	0.063	
π C5-C6 (2)	0.7182 $p_{(C5)+}$ 0.6959 $p_{(C6)}$	0.81165	π^* C1-C2	$p_{(C1)-}$ $p_{(C2)}$	0.21090	5.26	0.53	0.068	
			π^* C3-C4	$p_{(C3)-}$ $p_{(C4)}$	0.21517	9.96	0.27	0.067	
			π^* C11-C16	$p_{(C11)-}$ $p_{(C16)}$	0.15472	7.45	0.29	0.060	
π C11-C16 (2)	0.6869 $p_{(C11)+}$ 0.7267 $p_{(C16)}$	0.91124	π^* C5-C6	$p_{(C5)-}$ $p_{(C6)}$	0.22352	9.93	0.30	0.073	
			π^* C11-C16	$p_{(C11)-}$ $p_{(C16)}$	0.15472	0.55	0.31	0.017	
σ C12-H17 (1)	0.7832 $sp^{3.54}_{(C12)+}$ 0.6218 $s_{(H17)}$	0.98256	π^* C11-C16	$p_{(C11)-}$ $p_{(C16)}$	0.15472	2.40	0.55	0.049	
σ C12-H21 (1)	0.7818 $sp^{3.42}_{(C15)+}$ 0.6235 $s_{(H21)}$	0.98682	π^* C11-C16	$p_{(C11)-}$ $p_{(C16)}$	0.15472	1.08	0.55	0.033	
σ C15-H19 (1)	0.7799 $sp^{3.49}_{(C15)+}$ 0.6259 $s_{(H19)}$	0.98692	π^* C11-C16	$p_{(C11)-}$ $p_{(C16)}$	0.15472	1.21	0.54	0.035	
σ C15-H20 (1)	0.7768 $sp^{3.57}_{(C15)+}$ 0.6298 $s_{(H20)}$	0.98566	π^* C11-C16	$p_{(C11)-}$ $p_{(C16)}$	0.15472	2.11	0.54	0.046	
LP (1) N23	p	0.81646	π^* C3-C4	$p_{(C1)-}$ $p_{(C2)}$	0.21517	20.21	0.29	0.098	
			π^* C11-C16	$p_{(C11)-}$ $p_{(C16)}$	0.15472	18.25	0.31	0.096	
LP (1) N30	$sp^{0.92}$	0.98481	σ^* C26-C27	$sp^{2.93}_{(C26)-}$ $sp^{0.86}_{(C27)}$	0.01076	5.22	1.01	0.092	

*E(2) stabilization energy; ϵ_i and ϵ_j are diagonal elements, and F_{ij} is the off-diagonal NBO Fock matrix element.

Fig. 4 presents the HOMO and LUMO visualization of all conformers by using the B3LYP/6-311++G(d,p) level of the theory in the water phase. From Fig.4 it can be seen that the HOMO is mainly localized on the aromatic part (RA and RB) and partly on the C12 and C15 atoms on the non-aromatic ring (RC) for all stable conformers. It can be said that the nucleophilic site for all stable conformers is around the RA, RB, and partly RC. It is clear that the electrophilic site is around the aromatic part and the C12 atom for all stable conformers. The MEP diagrams can be also used to illustrate the electrophilic and nucleophilic attack sites of the sample molecular system, as well as to predict the H-bonding tendency, chemical

reactivity behavior of the biologically or pharmaceutically important molecules. Fig. 5 shows the MEP diagrams for all stable conformers in the water phase at 6-311++G(d,p) basis set. The electrostatic potential based on the total electron density surface of the stable conformers has changed as follows: Conf2 ($\pm 0.107e$) = Conf3 ($\pm 0.107e$) < Conf1 ($\pm 0.117e$). Also, the color scheme indicates the electron poor (blue color) and electron rich (red color) region of the sample molecular system. It is clearly seen that the red color on the Conf2 is darker than that of the other conformers due to the possibility of intra-molecular charge transfer between the acetonitrile group and the ring part of this conformer.

Table 4. The quantum chemical and physicochemical identifiers of the three stable conformers

Conformer	E_{HOMO}	E_{LUMO}	ΔE	μ	η	ω	ΔN_{max}
<u>6-31G(d,p)</u>							
Conf1	-0.19874	-0.00848	5.17724	-2.81937	2.58862	1.53535	1.08914
Conf2	-0.19001	-0.00070	5.15139	-2.59474	2.57570	1.30697	1.00740
Conf3	-0.19805	-0.00743	5.18704	-2.79570	2.59352	1.50682	1.07796
<u>6-311++G(d,p)</u>							
Conf1	-0.21130	-0.02615	5.03819	-3.23067	2.51910	2.07163	1.28247
Conf2	-0.20242	-0.02753	4.75900	-3.12863	2.37950	2.05680	1.31483
Conf3	-0.21059	-0.02543	5.03846	-3.21122	2.51923	2.04664	1.27468
<u>6-31G(d,p)</u>							
Conf1	-0.19667	-0.00848	5.12091	-2.79121	2.56046	1.52138	1.09012
Conf2	-0.19524	-0.00811	5.09207	-2.76672	2.54603	1.50327	1.08668
Conf3	-0.19665	-0.00829	5.12554	-2.78835	2.56277	1.51690	1.08802
<u>6-311++G(d,p)</u>							
Conf1	-0.20829	-0.02519	4.98241	-3.17666	2.49120	2.02536	1.27515
Conf2	-0.20706	-0.02506	4.95247	-3.15816	2.47624	2.01393	1.27538
Conf3	-0.20829	-0.02502	4.98703	-3.17435	2.49352	2.02053	1.27304

* ΔE (Energy Gap), χ, η, ω and ΔN_{max} are in eV; HOMO and LUMO energies are in au.

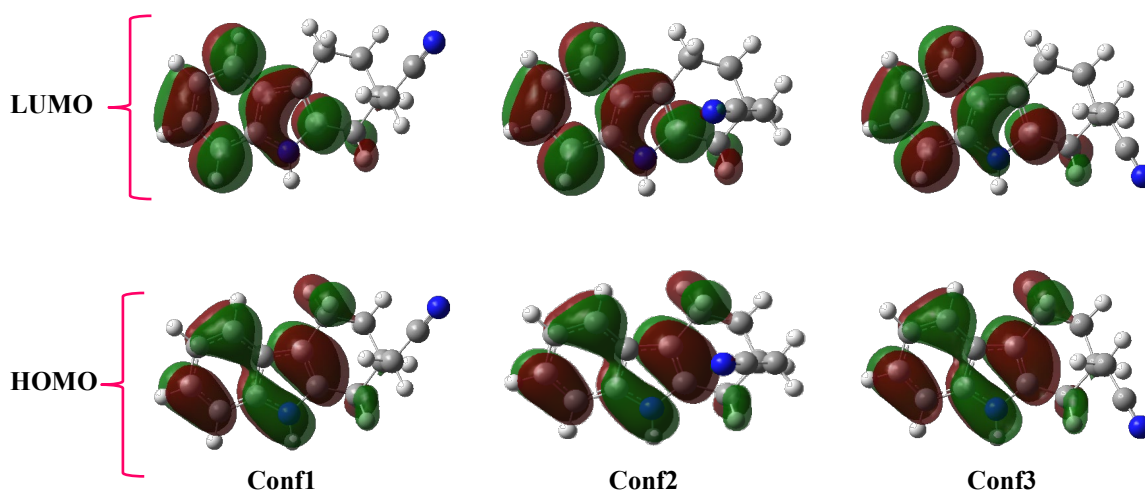


Fig. 4. HOMO and LUMO visualizations of the three stable conformers for the B3LYP/6-311++G(d,p) level in the water phase (isoval:0.02).

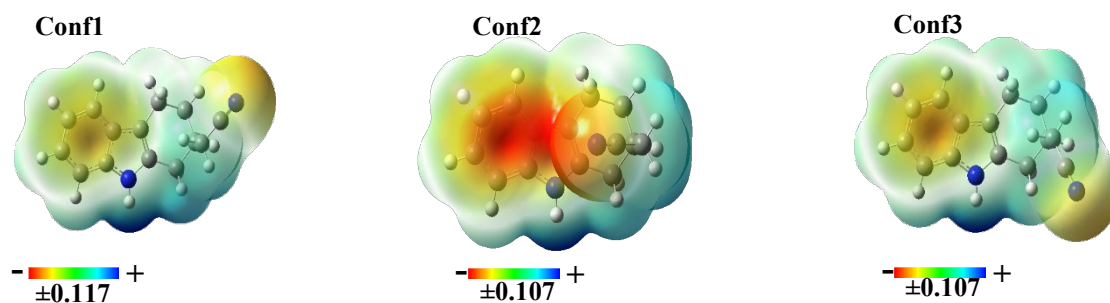


Fig. 5. The total electron density surface with ESP for the three stable conformers for using the 6-311++G(d,p) basis set in the water phase (Iso value:0.0004)

Vibrational analysis

Table 5 shows the selected vibrational modes of the studied compound obtained by FT-IR and simulated by the DFT method. The simulated frequencies for the stable conformers were scaled down by using a scaling factor of 0.9668 [24] for B3LYP/6-311++G(d,p) level of the theory to further match the vibrational mode values to the corresponding experimental values. The potential energy distribution (PED) analysis was employed to assign the vibrational frequencies of Conf3 and to verify them by the GaussView 6.0 package. The selected vibrational modes of each stable conformer of the studied compound and corresponding observed values are given in Table 5.

As it is well known, the N-H stretching and out-of-plane N-H bending (opb N-H) vibrational modes are very good wavenumbers to predict the functional groups of the specific molecular system but the in-plane N-H bending (ipb N-H) mode may not be good to predict wavenumber because it can be variable in the IR spectrum in terms of the location and intensity. It is well known that the N-H stretching band for the secondary amines occurs in the range 3500-3300 cm^{-1} [32]. In addition, the ipbH-N modes contaminated by the other modes, especially the ring vibrational modes, were simulated in the range 1218- 1221 cm^{-1} by DFT method at observed in 1221 cm^{-1} [33]. In addition, the opbH-N bending modes were found out at 483 and 435 cm^{-1} by FT-IR and calculated in the range 486-358 cm^{-1} by the DFT method [33]. In our previous study, the N-H stretching mode was recorded at 3230 cm^{-1} and simulated at 3523 cm^{-1} by HF method (chloroform phase) for the substituted carbazole compound [12]. In this work, we have observed the N-H stretching mode at 3268 cm^{-1} and simulated at 3525 cm^{-1} (Conf3) by DFT method. It can be noticed from Table 5 that the in-plane N-H bending modes were calculated as a mixed mode with in-plane bending ring vibrations and predicted between 1599- 1186 cm^{-1} by the DFT method. On

the other hand, the out-of-plane H-N bending frequencies were calculated between 630-389 cm^{-1} by DFT method and this band was also predicted as a mixed mode with out-of-plane ring vibrations. The N-C stretching mode for the nitrile group of the studied compound was computed at 2257 cm^{-1} (91% PED) and observed at 2165 cm^{-1} .

As it is expected from literature data, the C-C stretching modes for the aromatic rings of the compound have been observed in the range 1607-1242 cm^{-1} and simulated in 1599-1280 cm^{-1} by DFT.

Here, it is important to note that C-C stretching modes for the aromatic ring were generally as a mixed mode with the aromatic ring bending modes such as in-plane H-N and C-H bending modes. In addition, the symmetric and asymmetric C-H stretching vibrations in the aromatic ring for the Conf3 were simulated at 3081 cm^{-1} (94%, PED) and in the range 3071-3054 cm^{-1} , respectively. On the other hand non-aromatic ring and aliphatic C-H stretching modes for Conf3 were calculated in the range 2966-2947 cm^{-1} .

The non-aromatic ring bending modes for Conf3 were calculated in the range 1444-1418 cm^{-1} (scissoring, σCH_2), 1357-1299 cm^{-1} (wagging, ωCH_2), 1247-1142 (rocking, ρCH_2), 960-844 cm^{-1} (twisting, τCH_2) respectively. It is important to keep in mind that Table 5 shows a selection of both observed and calculated results. It is clear that, as expected, the CH₂ bending modes decreased in the following order: $\sigma\text{CH}_2 > \omega\text{CH}_2 > \tau\text{CH}_2 > \rho\text{CH}_2$ according to the wavenumber.

¹³C and ¹H NMR spectral studies

NMR spectroscopy as an analytical technique is used in many kinds of research fields to estimate the molecular structure and the molecular conformation in solution when the basic structure is known in addition to studying content and purity. Table 6 shows the ¹³C and ¹H NMR chemical shifts for the three stable conformers of the studied compound.

Table 5. Selected observed and calculated vibrational frequencies (in cm⁻¹) of the studied compound in the water phase at B3LYP/6-311++G(d,p) level.

Exp.	Conf1			Conf2			Conf3			PED % (Conf3)
	Unscal.	Scal.	I _{IR}	Unscal.	Scal.	I _{IR}	Unscal.	Scal.	I _{IR}	
3268	3645	3524	140	3645	3524	138	3646	3525	139	vN ₂₃ H (100)
	3187	3081	32	3186	3081	32	3187	3081	32	vCH RA(94)
	3176	3071	49	3176	3071	50	3176	3071	49	v _{as} CH RA(92)
	3088	2986	10	3079	2977	5	3089	2986	10	v _{as} C ₂₆ H ₂ (95)
	3069	2967	65	3064	2962	79	3068	2966	70	v _{as} C ₁₄ H ₂ RC (92)
	3049	2948	12	3041	2940	15	3048	2947	13	vC ₂₆ H ₂ (87)
	3046	2945	27	3040	2939	11	3046	2945	27	v _{as} C ₁₂ H RC (89)
2925	2990	2890	73	3000	2900	70	2991	2892	71	vC ₁₅ H RC (95)
2165	2335	2257	80	2333	2255	57	2335	2257	81	vN ₃₀ C (91)
1607	1654	1599	13	1655	1600	15	1654	1599-1465	12	vCC RAB (60)+ ipb HN ₂₃ C
1455	1495	1445	8	1494	1444	9	1494	1444-1418	7	σ CH ₂ RC (73)
1396	1459	1411	11	1455	1406	22	1458	1410	16	σ C ₂₆ H ₂ (56)
	1404	1357	13	1405	1358	10	1404	1357	13	ω CH ₂ RC+ ipb HN ₂₃ C (71)
1319	1360	1315	42	1360	1315	50	1359	1314	58	vCC RAB+ ω CH ₂ RC(69)
	1327	1283	36	1328	1284	59	1324	1280	39	vCC RAB+ ω CH ₂ RC (34)
1242	1289	1246	11	1295	1252	41	1290	1247	8	τ CH ₂ RC (54)
	1261	1219	5	1271	1229	13	1275	1232	3	τ CH ₂ RC (50)
	1256	1214	32	1254	1212	23	1255	1213	32	ipb HCC RA (43)
	1231	1190	3	1234	1193	1	1226	1186	6	ipb HN ₂₃ C (43)
	1222	1181	5	1225	1184	6	1212	1172	2	τ C ₂₆ H ₂ (68)
	1189	1150	4	1196	1156	1	1200	1161	1	τ CH ₂ RC (52)
1131	1170	1131	14	1172	1133	13	1170	1131-995	13	ipb HCC RA (64)
979	983	950	2	990	957	3	993	960	6	ρ CH ₂ RC (53)
930	948	916	2	941	910	4	942	942-723	3	opb HCC RA (91)
655	652	630	17	665	643	6	652	630-389	16	opb HN ₂₃ C (59)

The PED results are given for Conf3 (most stable structure). I_{IR}, IR intensity, The abbreviations are: v, symmetric stretching; v_{as}, asymmetric stretching; ω, wagging; τ, twisting; ρ, rocking; σ, scissoring; ipb, in-plane bending; opb, out-plane bending; R, ring.

In the past, the ¹³C NMR chemical shifts for the C atoms in the aromatic ring were found in the range 114-143 ppm and simulated in the range 112-146 ppm, by B3LYP/6-311++G(d,p) level of the theory, in the gas phase [34]. In the literature, it was reported that ¹³C NMR shifts for the C atoms in the non-aromatic ring were observed in the range 25-48 ppm in DMSO-*d*₆ and simulated in the range 26-56 ppm by B3LYP/631G(d) level of the theory [35]. In this paper, the ¹³C NMR chemical shifts for the aromatic and non-aromatic rings for Conf3 were recorded in the range 108.9-135.9 ppm and in the range 19.3-32.1 ppm, respectively, and computed in the range 115.7-143.3 and 21.2-38.1 ppm (gas phase). It is worth noticing that ¹³C NMR chemical shift for the C27 is observed at 118.1 ppm and calculated at 129.7 ppm (Conf3) in the water phase.

On the other hand, the ¹H NMR chemical shifts of the aromatic and non-aromatic ring for the substituted benzimidazole hydrate compound were recorded in the range 7.22-7.89 [34] and 1.5-1.8 ppm [35] whereas they were simulated in 7.35-7.85 ppm [34] and 1.5- 1.8 ppm by the DFT method [35]. In this work, the ¹H NMR chemical shifts of

the aromatic and non-aromatic rings for Conf3 were observed in the range 7.24-7.78 and 1.78-2.94 ppm, whereas they have been computed in the 7.35-7.76 and 1.99-3.21 ppm by the DFT method (water). It is clear that the chemical shift values of the hydrogen atoms closer to the electronegative atom are higher than the chemical shift values of the other hydrogen atoms.

Last, the linear regression analysis for both the ¹³C and ¹H NMR chemical shifts was employed to show the relationship between the observed and calculated chemical shifts; the regression equations are given in Table 7. Accordingly, the best correlation coefficient between the observed and simulated ¹³C NMR chemical shifts is determined as R²= 0.9992 (with the std. err. S= 1.3887) for Conf2 (gas) while the best correlation coefficient between the observed and calculated ¹H NMR chemical shifts is found to be R²= 0.9967 (with the std. err. S= 0.2564) for Conf3 (gas). These results indicate that the simulated ¹³C and ¹H NMR chemical shifts agree with the corresponding observed values.

Table 6. The observed and calculated ^1H and ^{13}C NMR isotropic chemical shifts (in ppm) for the studied compound, at 6-311++G(d,p) basis set.

^{13}C	Gas phase				Water phase		
	<i>Exp.</i>	Conf1	Conf2	Conf3	Conf1	Conf2	Conf3
1C	119.3	126.1	125.7	126.0	124.8	124.7	124.8
2C	121.4	128.1	127.8	128.0	126.5	126.5	126.5
3C	108.9	114.4	114.3	114.7	115.7	115.7	115.7
4C	135.9	143.2	143.4	143.2	143.3	143.3	143.3
5C	127.4	134.7	134.8	134.6	134.8	134.7	134.8
6C	118.9	123.5	123.6	123.0	122.9	122.9	122.9
11C	131.6	135.6	135.5	136.5	140.1	140.7	140.0
12C	28.9	33.5	30.8	30.2	32.9	30.4	30.3
13C	32.1	37.6	36.6	38.1	37.0	35.7	37.6
14C	28.1	29.1	34.1	33.0	29.2	33.2	32.6
15C	19.3	20.5	22.1	21.2	20.4	22.0	20.8
16C	111.2	116.3	118.0	114.6	114.9	116.8	114.8
26C	22.8	21.9	25.7	21.8	21.2	24.4	21.3
27C	118.1	123.2	122.3	123.8	129.2	129.3	129.7
^1H	<i>Exp.</i>	Conf1	Conf2	Conf3	Conf1	Conf2	Conf3
7H	7.24	7.31	7.27	7.29	7.35	7.35	7.35
8H	7.34	7.32	7.31	7.33	7.38	7.39	7.38
9H	7.45	7.30	7.30	7.34	7.59	7.61	7.60
10H	7.78	7.67	7.64	7.61	7.78	7.78	7.76
17H	2.94	3.23	3.28	3.08	3.29	3.35	3.21
18H	1.78	2.49	1.99	1.85	2.33	2.15	1.99
19H	2.79	2.89	2.91	2.87	2.93	2.98	2.88
20H	2.61	2.84	3.25	2.66	2.85	3.10	2.72
21H	2.79	2.30	2.65	3.02	2.58	2.85	3.00
22H	2.19	1.91	2.12	2.05	2.02	2.14	2.08
24H	7.17	6.92	6.99	7.07	7.72	7.81	7.80
25H	2.54	2.41	2.20	2.41	2.58	2.47	2.57
28H	2.54	2.10	2.38	2.48	2.45	2.62	2.56
29H	2.42	2.52	2.55	2.11	2.59	2.82	2.43

Table 7. Regression equations between observed and calculated ^1H and ^{13}C NMR shifts of the studied compound at B3LYP/6-311++G(d,p) level.

Method/ phase	Conformer	^{13}C	^1H
B3LYP/ gas	Conf1	$\delta_{\text{exp}} = 0.9618\delta_{\text{calc}} - 1.0410$ ($R^2 = 0.9989$, $S = 1.6820$)	$\delta_{\text{exp}} = 1.0098\delta_{\text{calc}} - 0.0151$ ($R^2 = 0.9836$, $S = 0.3260$)
	Conf2	$\delta_{\text{exp}} = 0.9759\delta_{\text{calc}} - 2.8283$ ($R^2 = 0.9992$, $S = 1.3887$)	$\delta_{\text{exp}} = 1.0258\delta_{\text{calc}} - 0.1288$ ($R^2 = 0.9899$, $S = 0.2564$)
	Conf3	$\delta_{\text{exp}} = 0.9650\delta_{\text{calc}} - 1.4070$ ($R^2 = 0.9987$, $S = 1.8087$)	$\delta_{\text{exp}} = 1.0074\delta_{\text{calc}} - 0.0022$ ($R^2 = 0.9967$, $S = 0.1472$)
B3LYP/ water	Conf1	$\delta_{\text{exp}} = 0.9492\delta_{\text{calc}} - 0.2385$ ($R^2 = 0.9981$, $S = 2.1757$)	$\delta_{\text{exp}} = 0.9848\delta_{\text{calc}} - 0.0659$ ($R^2 = 0.9912$, $S = 0.2387$)
	Conf2	$\delta_{\text{exp}} = 0.9579\delta_{\text{calc}} - 1.5430$ ($R^2 = 0.9986$, $S = 1.8600$)	$\delta_{\text{exp}} = 0.9972\delta_{\text{calc}} - 0.1905$ ($R^2 = 0.9919$, $S = 0.2294$)
	Conf3	$\delta_{\text{exp}} = 0.9522\delta_{\text{calc}} - 0.6637$ ($R^2 = 0.9978$, $S = 2.3433$)	$\delta_{\text{exp}} = 0.9786\delta_{\text{calc}} - 0.0313$ ($R^2 = 0.9952$, $S = 0.1762$)

CONCLUSIONS

In summary, we have completed divergent and efficient routes for the synthesis of 2-(2,3,4,9-tetrahydro-1*H*-carbazol-2-yl)acetonitrile. This method could be extended to the syntheses of other alkaloids. Finally, we believe that congeners of the

nitrile **3** will become versatile starting materials for the synthesis of diverse alkaloids bearing carbazole units. The PES scan carried out in the gas phase by the DFT method revealed three stable conformers that are very close to each other in terms of the energy. NBO analysis indicated that the resonance interactions ($\pi \rightarrow \pi^*$ and $n \rightarrow \pi^*$) for all stable

conformers have mainly contributed to the lowering of the molecular stability. The pictorial representation of HOMO shows that the nucleophilic attack site is around the aromatic ring (partly non-aromatic ring) of each stable conformer. Also, we have observed the NMR and FT-IR spectra of the studied compound and compared each of them with the computational results we have performed. This study has shown that the observed and simulated spectroscopic results are in good agreement with each other.

Acknowledgements: This work was financially supported by the Scientific and Technological Research Council of Turkey (TUBITAK Project No.112T503) and Sivas Cumhuriyet University Scientific research projects department (Project No: CUBAP: EGT-072). All simulations have been carried out at TUBITAK ULAKBIM, High Performance and Grid Computing Center (TR-Grid e-Infrastructure).

REFERENCES

1. T. Kametani, T. Suzuki, *J. Chem. Soc. C*, 1053 (1971).
2. J. Diez, P. Castells, M. Forns, D. Rubiralta, S. Grierson, H.-P. Husson, X. Solons, M. Font-Bardia, *Tetrahedron*, **50**, 6585 (1994).
3. C. Seide, A. De Moraes Santos, A. De Simone, M. Bartolini, A. M. Weffort-Santos, V. Andriassano, *Curr. Alzheimer. Res.*, **14**, 317 (2017).
4. H. Baggio, G. De Martini Otofujii, W. M. Souza, C. A. De Moraes Santos, L. M. Torres, L. Rieck, M. C. De Andrade Marques, S. Mesia-Vela, *Planta Med.*, **71**, 733 (2005).
5. J. M. Nardin, W. M. De Souza, J. F. Lopes, A. Florao, C. A. De Moraes Santos, A. M. Weffort-Santos, *Planta Med.*, **74**, 1253 (2008).
6. F. Tang, M. G. Banwell, A. C. Willis, *J. Org. Chem.*, **81**, 2950 (2016).
7. M. Amat, M. Perez, N. Llor, M. Martinelli, E. Mollins, *J. Chem. Commun.*, **14**, 1602 (2004).
8. S. Patir, N. Uludag, *Tetrahedron*, **65**, 115 (2009).
9. N. Uludag, R. Yilmaz, O. Asutay, N. Colak, *Chem. Heterocycl. Compd.*, **52**, 196 (2016).
10. N. Uludag, M. Sanda, O. Asutay, N. Coskun, *Org. Prep. Proc. Int.*, **46**, 551 (2014).
11. N. Uludag, M. Yakup, *Org. Prep. Proc. Int.*, **47**, 454 (2015).
12. N. Uludag, G. Serdaroglu, A. Yinanc, *J. Mol. Struct.*, **1161**, 152 (2018).
13. G. Serdaroglu, N. Uludag, *J. Mol. Struct.*, **1166**, 286 (2018).
14. T. A. Reekie, M. G. Banwell, A. C. Willis, *J. Org. Chem.*, **77**, 10773 (2012).
15. N. Uludag, G. Serdaroglu, *J. Mol. Struct.*, **1155**, 548 (2018).
16. A. D. Becke, *J. Chem. Phys.*, **98**, 1372 (1993).
17. C. Lee, W. Yang, R. G. Parr, *Phys. Rev.*, **B37**, 785 (1988).
18. J. B. Foresman, T. A. Keith, K. B. Wiberg, J. Snoonian, M. J. Frisch, *J. Phys. Chem.*, **100**, 16098 (1996).
19. J. Tomasi, B. Mennucci, R. Cammi, *Chem. Rev.*, **105**, 2999 (2005).
20. F. Weinhold, C. R. Landis, E. D. Glendening, *Int. Rev. in Phys. Chem.*, **35**, 399 (2016).
21. A. E. Reed, L. A. Curtiss, F. Weinhold, *Chem. Rev.*, **88**, 899 (1988).
22. M. Rohlfing, C. Leland, C. Allen, R. Ditchfield, *Chem. Phys.*, **87**, 9 (1984).
23. K. Wolinski, J. F. Hinton, P. Pulay, *J. Am. Chem. Soc.*, **112 (23)**, 8251 (1990).
24. G. Shakila, H. Saleem, N. Sundaraganesan, *World Scientific News*, **61(2)**, 150 (2017).
25. M. H. Jamroz, *Vibrational Energy Distribution Analysis VEDA 4*, Warsaw, (2004-2010).
26. M. J. Frisch, G. W. Trucks, H. B. Schlegel, G. E. Scuseria, M. A. Robb, J. R. Cheeseman, G. Scalmani, V. Barone, B. Mennucci, G. A. Petersson, H. Nakatsuji, M. Caricato, X. Li, H. P. Hratchian, A. F. Izmaylov, J. Bloino, G. Zheng, J. L. Sonnenberg, M. Hada, M. Ehara, K. Toyota, R. Fukuda, J. Hasegawa, M. Ishida, T. Nakajima, Y. Honda, O. Kitao, H. Nakai, T. Vreven, J. A. Montgomery, Jr., J. E. Peralta, F. Ogliaro, M. Bearpark, J. J. Heyd, E. Brothers, K. N. Kudin, V. N. Staroverov, T. Keith, R. Kobayashi, J. Normand, K. Raghavachari, A. Rendell, J. C. Burant, S. S. Iyengar, J. Tomasi, M. Cossi, N. Rega, J. M. Millam, M. Klene, J. E. Knox, J. B. Cross, V. Bakken, C. Adamo, J. Jaramillo, R. Gomperts, R. E. Stratmann, O. Yazyev, A. J. Austin, R. Cammi, C. Pomelli, J. W. Ochterski, R. L. Martin, K. Morokuma, V. G. Zakrzewski, G. A. Voth, P. Salvador, J. J. Dannenberg, S. Dapprich, A. D. Daniels, O. Farkas, J. B. Foresman, J. V. Ortiz, J. Cioslowski, and D. J. Fox, Gaussian 09 D.01. Gaussian, Inc, Wallingford CT (2013).
27. ChemOffice17 suite, Perkin Elmer, 2017.
28. GaussView6.0, Gaussian, Inc, Wallingford CT, 2016.
29. S. Murugavel, P. S. Kannan, A. Subbiah Pandi, T. Surendirand, S. Balasubramanian, *Acta Crystallogr. E*, **64**, o2433 (2008).
30. K. Fukui, *Science*, **218,4574**, 747 (1982).
31. R. G. Parr, L. V. Szentpaly, S. Liu, *J. Am. Chem. Soc.*, **121**, 1922 (1999).
32. T. Kavitha, G. Velraj, *J. Mol. Struct.*, **1141**, 335 (2017).
33. H. Singh, S. Singh, P. Agarwal, P. Tandon, R. D. Erande, D. H. Dethe, *J. Mol. Struct.*, **1153**, 262 (2018).
34. Y. E. Bakri, E. H. Anouar, Y. Ramli, E. M. Essassi, J. T. Mague, *J. Mol. Struct.*, **1152**, 154 (2018).
35. N. B. Arslan, C. Kazak, F. Aydın, *J. Mol. Struct.*, **1155**, 646 (2018).

ОТНОСНО СИНТЕЗА НА АЛКАЛОИДИ ОТ УЛЕИНОВ ТИП ЧРЕЗ ФИШЕРОВА РЕАКЦИЯ НА ИНДОЛОВ СИНТЕЗ: FT-IR, NMR СПЕКТРОСКОПСКО И ИЗЧИСЛИТЕЛНО ИЗСЛЕДВАНЕ НА ЗАМЕСТЕНО КАРБАЗОЛОВО СЪЕДИНЕНИЕ

Г. Сердароглу¹, Н. Улудаг^{2*}

¹Сивас Университет Джумхуриет, Департамент по наука и образование, 58040, Сивас, Турция

²Университет Намик Кемал, Департамент по химия, 59030, Текирдаг, Турция

Постъпила на 1 юли, 2018 г.; приета на 1 октомври, 2018 г.

(Резюме)

Представен е ефективен директен метод за синтез на 2-(2,3,4,9-тетрахидро-1*H*-карбазол-2-ил) ацетонитрил чрез Фишера реакция между фенилхидразин хидрохлорид и 2-(3-оксоциклохексил) ацетонитрил в присъствие на етанол. Предимства на тази процедура са меките реакционни условия, добрите добиви на реакционните продукти, краткото време на реакцията и простотата на изпълнение. Повърхността на потенциалната енергия е сканирана за определяне на стабилните конформери на изучаваното съединение в газова фаза на ниво ВЗЛУР/6-31G(d,p) на теорията. Наблюдавани са ¹H и ¹³C NMR химични отмествания за всеки стабилен конформер, които са симулирани чрез DFT метода в газова и водна фаза. Регистрираният FT-IR спектър на изучаваното съединение е сравнен със симулираните вибрационни режими за всеки стабилен конформер. NBO е използван за предсказване на важни межумолекулни взаимодействия, допринасящи за понижаване на молекулната енергия на стабилизация на всеки стабилен конформер. FMO анализ и MEP диаграми са използвани за предсказване на физикохимичните и квантово-химични параметри за оценка на химичната реактивност и реактивните центрове на всеки стабилен конформер.

Mechanism of the electron-exchange reactions between mixed ligand Fe(III) complexes and cyano complex of Fe(II)

Rozina Khattak^{1,2*}, Muhammad Sufaid Khan³, Iftikhar Imam Naqvi²

¹Department of Chemistry, Shaheed Benazir Bhutto Women University, Peshawar, Pakistan

²Department of Chemistry, University of Karachi, Karachi-75270, Pakistan

³Departamento de Fisico-Química, Instituto de Química, Universidade Estadual Paulista (UNESP) - Araraquara 14800-900, SP, Brazil

Received July 1, 2018; Accepted October 1, 2018

Our interest was to study the reactions of those mixed ligand complexes of Fe(III), where cyanide plays its role as a ligand. We synthesized the mixed ligand complexes of Fe(III) with diimine and cyanide as ligands to form octahedral geometry with high stability. We adopted previously cited procedures with improvements. The synthesized complexes, $[\text{Fe}^{\text{III}}(\text{phen}/\text{bpy})_2(\text{CN})_2]^+$ were reduced by the hexacyano complex of Fe(II) that is well-known for its high stability and octahedral geometry. The reduction was performed in aqueous medium at constant ionic strength of 0.06. The progress of the reactions was monitored spectrophotometrically by measuring the formation of $[\text{Fe}^{\text{II}}(\text{phen}/\text{bpy})_2(\text{CN})_2]$, i.e., the increase in absorbance with time. We found that the reduction of the mixed ligand Fe(III) complexes takes place in two phases. The first phase, when the Fe(III) complex is reduced to the neutral Fe(II) complex following zeroth order kinetics. The second phase was observed to be the rate-determining or slow step in the reduction of each complex, and the electron-exchange took place by an overall second order kinetics. In order to refine our results and to differentiate between the species which were taking part in the rate-determining step (slow step) and those which were taking part in the fast step, we studied the effect of protons and ionic strength on the rate constants in aqueous medium. We proposed an outer-sphere mechanism for the electron-exchange between Fe(III) and Fe(II) complexes.

Keywords: Dicyanobis(phen)iron(III), Dicyanobis(bpy)iron(III), Hexacyanoferrate(II)

INTRODUCTION

The redox chemistry of the coordination complexes is specifically important considering the wide ranging applications of those compounds [1-5]. We chose the redox reactions of Fe(III)/Fe(II) complexes, and studied the electron-exchange mechanism of the reactions of the mixed ligand complexes of Fe(III) with a well-known stable cyano complex of Fe(II). Dicyanobis(diimine)iron(III) was selected as an oxidizing agent due to its stability and solubility in aqueous medium, high molar absorptivity of its reduced form and the moderate value of the reduction potential (0.80 - 0.76 V) [6]. We selected 1,10-phenanthroline and 2,2'-bipyridine ligands as the representatives of the diimine group. Dicyanobis(phen/bpy)iron(III)/(II); $[\text{Fe}^{\text{III/II}}(\text{phen}/\text{bpy})_2(\text{CN})_2]^{+/0}$ were the outer-sphere mixed ligand complexes. They were synthesized in the 1960s [7] and their structure and properties, such as electrochemical behavior, were subsequently studied [8-17]. The derivatives of these compounds were also synthesized and characterized [18-20]. Later on, their applications were found through extensive research work on photosensitizing ability, acid hydrolysis,

solvatochromism, indicators (nonaqueous acid-base and redox), and kinetic studies [2, 21-52]. The kinetic studies involve the redox reactions of these compounds, but such reactions have rarely been studied since the compounds have been synthesized in the 1960s. $[\text{Fe}^{\text{II}}(\text{bpy})_2(\text{CN})_2]$ was oxidized by $\text{S}_2\text{O}_8^{2-}$, and the effect of various parameters were determined [36, 39, 40]. The effects of solvents and the solvation in the transition state, as well as the reorganization energy were discussed [41]. Bromate ion, BrO_3^- , has been used to oxidize $[\text{Fe}^{\text{II}}(\text{bipy})(\text{CN})_4]^{2-}$, $[\text{Fe}^{\text{II}}(\text{bipy})_2(\text{CN})_2]$ and $[\text{Fe}^{\text{II}}(\text{bipy})_3]^{2+}$ in acidic medium, and the kinetic parameters were reported [5, 43]. Meanwhile, the literature survey surfaced oxidation of a number of biologically active compounds by dicyanobis(bpy)iron(III); $[\text{Fe}^{\text{III}}(\text{bpy})_2(\text{CN})_2]^+$ and dicyanobis(phen)iron(III); $[\text{Fe}^{\text{III}}(\text{phen})_2(\text{CN})_2]^+$. Dicyanobis(phen/bpy)iron(III) is a sufficiently stable compound in aqueous, mixed aqueous and non aqueous media. This electrochemical stability draws the interest of the chemists to use this coordination complex in various redox reactions. Hydroquinone, ascorbic acid, sulfatoiron, rusticyanin, derivatives of ferrocene, Piloty's acid, iodide, cysteine and catechol were oxidized by

* To whom all correspondence should be sent:

E-mail: rznkhattak@sbbwu.edu.pk,
rznkhattak@yahoo.com

Rozina Khattak et al.: Mechanism of the electron-exchange reactions between mixed ligand Fe(III) complexes and ...

$[\text{Fe}^{\text{III}}(\text{phen/bpy})_2(\text{CN})_2]^+$ in different media under various conditions [2-4, 44-47, 49-52]. The kinetic parameters of these studies show that the reactions follow an outer-sphere mechanism which was discussed in the view of Marcus theory. We chose to oxidize hexacyanoferrate(II); $[\text{Fe}^{\text{II}}(\text{CN})_6]^{4-}$ by each of dicyanobis(phen)iron(III) and dicyanobis(bpy)iron(III) in order to compile the results of a thorough kinetic study. Hexacyanoferrate(II) has been oxidized by cumene hydroperoxide, chloroperoxidase compounds I and II, horseradish peroxidase compounds I and II, lactoperoxidase compound II, hydrogen peroxide, bromate, iodate, *N*-bromosuccinimide, and permanganate [53-62]. The kinetic parameters such as rate constants of some of these reactions were monitored and reported, and the mechanisms were discussed. Our study contributes the results of the kinetic study of the redox reactions between $[\text{Fe}^{\text{III}}(\text{phen/bpy})_2(\text{CN})_2]^+$ and $[\text{Fe}^{\text{II}}(\text{CN})_6]^{4-}$ in aqueous medium. We determined the effects of various parameters such as proton and ionic strength on the rate constants. In the view of the results and their comparison, we aimed to know the reactive species that were involved in the slow step(s) to control the mechanism(s).

EXPERIMENTAL

Anal grade materials were used. The nitrate salt of $[\text{Fe}^{\text{III}}(\text{phen/bpy})_2(\text{CN})_2]^+$ was synthesized and purified by implementing the reported procedures [2, 6, 7]. We purchased potassium salt of hexacyanoferrate(II), potassium nitrate, nitric acid and dioxane from Merck and used them without further purification. We used a rapid reaction monitoring system (home built) by following changes in absorbance with respect to time in the visible region [2, 6]. A total of 3 mL of the reaction mixture was put into the quartz cuvette (1 cm path length). We recorded the formation of dicyanobis(phen/bpy)iron(II) at 510 nm and 522 nm, respectively.

The reactions were studied under the condition of pseudo-first order in aqueous medium at 0.06 ionic strength and room temperature. The concentration of $[\text{Fe}^{\text{II}}(\text{CN})_6]^{4-}$ was always in excess over $[\text{Fe}^{\text{III}}(\text{phen/bpy})_2(\text{CN})_2]^+$. The results helped to conclude that the electron-exchange reaction of dicyanobis(phen/bpy)iron(III) with hexacyanoferrate(II) was completed in three phases (Fig. 1). We observed the first phase soon after starting the reaction(s). In this phase, the rate of reaction(s) remained independent of the concentrations of the reactants, and the order of reaction(s) with respect to the oxidant and reductant was zero. A ~69 (bpy system) and ~72 (phen

system) percent fraction of the reactions obeyed an overall zeroth order. The second phase started soon after the first phase. In this phase, the order of reaction with respect to the oxidant and the reductant was first, and we observed an overall second order. The third phase was the competition phase. The competition occurred between the rate of redox reaction(s) and the rate of precipitation of the neutral product, dicyanobis(phen/bpy)iron(II); $[\text{Fe}^{\text{II}}(\text{phen/bpy})_2(\text{CN})_2]$. We followed the progress of reaction(s) by monitoring the formation of product species, $[\text{Fe}^{\text{II}}(\text{phen/bpy})_2(\text{CN})_2]$, i.e., the increase in absorbance with respect to time. The monovalent oxidizing agent, $[\text{Fe}^{\text{III}}(\text{phen/bpy})_2(\text{CN})_2]^+$, was gaining an electron to yield neutral $[\text{Fe}^{\text{II}}(\text{phen/bpy})_2(\text{CN})_2]$. The increasing concentration of the neutral product near completion of the reaction(s) tended to decrease its solubility in aqueous medium. Due to this decrease in the solubility, we observed precipitates in the cuvette, and changes in the absorbance occurred. The decrease in absorbance changed the data near the end of each reaction. We implemented an integration method to determine the rate constant in each phase of the reaction(s). The values; observed zeroth order ($\epsilon \cdot k_{\text{obs}}$; s^{-1}) and observed pseudo-first order (k'_{obs} ; s^{-1}), are the average values of 3-6 experimental trials.

We collected data to characterize the synthesized complexes by using UV-Visible spectrophotometer (UV-160A Shimadzu) and elemental analyzer (Carlo Erba 1106). We used pH meter (HANNA HI 8314), and circulating water bath (Haake KT 33) to monitor pH and maintain temperature at a desired value, respectively.

RESULTS AND DISCUSSION

Kinetic parameters

We studied the effect of variation in the concentration of $[\text{Fe}^{\text{III}}(\text{phen/bpy})_2(\text{CN})_2]^+$, and or, $[\text{Fe}^{\text{II}}(\text{CN})_6]^{4-}$ upon the product of molar absorptivity of $[\text{Fe}^{\text{II}}(\text{phen/bpy})_2(\text{CN})_2]$ and observed zeroth order rate constant ($\epsilon \cdot k_{\text{obs}}$) i.e., the first phase of the reaction(s), and, observed pseudo-first order rate constant (k'_{obs}) i.e., the second phase of the reaction(s). There was no effect of $[\text{Fe}^{\text{III}}(\text{phen/bpy})_2(\text{CN})_2]^+$ on ' $\epsilon \cdot k_{\text{obs}}$ ' and ' k'_{obs} ' (Fig. 2). This confirms the zeroth order with respect to $[\text{Fe}^{\text{III}}(\text{phen/bpy})_2(\text{CN})_2]^+$ and the suitability of the pseudo-first order condition to probe the reaction(s) according to the following Eqns. 1-3.

$$\text{Rate} = k_{\text{obs}}[\text{Fe}^{\text{III}}(\text{phen/bpy})_2(\text{CN})_2]^0 + k'_{\text{obs}}[\text{Fe}^{\text{III}}(\text{phen/bpy})_2(\text{CN})_2]^+ \quad (1)$$

Rozina Khattak et al.: Mechanism of the electron-exchange reactions between mixed ligand Fe(III) complexes and ...

where, $[\text{Fe}^{\text{II}}(\text{CN})_6^{4-}] \gg [\text{Fe}^{\text{III}}(\text{phen/bpy})_2(\text{CN})_2^+]$

$k_{\text{obs}} = \text{observed zeroth order rate constant} = k_1[\text{Fe}^{\text{II}}(\text{CN})_6^{4-}]^0$ (2)

$k'_{\text{obs}} = \text{observed pseudo-first order rate constant} = k_2[\text{Fe}^{\text{II}}(\text{CN})_6^{4-}]$ (3)

The value of ' k'_{obs} ' varied in a sine-wave pattern and ' $\epsilon \cdot k_{\text{obs}}$ ' remained unchanged with respect to $[\text{Fe}^{\text{II}}(\text{CN})_6^{4-}]$ (Fig. 3).

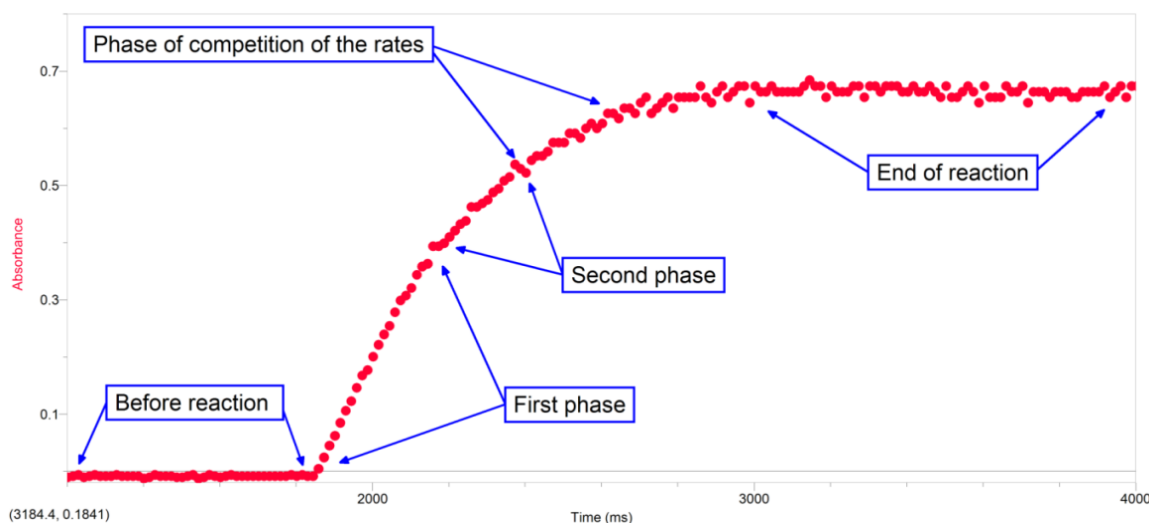


Fig. 1. A representative plot to show the phases of the reaction of $[\text{Fe}^{\text{III}}(\text{phen})_2(\text{CN})_2]^+$ with $[\text{Fe}^{\text{II}}(\text{CN})_6^{4-}]$ at $[\text{Fe}^{\text{III}}(\text{phen})_2(\text{CN})_2^+] = 0.1 \text{ mM}$, $[\text{Fe}^{\text{II}}(\text{CN})_6^{4-}] = 1.3 \text{ mM}$, $I = 0.06$, $T = 298 \pm 0.5 \text{ K}$ and $\lambda_{\text{max}} = 510 \text{ nm}$.

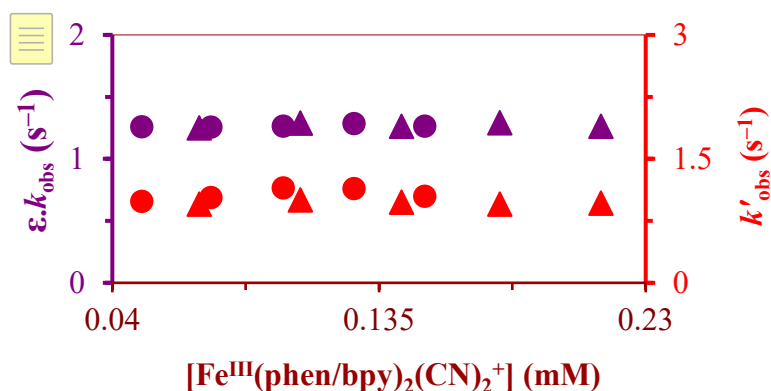


Fig. 2. Effect of the concentration of $[\text{Fe}^{\text{III}}(\text{phen/bpy})_2(\text{CN})_2]^+$ on the rate constants " $\epsilon \cdot k_{\text{obs}}$ " and " k'_{obs} " at $298 \pm 0.5 \text{ K}$, $[\text{Fe}^{\text{II}}(\text{CN})_6^{4-}] = 1.8/1.3 \text{ mM}$, and $I = 0.06$ (● phenanthroline and ▲ bipyridine systems).

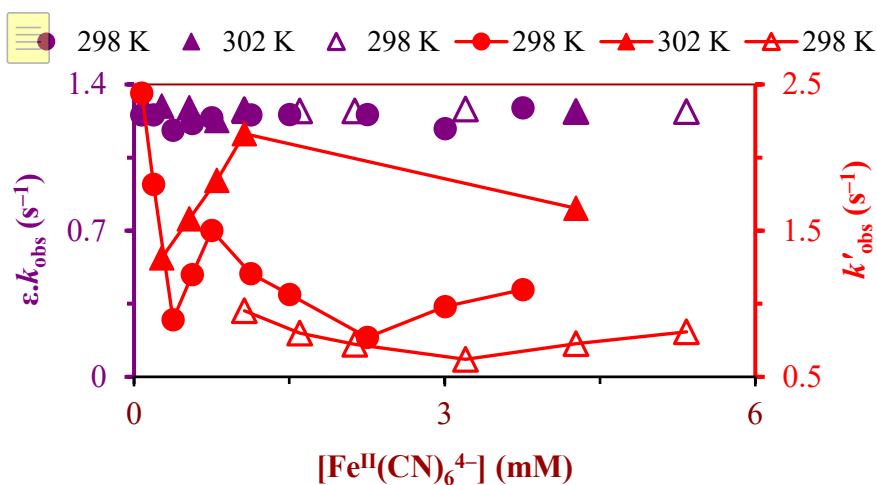


Fig. 3. Effect of the concentration of $[\text{Fe}^{\text{II}}(\text{CN})_6^{4-}]$ on the rate constants " $\epsilon \cdot k_{\text{obs}}$ " and " k'_{obs} " at $298/302 \pm 0.5 \text{ K}$, $[\text{Fe}^{\text{III}}(\text{phen/bpy})_2(\text{CN})_2^+] = 0.08/0.11 \text{ mM}$, and $I = 0.06$ (● phenanthroline and Δ/\blacktriangle bipyridine systems).

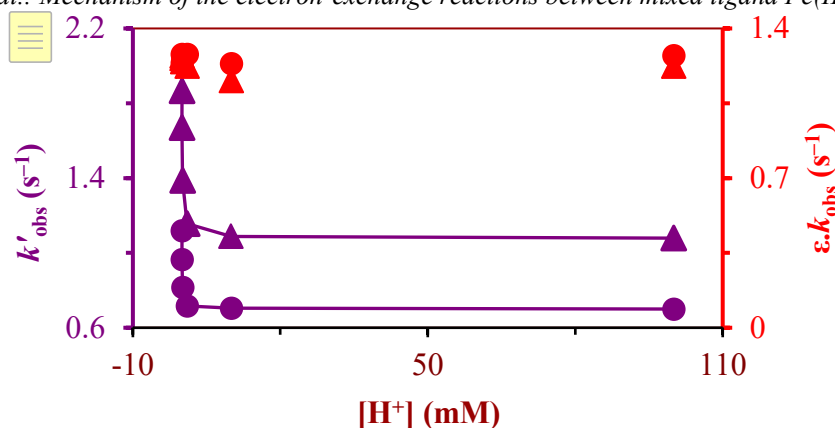


Fig. 4. Effect of the concentration of H^+ on the rate constants “ $\epsilon.k_{obs}$ ” and “ k'_{obs} ” at $298/302 \pm 0.5$ K, $[Fe^{III}(phen/bpy)_2(CN)_2^+] = 0.08/0.11$ mM, $[Fe^{II}(CN)_6^{4-}]_T = 0.8/1.1$ mM, and $I = 0.12$ (● phenanthroline and ▲ bipyridine systems).

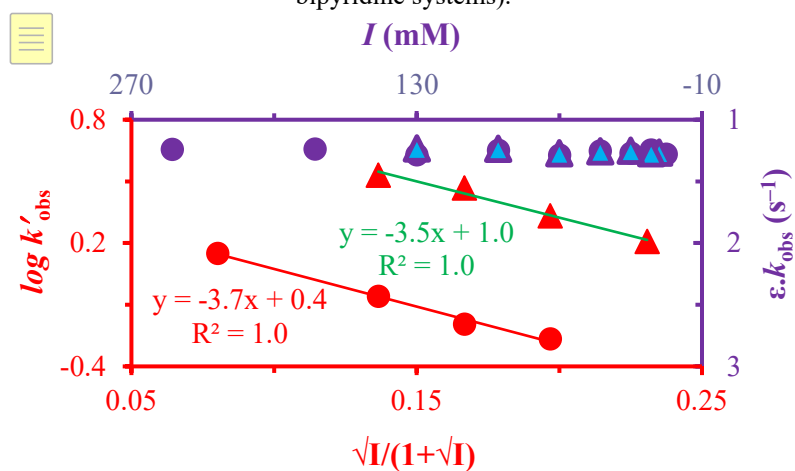


Fig. 5. Effect of the ionic strength on the rate constants “ $\epsilon.k_{obs}$ ” and “ k'_{obs} ” in aqueous medium at $300/302 \pm 0.5$ K, $[Fe^{III}(phen/bpy)_2(CN)_2^+] = 0.08/0.11$ mM, and $[Fe^{II}(CN)_6^{4-}]_T = 0.8/1.1$ mM (● phenanthroline and ▲ bipyridine systems).

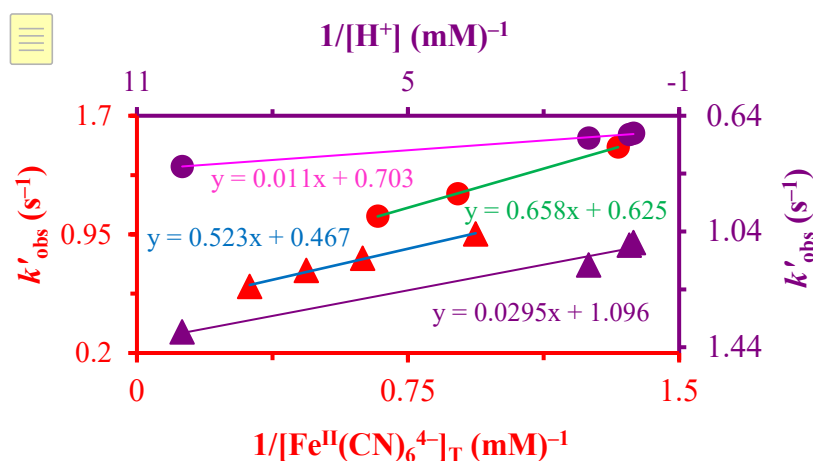


Fig. 6. The plot of k'_{obs} against $1/[Fe^{II}(CN)_6^{4-}]_T$ or $1/[H^+]$ at 298 ± 0.5 K, $[Fe^{III}(phen/bpy)_2(CN)_2^+] = 0.08/0.11$ mM, $[Fe^{II}(CN)_6^{4-}]_T = 0.8/1.1$ mM, and $I = 0.06/0.12$ (● phenanthroline and ▲ bipyridine systems).

We observed a similar effect for each reaction. The results confirmed an initial zeroth and then first order with respect to $[Fe^{II}(CN)_6^{4-}]$ in the first and second phase of the reaction, respectively. The sine-wave pattern corresponding to the increasing concentration of $[Fe^{II}(CN)_6^{4-}]$ shows that the

oxidation of $[Fe^{II}(CN)_6^{4-}]$ may involve its protonated species as well.

Hexacyanoferrate(II) may protonate and form $H[Fe^{II}(CN)_6]^{3-}$, $H_2[Fe^{II}(CN)_6]^{2-}$, $H_3[Fe^{II}(CN)_6]^{-}$, and $H_4[Fe^{II}(CN)_6]$, which depends upon the acidity of the reaction mixture, concentration of $[Fe^{II}(CN)_6]^{4-}$, and the conditions employed [6]. However, there is no evidence of protonation of $[Fe^{III}(phen/bpy)_2(CN)_2]^+$ under the experimental conditions [7]. In order to rectify the outcomes (Fig. 3), we varied the concentration of protons (H^+) in the reaction mixture by adding HNO_3 and determined its effect on the rate constants. The pseudo-first order condition was maintained by keeping $[Fe^{II}(CN)_6^{4-}]$ in a 10-fold excess over $[Fe^{III}(phen/bpy)_2(CN)_2]^+$, and $[H^+]$ in excess over $[Fe^{II}(CN)_6^{4-}]$. We did not observe any change in ' $\epsilon.k_{obs}$ '. This was obvious due to the zeroth order rate law in the first phase of the reaction(s). The value of k'_{obs} decreased gradually with increase in $[H^+]$ and became constant at the higher concentration of proton. Each reaction underwent similar effect (Fig. 4). The results confirm the formation and participation of $H[Fe^{II}(CN)_6]^{3-}$ and $H_2[Fe^{II}(CN)_6]^{2-}$ in the reaction(s) because under the experimental conditions, the existence of $H_3[Fe^{II}(CN)_6]^{-}$ and $H_4[Fe^{II}(CN)_6]$ is not possible. The value of k'_{obs} became constant at the higher concentration of proton because of the constant concentration of the limiting reactant i.e., $[Fe^{II}(CN)_6^{4-}]$. The decrease in the value of k'_{obs} indicates that the rate-determining step involves free $[Fe^{II}(CN)_6^{4-}]$. The findings were confirmed by studying the effect of ionic strength on the rate constants.

Effect of ionic strength on the rate constants

The effect of ionic strength was studied by adding KNO_3 in the reaction mixture and maintaining

$$-\frac{d[Fe(II)]}{dt} = k_1 + k_2 [Fe(III)][Fe(II)]_T + \frac{k_3 [Fe(III)]}{K_2 [H^+][Fe(II)]_T} \dots \dots \dots (4)$$

According to Eqn. (4) the rate should be independent of the reactants in the first phase, and should be of first order with respect to each reactant in the second phase. Our results are in conformity with the rate law (Figs. 2-3). The conversion of free hexacyanoferrate(II) into mono and diprotonated species reduces the concentration of the reactive entity $[Fe^{II}(CN)_6^{4-}]$ that controls the rate-determining step and leads to the decrease in the value of the rate constant upon increasing $[H^+]$ and $[Fe^{II}(CN)_6^{4-}]$, (Figs. 3-4). If we plot k'_{obs} versus the reciprocal of $[H^+]$, and or, $[Fe^{II}(CN)_6^{4-}]$, the straight line should yield a +ve slope, which may be used to

deduce k_3 . Our results are consistent with the rate law (Fig. 6). From our results we calculated the values of the rate constants for each reaction as follows.

- k_1 , k_2 , and k_3 for $[Fe^{III}(phen)_2(CN)_2]^+ + [Fe^{II}(CN)_6]^{4-}$ reaction = $2.1 \times 10^{-5} M s^{-1}$, $1.63 \times 10^3 M^{-1} s^{-1}$, and $2.94 \times 10^{-8} M s^{-1}$ respectively at $298 \pm 0.5 K$
- k_1 , k_2 , and k_3 for $[Fe^{III}(bpy)_2(CN)_2]^+ + [Fe^{II}(CN)_6]^{4-}$ reaction = $1.1 \times 10^{-4} M s^{-1}$ at $302 \pm 0.5 K$, $1.1 \times 10^3 M^{-1} s^{-1}$ at $302 \pm 0.5 K$, $2.34 \times 10^{-8} M s^{-1}$ at $298 \pm 0.5 K$

CONCLUSION

The results of our studies enabled us to propose a common outer-sphere electron-exchange mechanism for the two reactions. Following rate-law was proposed for the reactions:

We concluded from the results that the phen complex (0.80 V, [6]) has a high affinity of electron-exchange with hexacyanoferrate(II) (0.4 V, [6]) than that of bpy complex (0.74 V, [6]).

REFERENCES

- R. Khattak, I. I. Naqvi, M. A. Farrukh, *J. Iran. Chem. Soc.*, **5**, 631 (2008).
- R. Khattak, I. I. Naqvi, S. Summer, M. Sayed, *Arabian Journal of Chemistry*, (2016), DOI: <https://doi.org/10.1016/j.arabjc.2016.05.007>
- R. Khattak, M. Nazir, S. Summer, M. Sayed, A. Minhaz, I. I. Naqvi, *Chemical Papers*, **72**, 883 (2018).
- R. Khattak, M. Nazir, S. Summer, M. Sayed, A. Minhaz, I. I. Naqvi, *Chemical Papers*, **72**, 895 (2018).
- S. Summer, I. I. Naqvi, R. Khattak, S. Gulzar, F. Reyaz, *J. Chem. Soc. Pak.*, **38**, 384 (2016).
- R. Khattak, Department of Chemistry, University of Karachi, Karachi, Pakistan, 2011.
- A. A. Schilt, *J. Am. Chem. Soc.* **82**, 3000 (1960).
- Sh. Zhan. Q. Meng, X. You. G. Wang, P.-J. Zheng, *Polyhedron*, **15**, 2655 (1996).
- T.-H. Lu, H.-Y. Kao, D. I. Wu, K. C. Kong, C. H. Cheng, *Acta Cryst. C* **44**, 1184 (1988).
- W. M. Reiff, R. E. Desimone, *Inorg. Chem.*, **12**, 1793 (1973).
- J. R. Winkler, N. Sutin, *Inorg. Chem.*, **26**, 220 (1987).
- T. Sagij, S. Aoyagui, *Bull. Chem. Soc. Jpn.*, **49**, 1399 (1976).
- M. F. A. Dove, J. G. Hallett, *J. Chem. Soc. A*, 1204 (1969).
- H. Kobayashi. B. V. Agarwala, Y. Kaizu, *Bull. Chem. Soc. Jpn.*, **48**, 465 (1975).
- O. S. Esan. C. O. Aboluwoye. N. A. Oladoja, O. Bankole, *Int. J. Phys. Sci.*, **4**, 764 (2009).
- O. S. Esan, C. O. Aboluwoye, N. A. Oladoja, J. Ige, O. Owoyomi, G. O. Ogunlusi, *Afr. J. Pure Appl. Chem.*, **2**, 92 (2008).
- A. Yamagishi, *Inorg. Chem.*, **21**, 1778 (1982).
- S. Gou, F. Renz, Y. Fukuda, W. Linert, *Inorg. Chim. Acta*, **287**, 95 (1999).
- D. F. Shriver, J. Posner, *J. Am. Chem. Soc.*, **88**, 1672 (1966).
- B. J. C. Lima, F. David, P. G. David, *J. Chem. Soc., Dalton Trans.*, 680 (1974).
- S. Ferrere, *Inorg. Chim. Acta*, **329**, 79 (2002).
- S. Ferrere, *Chem. Mater.*, **12**, 1083 (2000).
- V. Balzani, V. Carassiti, L. Moggi, *Inorg. Chem.*, **3**, 1252 (1964).
- Y. Zimmermann, S. Spange, *New J. Chem.*, **26**, 1179 (2002).
- A. Taha, A. A. T. Ramadan, M. A. El-Behairy, A. I. Ismail, M. M. Mahmoud, *New J. Chem.*, **25**, 1306 (2001).
- R. Lungwitz, M. Friedrich, W. Linert, S. Spange, *New J. Chem.*, **32**, 1493 (2008).
- K. Harada, J. Yuzurihara, Y. Ishii, N. Sato, H. Kambayashi, Y. Fukuda, *Chem. Lett.*, 887 (1995).
- A. Alousy, N. J. Blundell, J. Burgess, C. D. Hubbard, R. V. Eldik, *Transition Met. Chem.*, **27**, 244 (2002).
- M. J. Blandamer, J. Burgess, B. Shraydeh, *J. Chem. Soc., Faraday Trans.*, **89**, 531 (1993).
- A. A. Schilt, *Anal. Chim. Acta*, **26**, 134 (1962).
- A. A. Schilt, J. Bacon, *Anal. Chem.*, **41**, 1669 (1969).
- A. A. Schilt, J. W. Sutherland, *Anal. Chem.*, **36**, 1805 (1964).
- O. O. Soriyan, O. Owoyomi, J. Ige, *Transition Met. Chem.*, **33**, 121 (2008).
- P. Cokie, J. E. Erman, *Biochim. Biophys. Acta*, **913**, 257 (1987).
- O. O. Soriyan, J. Ige, A. O. Fadiran, O. Owoyomi, *J. Applied Sci.*, **5**, 773 (2005).
- F. Sánchez, M. L. Moyá, A. Rodríguez, R. Jiménez, C. Gómez-Herrera, C. Yánes, P. López-Cornejo, *Langmuir*, **13**, 3084 (1997).
- J. Benko, O. Vollarová, J. Burgess, P. López, *Transition Met. Chem.*, **25**, 674 (2000).
- J. Benko, J. Burgess, P. L. Cornejo, O. Vollarová, *Croatica Chemica Acta (CCACAA)*, **74**, 607 (2001).
- M. J. Blandamer, J. Burgess, N. V. Reed, P. Wellings, *J. Inorg. Nucl. Chem.*, **43**, 3245 (1981).
- J. Blandamer, J. Burgess, *J.C.S. Chem. Comm.*, **963**, (1978).
- M. S. Matamoros-Fontenla, P. López-Cornejo, P. Pérez, R. Prado-Gotor, R. D. L. Vega, M. L. Moya, F. Sanchez, *New J. Chem.*, **39** (1998).
- O. Horváth, K. L. Stevenson, *J. Photochem. Photobiol. A: Chem.*, **120**, 185 (1999).
- J. P. Birk, S. G. Kozub, *Inorg. Chem.*, **17**, 1186 (1978).
- E. Pelizzetti, E. Mentasti, E. Pramauro, *Inorg. Chem.*, **17**, 1181 (1978).
- H. D. Takagi, N. Kagayama, M. Matsumoto, T. Tarumi, S. Funahashi, *J. Mol. Liq.*, **65-66**, 277 (1995).
- M. Matsumoto, T. Tarumi, K.-I. Sugimoto, N. Kagayama, S. Funahashi, H. D. Takagi, *Inorg. Chim. Acta*, **255**, 81 (1997).
- R. Blake, K. J. White, E. A. Shute, *J. Biol. Chem.*, **266**, 19203 (1991).
- T. Saji. T. Yamada, S. Aoyagui, *Bull. Chem. Soc. Jpn.*, **48**, 1641 (1975).
- P. C. Wilkins, H. K. Jacobs, M. D. Johnson, A. S. Gopalan, *Inorg. Chem.*, **43**, 7877 (2004).
- X. Wang, D. M. Stanbury, *J. Phys. Chem. A*, **108**, 7637 (2004).
- X. Wang, D. M. Stanbury, *Inorg. Chem.*, **45**, 3415 (2006).
- X. Wang, D. M. Stanbury, *Inorg. Chem.*, **47**, 1224 (2008).
- D. M. Kardel, H. B. Dunford, S. Alexandre, *Eur. J. Biochem.*, **194**, 259 (1990).
- A.-M. Lambeir, H. B. Dunford, M. A. Pickard, *Eur. J. Biochem.*, **163**, 123 (1987).
- H. Boardman, *J. Am. Chem. Soc.*, **75**, 4268 (1953).

- Rozina Khattak et al.: Mechanism of the electron-exchange reactions between mixed ligand Fe(III) complexes and ...*
56. B. B. Hasinoff, H. B. Dunford, *Biochemistry*, **9**, 4930 (1970).
57. M. L. Cotton, H. B. Dunford, *Can. J. Chem.*, **51**, 582 (1973).
58. G. Rabai, I. R. Epstein, *Inorg. Chem.*, **28** 732 (1989).
59. A. A. Abdel-Khalek, *Transition Met. Chem.*, **11**, 67 (1986).
60. G. Rabai, K. Kustin, I. R. Epstein, *J. Am. Chem. Soc.*, **111**, 8271 (1989).
61. M. A. Rawoof, J. R. Sutter, *J. Phys. Chem.*, **71**, 2767 (1967).
62. A. E. M. Abdel-Hady, *Transition Met. Chem.*, **33**, 887 (2008).

МЕХАНИЗЪМ НА РЕАКЦИИТЕ НА ОБМЕН НА ЕЛЕКТРОНИ МЕЖДУ СМЕСЕНИ ЛИГАНДНИ КОМПЛЕКСИ НА Fe(III) И ЦИАНО КОМПЛЕКС НА Fe(II)

Розина Хатак^{1,2*}, Мухамад Суфаид Хан³, Ифтихар Имам Накви²

¹ Департамент по химия, Женски университет Шахед Беназир Бхудо, Пешавар, Пакистан

² Департамент по химия, Университет на Карачи, Карачи-75270, Пакистан

³ Департамент по физикохимия, Институт по химия, Държавен университет Паулиста(UNESP)–Араракуара 14800-900, СП, Бразилия

Постъпила на 1 юли, 2018 г.; приета на 1 октомври, 2018 г.

(Резюме)

В статията са изследвани реакциите на смесени лигандни комплекси на Fe(III) с цианиденлиганд. Синтезирани са смесени лигандни комплекси на Fe(III) с лиганди диимин и цианид, характеризиращи се с октаедрична геометрия и висока стабилност. За целта са модифицирани известни процедури. Синтезираните комплекси, $\text{Fe}^{\text{III}}(\text{фенантролин/бипиридил})_2(\text{CN})_2^+$ са редуцирани от хексациано комплекса на Fe(II), който е известен с високата си стабилност и октаедрична геометрия. Редукцията се извършва във водна среда при постоянна йонна сила = 0.06. Напредването на реакциите се проследява спектрофотометрично чрез измерване на нарастването на абсорбцията с времето, т.е. образуването на $[\text{Fe}^{\text{II}}(\text{фенантролин/бипиридил})_2(\text{CN})_2]$. Установено е, че редукцията на смесените лигандни комплекси на Fe(III) става на два етапа. Първият етап на редукция на Fe(III) комплекса до неутрален Fe(II) комплекс е с кинетика от нулев порядък. Вторият етап е скоростопределящ или бавен етап при редукцията на комплексите и електронният обмен е с обща кинетика от втори порядък. За прецизиране на резултатите и разграничаване на формите, участващи в скоростопределящия етап (бавен етап) и тези, участващи в бързия етап е изучено влиянието на протоните и йонната сила върху скоростните константи във водна среда. Предложен е външно-сферен механизъм на електронния обмен между комплексите на Fe(III) and Fe(II).

Possible reaction pathways of the acetamiprid molecule according to the DFT calculation method

B. Eren¹, Y. Yalcin Gurkan^{2*}

¹Namik Kemal University, Faculty of Agriculture, Tekirdag, Turkey

²Namik Kemal University, Department of Chemistry, Tekirdag, Turkey

Received July 1, 2018; Accepted October 1, 2018

Acetamiprid, the major active ingredient of some pesticides, is a subclass of the neonicotinoid group and is used especially against whitefly, aphididae, leaf bugs, potato bugs which affect products such as cotton, tobacco, potato, tomato, nut, citrus, planted in greenhouses and fields. Quantum chemical calculations of density functional theory (DFT) were used to investigate the structural and physical characteristics of acetamiprid. The analysis was made on the probable reaction path of acetamiprid molecule with OH radicals. The calculation of the optimized geometry and the geometric optimization for determination of the lowest energy status were made by the Gauss View 5 and the Gaussian 09 program. Activation energy for the probable reaction paths was calculated and its most stable states from the thermodynamic perspective were determined for the different phases. The aim of this study is to estimate the degradation mechanism of acetamiprid molecule in gaseous phase, in ethanol and water as polar solvents, and in chloroform as a partially polar solvent, all of which were analysed through the conductor-like screening solvation model (COSMO) as the solvation model. The probable reaction path of the activation energy was calculated, and its most stable state in the thermodynamic frame was determined for these phases.

Keywords: Acetamiprid, DFT, Pesticide

INTRODUCTION

Recently, chemical treatments are widely used for high fertility in agricultural fields. These chemicals are used for the combat with insects, fungi, flies, disease agents, and weeds. Pesticides are beneficial when used at proper amounts and time whereas their improper use in terms of excess and improper time results in problems in human health, as well as in the increase of environmental pollution beside its negative effect on other livings. Pesticides are known to be highly poisonous but still are widely used in great amounts in agriculture. Thus, it is obvious that pesticides are extremely dangerous in both use and production.

In developing countries, mortality caused by pesticide poisoning, suicide attempts due to the easy accessibility of pesticides on the market, the occurrence of leucemias, urinary bladder or pancreatic cancers, as well as lymphomas due to pesticides have been reported widely in researches carried out recently. Moreover, it has also been reported that there has been an increase in congenital disorders in children of parents exposed to pesticides. The use of the same pesticides in great amounts throughout many years caused many pest populations to desensitise and become resistant to these chemicals. Therefore, it is essential that insecticides be renewed continuously. As a result, the use of organochlorine and organophosphorous

insecticides has been reduced in time, pyrethroides have been used as an alternative, and later the use of neonicotinoids has progressively increased [1-8].

There are many ways for organic contaminants to enter the environment. The excessive use of insecticides including organic contaminants leads to residuals of these compounds at high levels. The cycle starts with soil, ground and surface waters, then with fruits and vegetables regardless of their being fresh or processed, and finally reaches the human beings through consumption [9,10].

Acetamiprid, being an odorless neonicotinoid insecticide, is an organic compound with the chemical formula $C_{10}H_{11}ClN_4$. As stated in many studies, organic contaminants are known to exist in water at very low concentrations. Thus, it is crucial that drinking water be purified from the organic contaminants. Solar light on earth provides natural purification of water systems such as pools, lakes, creeks, and rivers. Large organic molecules are degraded into smaller basic molecules through sunbeams, and finally form CO_2 , H_2O , NH_4^+ and other small molecules [11-13].

OH radical acts like an electrophile in its reaction with any organic molecule and therefore readily attacks the unsaturated bonds, while O radical is a nucleophile, and thus does not attack these bonds. If there is an aliphatic side chain readily bound to an aromatic molecule, radical H attacks O, whereas OH radical preferentially attacks

* To whom all correspondence should be sent:

E-mail: yyalcin@nku.edu.tr

the aromatic ring, which can result in the formation of various products when pH reaches a range in which O radical is the reactant rather than OH radical. Hydroxyl radical, known to be the most reactive type in biological systems, goes into reaction with every biomolecule it confronts, including water. Potentially, every biomolecule is a hydroxyl radical scavenger at different speeds. Aromatic compounds are good detectors since they hydroxylate. In addition, the position of attack to the ring depends on the electron withdrawal and the repulsion of previously present substituents. The attack of any hydroxyl radical to an aromatic compound results in the formation of a hydroxylated product [13-16].

This study was conducted in order to find out whether this molecule, being named D molecule in our study, would be fragmented in the nature under the formation of small molecules. The kinetics of the degradation reaction path of D molecule with OH radical was theoretically analysed through the density functional theory (DFT) method.

COMPUTATIONAL SET-UP AND METHODOLOGY

Computational models

The models of the molecules were formed by the use of the mean bond distances and the geometric parameters of the closed ring. Tetrahedral angles were used for the sp^3 -hybridized carbon and oxygen atoms and 120° for the sp^2 -hybridized carbon atoms was used in the computational modelling. The aromatic ring was left planar, excluding the position of attack. Due to the change in the hybridization state of the carbon at the addition centre from sp^2 to sp^3 , the attacking $\bullet OH$ was presumed to create a tetrahedral angle with the C-H bond [17].

Molecular orbital calculations

In photocatalytic degradation reactions of the D molecule it is possible that products more harmful than those in the original material could be formed. Therefore, before experimentally realizing a photocatalytic degradation reaction, it is essential to know the nature of the primary intermediate products. The most reliable and accurate information is gathered through calculations realized with quantum mechanical methods. Thus, since the yield produced was the same, photocatalytic degradation reactions of the D molecule and its hydroxy derivatives are based on the direct reaction of these molecules with $\bullet OH$.

With this aim, the kinetics of the reactions of the D molecule with $\bullet OH$ were theoretically analysed.

The study was initiated with the D molecule which was then exposed to reaction with $\bullet OH$ and the reaction yields were modelled in different phases. Experimental results in the scientific literature showed that $\bullet OH$ detaches a hydrogen atom from saturated hydrocarbons, and $\bullet OH$ is added to unsaturated hydrocarbons and materials with this structure [18,19]. For this purpose, all reaction paths for the analysed reactions were determined. For these fragmentation paths, molecular orbital calculations of the D molecule were performed with the density functional theory (DFT), their molecular orbital calculations were realized and their geometries optimized. In order to explore the conformational landscape of the molecules, a potential energy surface scan was performed along the torsional coordinates mentioned above in a relaxed manner. The scan was calculated using the B3LYP/6-31G* method [20].

Kinetic data treatment

The aim of this study was to develop a model providing the outcome of the photocatalytic degradation reactions. The vibration frequencies, the thermodynamic and electronic features of every structure were calculated using the obtained optimum geometric parameters.

Subsequently, based on the quantum mechanical calculation results, the rate constant and activation energy (E_a) of every reaction was calculated at a temperature of $25^\circ C$. In order to enable the calculation of the rate constant, it is necessary initially to calculate the partition function of the activated complex. To realize this calculation, it is essential to know the geometry of the complex and the moments of inertia. In addition, E_a should be known in order to determine the rate constant. The activation energy, as the vibration frequency, can only be calculated quantum mechanically. The optimized geometric structures were drawn *via* GaussView 5, and the calculations were realised within the Gaussian 09 programme packet [20].

Methodology

The investigated reaction system was composed of $\bullet OH$, which are open-shell species. It is known that open-shell molecules cause severe problems in quantum mechanical calculations. The self-consistent field method (SCF) calculation will proceed for an open-shell case in the same way as for a closed-shell case. However, since two sets of equations have to be dealt with, at each iteration, the program has to consider, either simultaneously or successively, the closed-shell and the open-shell equations. In this respect, the computational burden could be two-times larger for an open shell than

that for a closed-shell. Another point raised in connection with the optimization of the SCF process for open-shell molecules is the relative intricacy of the sequence of calculations for the closed-shell Hamiltonian and the open-shell Hamiltonian [21].

DFT methods, taking the electron correlation into account, use the precise electron density to calculate molecular properties and energies. Spin contamination does not affect them and hence, for calculations involving open-shell systems, they become favourable. DFT calculations were made by the hybrid B3LYP functional combining the HF and Becke exchange terms with the Lee–Yang–Parr correlation functional. It is essential in such calculations to choose the basis set. Based upon the obtained results, optimization in the current study was carried out at the B3LYP/6-31G(d) level [13,20].

Solvent effect model

The energetics of the degradation reactions of all organic compounds are affected by water molecules in aqueous media. In addition, geometry relaxation on the solutes is induced by H₂O. Solvation is based on the affinity between molecules. In order to be able for a solvent to solve a substance, affinity between the solvent and molecules of the solute has to be greater than the affinity between the solvent and the own molecules of the solute. Generally, solvation occurs in situations where solvent and solute have the same construct. If a molecule consists of different atoms, the affinity of each atom towards electrons is different. As a result, there is an electron surplus; therefore partial negative load in part of the molecule, and there is lack of electrons; therefore partial positive load in the remaining part of the molecule. These kinds of molecules are called polar molecules. If the conditions mentioned above do not exist; in other words, they do not reveal any polarization, these are called apolar molecules [22].

C-H and C-C bonds of the ethanol molecule are apolar, whereas its O-H and C-O bonds are polar. Thus, since one end reveals polar, and the other reveals apolar characteristics, ethanol is a good solvent for both polar and apolar substances. Chloroform is a heavy, colourless liquid solvent that is slowly oxidised under the influence of light, and can evaporate easily. Beside being a partially polar solvent, chloroform, or trichloromethane was chosen to be the solvent for our molecule because of its partial negative loaded ends of the chlorine atoms.

On the other hand, it was indicated in previous studies that there is an insignificant effect of

geometry changes on the energy of the solute for both open- and closed-shell structures [23].

In this study, DFT/B3LYP/6-31+G(d) calculations were realised for the optimized structures of the reactants, the pre-reactive and the transition state complexes and the product radicals, by using the COSMO (conductor-like screening solvation model) as the solvation method in order to consider the effect of H₂O on the energetics and the kinetics of D molecule reactions with •OH. Water at 25 °C was used as a solvent with dielectric constant, $\epsilon = 78.39.28$

The COSMO method explains the solvent reaction field through apparent polarization charges distributed on the cavity surface, determined by presuming that the total electrostatic potential cancels out at the surface. The solvation in polar liquids can be described by this condition. Therefore, this method was chosen to be appropriate for the present study [24].

RESULTS AND DISCUSSION

As seen from different angles in an optimized form, lincomycin molecule (D) has a conformation far from a planar structure in terms of geometric shape (Fig. 1).

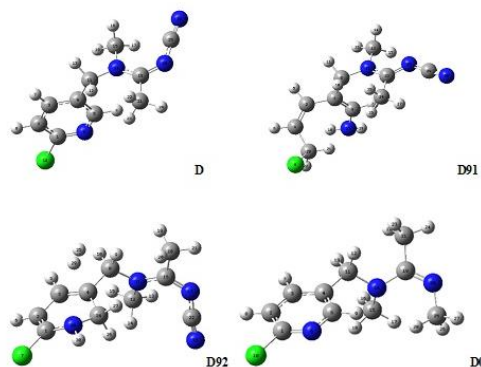


Figure 1. Optimized figures of the D molecule and its three stable fragments D91, D92, and D0. (Grey, C; green, Cl; white, H; blue, N)

Reaction centres can be explained through Mulliken charge distribution of the molecule. According to the data in Table 1, the degradation reaction occurred due to the electronegativity of Cl, and N.

When Mulliken charges of the D molecule are analysed, N₆, N₁₅, N₂₀ and N₂₆ are determined to be atoms with high electronegativity. Various fractions were obtained through fragmentation from bonds close to these atoms.

The molecule was analysed whether stable fractions found through the analysis of bond lengths and angles shown in Table 2 were compatible with thermodynamic values found in Table 3. In addition

to predicting that the fragmentation occurs from the electronegative atoms in molecules, bond lengths, bond lengths starting from long to short ones, bond angles and by taking into consideration the molecules are divided into fractions by stable-close ring.

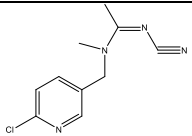
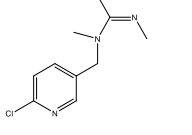
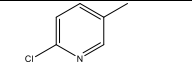
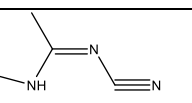
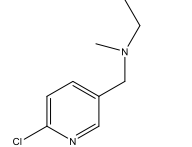
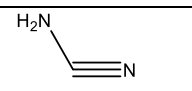
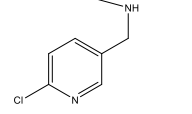
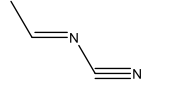
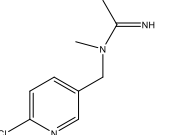
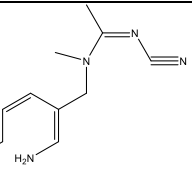
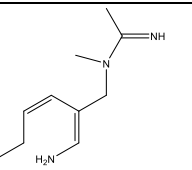
Table 1. Mulliken loads of the studied fragments

D		D0		D1		D2		D3	
C ₂	-0.122839	C ₂	-0.123041	C ₂	-0.122975	N ₁	-0.575866	C ₂	-0.224276
C ₃	-0.141567	C ₃	-0.148100	C ₃	-0.139127	C ₂	-0.316119	C ₃	-0.159563
C ₅	-0.004049	N ₆	-0.405381	C ₅	-0.015604	N ₇	-0.503063	C ₄	-0.062557
N ₆	-0.401661	Cl ₁₀	-0.009623	N ₆	-0.403007	C ₈	-0.535133	N ₆	-0.504356
Cl ₁₀	0.005156	C ₁₁	-0.212164	Cl ₁₀	-0.015134	N ₁₃	-0.499836	Cl ₁₀	0.002413
C ₁₁	-0.239135	N ₁₄	-0.426162	C ₁₁	-0.535898			C ₁₁	-0.129139
N ₁₅	-0.403753	C ₁₅	-0.317742					N ₁₄	-0.569425
C ₁₅	-0.342771	N ₂₀	-0.405623					C ₁₅	-0.294353
N ₂₀	-0.504061	C ₂₁	-0.510021					C ₁₉	-0.481934
C ₂₁	-0.536110	C ₂₅	-0.335521					C ₂₃	-0.114721
N ₂₆	-0.493369								
D4		D5		D6		D7		D8	
N ₂	-0.446855	C ₂	-0.123412	N ₂	-0.394345	C ₂	-0.122372	N ₂	-0.358128
N ₃	-0.752971	C ₃	-0.149817	C ₃	-0.506851	C ₃	-0.149256		
		N ₆	-0.406789	N ₈	-0.452780	N ₆	-0.404164		
		Cl ₁₀	-0.017616			Cl ₁₀	-0.007115		
		C ₁₁	-0.213183			C ₁₁	-0.222627		
		N ₁₄	-0.534391			N ₁₄	-0.404996		
		C ₁₅	-0.310549			C ₁₅	-0.340831		
						N ₂₀	-0.628160		
						C ₂₁	-0.522725		
D91		D92		D10		D11		D12	
C ₁	-0.158579	C ₂	-0.277066	C ₂	-0.123495	C ₂	-0.136641	N ₂	-0.450958
C ₂	-0.211035	C ₃	-0.170426	C ₃	-0.148966	C ₃	-0.150912	C ₃	-0.511351
C ₃	-0.094373	C ₄	-0.002703	N ₆	-0.406735	N ₆	-0.403561	N ₈	-0.467603
Cl ₈	-0.110206	Cl ₇	0.017264	Cl ₁₀	-0.017595	C ₁₀	-0.242085	C ₉	-0.522648
C ₉	-0.117457	C ₈	-0.180448	C ₁₁	-0.210702	N ₁₃	-0.399893		
N ₁₂	-0.671279	N ₁₁	-0.661729	N ₁₄	-0.715092	C ₁₄	-0.341379		
C ₁₃	-0.276052	C ₁₂	-0.310825			N ₁₉	-0.507336		
N ₁₇	-0.869382	N ₁₇	-0.661817			C ₂₀	-0.536669		
C ₂₀	-0.417418	C ₁₈	-0.566280			N ₂₅	-0.496034		
C ₂₄	-0.589520	N ₂₃	-0.494814						
N ₂₈	-0.683934	C ₂₄	-0.113899						
N ₃₀	-0.489022	N ₂₈	-0.750932						

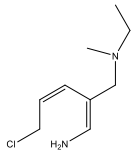
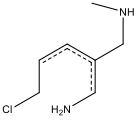
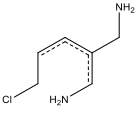
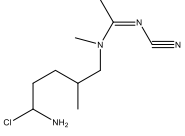
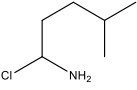
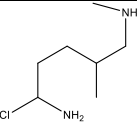
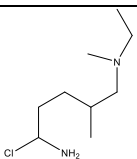
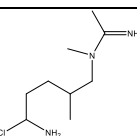
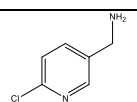
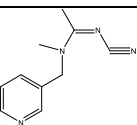
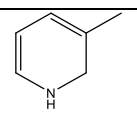
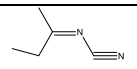
Table 2. Bond lengths and angles of stable fragments of the D molecule.

D	Bond Length	D91	Bond Length	D92	Bond Length	D0	Bond Length
C ₁ Cl ₁₀	1.75997	C ₂₉ N ₃₀	1.14137	C ₁₆ N ₁₇	1.28635	C ₁₉ N ₂₀	1.27758
C ₁ N ₅	1.31877	C ₂₉ N ₂₈	1.33081	C ₁₆ N ₁₁	1.34890	C ₁₉ N ₁₄	1.42779
C ₅ N ₅	1.34130	C ₂₃ N ₂₈	1.28942	C ₈ N ₁₁	1.46565	C ₁₅ N ₂₄	1.46504
C ₁₁ N ₁₄	1.46336	C ₂₃ N ₁₂	1.34220	C ₁₂ N ₁₁	1.46211	C ₂₅ N ₂₀	1.45043
C ₁₉ N ₁₄	1.36653	C ₁₃ N ₁₂	1.45812	C ₂₂ N ₁₇	1.33058	C ₁₁ N ₁₄	1.46205
C ₁₉ N ₂₀	1.30326	C ₉ N ₁₂	1.45292	C ₂₂ N ₂₃	1.14142	C ₁₅ N ₁₄	1.46504
C ₂₅ N ₂₀	1.32618	C ₂₀ Cl ₈	1.80507	C ₁ N ₂₈	1.37615	C ₅ N ₆	1.33903
C ₂₅ N ₂₆	1.17200	C ₄ N ₁₇	1.38821	C ₂₄ N ₂₈	1.45504	C ₁ N ₆	1.32123
D	Bond Angle	D91	Bond Angle	D92	Bond Angle	D0	Bond Angle
C ₁ N ₆ C ₅	117.47936	C ₂₃ N ₂₈ C ₂₉	120.04265	C ₁₆ N ₁₇ C ₂₂	125.39757	C ₁₉ N ₂₀ C ₂₅	121.35950
C ₁₁ N ₁₄ C ₁₉	122.32345	C ₁₃ N ₁₂ C ₂₃	118.76386	N ₁₁ C ₁₆ N ₁₇	127.56093	N ₁₄ C ₁₉ N ₂₀	124.52572
C ₁₁ N ₁₄ C ₁₅	114.47495	N ₁₂ C ₂₃ N ₂₈	117.29458	C ₈ N ₁₁ C ₁₆	123.13607	C ₁₉ N ₁₄ C ₁₅	116.24421
C ₁₅ N ₁₄ C ₁₉	122.97978	C ₉ N ₁₂ C ₁₃	117.19305	C ₈ N ₁₁ C ₁₂	114.66496	C ₁₁ N ₁₅ C ₁₄	112.54777
C ₁₉ N ₂₀ C ₂₅	128.05325	C ₉ N ₁₂ C ₂₃	123.92611	C ₁₂ N ₁₁ C ₁₆	122.15344	C ₁ N ₆ C ₅	117.32205

B. Eren, Y. Yalcin Gurkan: Possible reaction pathways of the acetamiprid molecule according to the DFT ...
Table 3. Gas phase of various fractions of the D molecule, energy, enthalpy, and Gibbs Free Energy electrochemical values within ethanol, water and chloroform solvent

D	Ethanol	Chloroform	Gas	Water	Molecule
$\Delta E(\text{Au})$	-1066.661533	-1066.657084	-1066.641435	-1066.662293	
$\Delta H(\text{Au})$	-1066.660589	-1066.656140	-1066.640491	-1066.661348	
$\Delta G(\text{Au})$	-1066.719894	-1066.715610	-1066.700286	-1066.720627	
D0	-1013.681701 -1013.680757 -1013.740041	-1013.679679 -1013.678735 -1013.738112	-1013.671802 -1013.670857 -1013.729670	-1013.682075 -1013.681131 -1013.740436	
D1	-747.093774 -747.092829 -747.133275	-747.092519 -747.091574 -747.132045	-747.087855 -747.086911 -747.127422		
D2	-320.766542 -320.765598 -320.808013	-320.762939 -320.761995 -320.804441	-320.750306 -320.749362 -320.793758	-320.767160 -320.766216 -320.808819	
D3	-916.515967 -916.515023 -916.566908	-916.514308 -916.513364 -916.565271	-916.508022 -916.507077 -916.558717	-916.516245 -916.515301 -916.567178	
D4	-148.754966 -148.754022 -148.782103	-148.752353 -148.751409 -148.779497	-148.742299 -148.741355 -148.769488	-148.755400 -148.754456 -148.782536	
D5	-841.694576 -841.693632 -841.740179	-841.692942 -841.691998 -841.738498	-841.686802 -841.685858 -841.732216	-841.694850 -841.693906 -841.740459	
D6	-226.126057 -226.125113 -226.159532	-226.123925 -226.122981 -226.157407	-226.116154 -226.115210 -226.149667	-226.126418 -226.125473 -226.159892	
D7	-974.414056 -974.413112 -974.470948	-974.411268 -974.410323 -974.465849	-974.401101 -974.400157 -974.455140	-974.414487 -974.413542 -974.469627	
D8	-93.410013 -93.409069 -93.431904	-93.408692 -93.407748 -93.430587	-93.403610 -93.402666 -93.425523	-93.410232 -93.409288 -93.432123	
D91	-1064.369962 -1064.369018 -1064.432278		-1064.353352 -1064.352407 -1064.415887	-1064.370790 -1064.369846 -1064.433133	
D91a	-972.625517 -972.624573 -972.685408	-972.622686 -972.621742 -972.680922	-972.617066 -972.616122 -972.674740	-972.626051 -972.625107 -972.685981	

B. Eren, Y. Yalcin Gurkan: Possible reaction pathways of the acetamidiprid molecule according to the DFT ...

D91b	-918.745749 -918.744805 -918.802374	-918.742527 -918.741582 -918.798706	-918.746047 -918.745103 -918.802688		
D91c	-840.747044 -840.746100 -840.797646	-840.741632 -840.740687 -840.790546			
D91d	-801.738985 -801.738041 -801.787067	-801.749466 -801.748522 -801.796536	-801.746628 -801.745684 -801.792172		
D92	-1064.361834 -1064.360890 -1064.424135	-1064.317001 -1064.316057 -1064.383316	-1064.362618 -1064.361673 -1064.424920		
D92a		-746.750810 -746.749866 -746.794447	-746.753241 -746.752297 -746.797424		
D92b	-840.597931 -840.596987 -840.653717	-840.724588 -840.723643 -840.778518	-840.667576 -840.666632 -840.713670	-840.599520 -840.598576 -840.654981	
D92c	-918.748967 -918.748023 -918.805843	-918.724593 -918.723649 -918.785350	-918.667209 -918.666265 -918.719474	-918.749241 -918.748297 -918.806614	
D92d	-972.566402 -972.565458 -972.620443	-972.598733 -972.597788 -972.661499	-972.534998 -972.534053 -972.589067	-972.567422 -972.566478 -972.621462	
D10	-802.416626 -802.415682 -802.459099	-802.414736 -802.413792 -802.457004	-802.407640 -802.406696 -802.449665	-802.420704 -802.419760 -802.462825	
D11	-607.035785 -607.034841 -607.091209	-607.054447 -607.053503 -607.109709	-607.046025 -607.045081 -607.101890	-607.055139 -607.054195 -607.110378	
D11a	-287.845853 -287.844909 -287.886376	-287.817814 -287.816870 -287.863549	-287.813317 -287.812373 -287.858430		
D12			-265.411123 -265.410178 -265.448924		

For each fraction, physicochemical calculations in gaseous phase, ethanol and water solvents which are polar, as well as in chloroform revealing partial polarity, were performed. ΔE energy, ΔH enthalpy

and ΔG Gibbs free energy values given in Table 3 are stated for each fragment separately.

Three probable stable fragmentation pathways of the D molecule are given in Figures 2, 3 and 4.

CONCLUSIONS

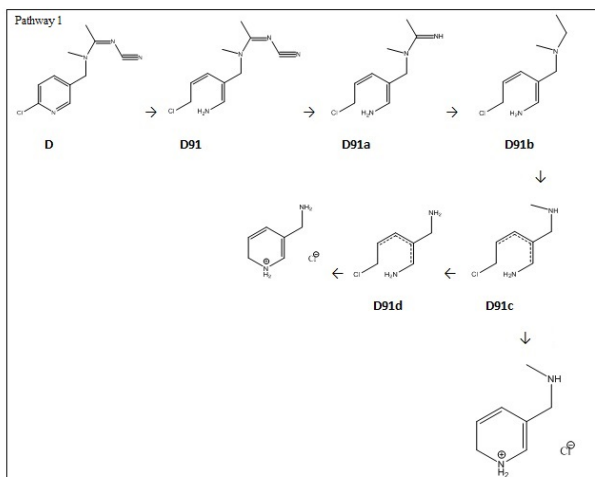


Figure 2. The assumed 1st fragmentation path of the most stable D91 fragment of the D molecule.

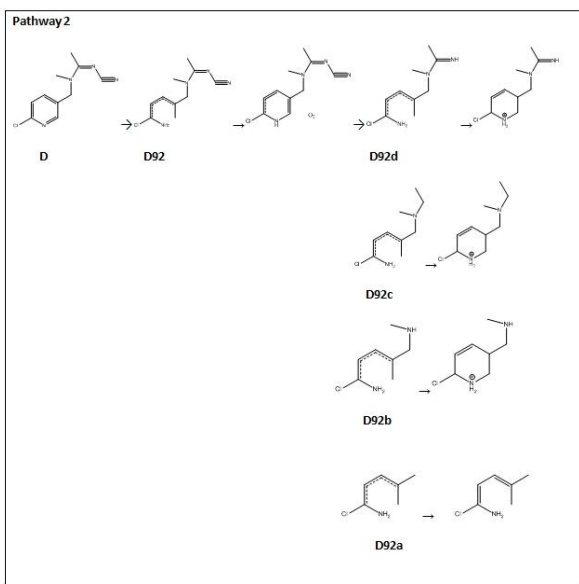


Figure 3. The assumed 2nd fragmentation path of the stable D92 fragment of the D molecule.

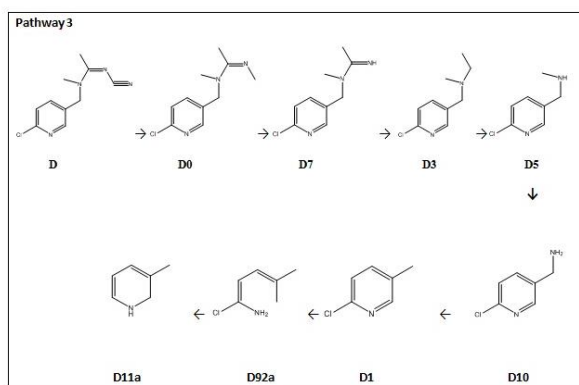


Figure 4. The assumed 3rd fragmentation path of the stable D0 fragment of the D molecule.

When ΔG Gibbs free energy values were analysed, it was seen that ΔG value of each fragmentation was negative. These results show that fragmentation occurred spontaneously. Blank parts in Table 3 indicate that fragments either were not dissolved in those solvents or became deformed. Fragments with the lowest electrochemical energy, in other words, the most stable fragments are D91 with -1064.369962 Au, D92 with -1064.361834 Au, D0 with -1013.681701 Au, and D7 with -974.414056 Au, respectively.

D91 and D92 fragments are formed through the opening of right and left bonds of N atom bound to the closed ring. As known, closed rings do not fragment voluntarily due to their being stable. In our study, more investigation was conducted to find out whether there will be closure in the further phases of these molecules due to their having the lowest energy. D92 fragment closed immediately while there was no closure observed in the D91 fragment.

Three probable stable fragmentation pathways of the D molecule are given in Figures 2, 3 and 4. In Pathway 1, fragmentation process was conducted until the ring was closed. In Pathway 2, fragmentation process proceeded from different electronegative parts of the molecule, although the ring was closed at the first fragmentation, and thermochemical values in each fragmentation were calculated. When D0 fragment is analysed as the third most stable path, and the next fragment is D7, the latter is not mentioned once again as a different fragmentation path.

When energy, enthalpy and Gibbs free energy values of each fragment of the D molecule in Table 3 were analysed regarding the studied solvents, it was observed that solvation took place in water, ethanol and chloroform. Due to water being the solvent, it is the most appropriate one. When the three probable fragmentation pathways were analysed, it was seen that the D molecule was fragmented in aqueous media up to its smallest molecules.

Acknowledgements: The authors greatly appreciate Namik Kemal University Research Foundation for financial support. Project number: NKUBAP.01.GA.18.164 The authors declare that there is no conflict of interests regarding the publication of this paper.

REFERENCES

1. A. Blair, S. H. Zahm, *Environ Health Perspect.*, **103**, 205 (1995).

B. Eren, Y. Yalcin Gurkan: Possible reaction pathways of the acetamidiprid molecule according to the DFT ...

- L. M. Brown, A. Blair, R. Gibson, G. D. Everett, K. P. Cantor, L. M. Schuman, L. F. Burmeister, S. F. Van Lier, F. Dick, *Cancer Res.*, **50**, 6585 (1990).
- B. C-H. Chiu, D. D. Weisenburger S. H. Zahm, K. P. Cantor, S. M. Gapstur, F. Holmes, L. F. Burmeister, A. Blair, *Cancer Epidemiol. Biomarkers Prev.*, **13**(4), 525 (2004).
- M. Elestondd, L. Karalliedde, N. Buckley, R. Fernando, G. Hutchinson, G. Isbister, F. Konradsen, D. Murray, J. C. Piola, N. Senanayake, R. Sheriff, S. Singh, S. B. Siwach, L. Smit, *The Lancet*, **360**, 1163 (2002).
- N. V. Kovganko, Zh. N. Kashkan, *Russian J. of Organic Chem.*, **40**(12), 1709 (2004).
- J. F. Viel, B. Chalier, *Environ. Med.*, **52**(9), 587 (1995).
- T. Zheng, S. H. Zahm, K. P. Cantor, D. D. Weisenburger, Y. Zhang, A. Blair, *JOEM*, **43**, 641 (2001).
- B. T. Ji, D. T. Silverman, P.A. Stewart, A. Blair, G. M. Swanson, D. Baris, R. S. Greenberg, R. B. Hayes, L. M. Brown, K. D. Lillemoe, J. B. Schoenberg, L. M. Pottern, A. G. Schwartz, R. N. Hoover, *Am. J. Ind. Med.*, **39**(1), 92 (2001).
- D. Sharma, A. Nagpal, Y. B. Pakade, and J.K. Katnoria, *J. Environ. Res. Develop.*, **82**(4), 1077 (2010).
- E. Taillebois, Z. Alamiddine, C. Brazier, J. Graton, A.D. Laurent, S.H. Thany, J-Y. L. Questel, *BMC*, **23**, 1540 (2015).
- K. Verschueren, *Handbook of Environmental Data on Organic Chemicals*, 2nd ed., Wiley, New York, 1996.
- R. W. Matthews, D. Ollis, H. Al-Ekabi, Elsevier, New York, 1993, 121.
- B. Eren, Y. Yalcin Gurkan, *JSCS*, **82**(3), 277 (2017).
- V. G. Buxton, L. C. Greenstock, P. W. Helman, A. B. Ross, *Journal of Physical and Chemical Reference Data*, **17**, 513 (1988).
- M. Anbar, P. Neta, *Int. J. Appl. Radiat. Isot.*, **18**, 493 (1967).
- B. Halliwell, M. Grootveld, J. M.C. Gutteridge, *Methods Biochem. Anal.*, **33**, 59 (1998).
- A. Hatipoglu, D. Vione, Y. Yalcin, C. Minero, Z. Cinar, *Journal of Photochemistry and Photobiology A*, **215**, 59 (2010).
- P. W. Atkins, *Physical Chemistry*, 6th ed., Oxford University Press, New York, 1998
- K. Mierzejewska, J. Trylska, J. Sadlej, *J. Mol. Model.*, **18**, 2727 (2012).
- Gaussian 09, Revision B.04, Gaussian Inc., Pittsburgh, PA, 2009.
- H. F. Diercksen Geerd, B. T. Sutcliffe, A. Veillard, *Computational Techniques in Quantum Chemistry and Molecular Physics. Proceedings of the NATO Advanced Study Institute, Ramsau, Germany. 1974*, p. 4.
- T. W. Graham Solomons, B. Fryhle Craig, *Organic Chemistry*, 7th ed., Wiley, 1999.
- P. W. Atkins, R. S. Friedman, *Molecular Quantum Mechanics*, 4th ed., Oxford University Press Inc., New York, 2005.
- I. N. Levine, *Quantum Chemistry*, 2nd ed., Academic Press, Waltham, MA, 1993.

ВЪЗМОЖНИ РЕАКЦИОННИ ПЪТИЩА НА МОЛЕКУЛАТА НА АЦЕТАМИПРИД ПО DFT ИЗЧИСЛИТЕЛНИЯ МЕТОД

Б. Ерен¹, Я. Ялджин Гуркан^{2*}

¹ Университет Намик Кемал, Селскостопански факултет, Текирдаг, Турция

² Университет Намик Кемал, Департамент по химия, Текирдаг, Турция

Постъпила на 1 юли, 2018 г.; приета на 1 октомври, 2018 г.

(Резюме)

Ацетамиприд, основният активен ингредиент на някои пестициди, е подклас на неоникотиноидната група и се използва предимно срещу бяла муха, *aphididae*, листни бръмбари и картофени бръмбари, атакуващи продукти като памук, тютюн, картофи, домати, орехи и цитрусови плодове, отглеждани в парници и на полето. Квантово-химични изчисления с помощта на функционалната теория на плътността (DFT) са използвани за изследване на структурните и физични характеристики на ацетамиприда. Анализирани са възможните реакционни пътища на молекулата на ацетамиприда с ОН радикали. Изчисляването на оптимизираната геометрия за определяне на състоянието на най-ниска енергия е проведено чрез Gauss View 5 и програмата Gaussian 09. Изчислена е активиращата енергия на вероятните реакционни пътища и нейното най-стабилно състояние за различните фази от термодинамична гледна точка. Целта на настоящото изследване е да се определи механизъмът на разлагане на молекулата на ацетамиприда в газова фаза, в етанол и вода като полярни разтворители и в хлороформ като частично полярно разтворител. Анализите са проведени с използване на проводящия солватационен скрининг модел (COSMO). Изчислен е вероятният реакционен път на активационната енергия и е определено нейното най-стабилно състояние за тези фази от термодинамична гледна точка.

Investigation of *in vitro* salt stress on peroxidase enzyme of *Amsonia orientalis* and purification of peroxidase from non-stressed and salt-stressed plants

Y. Duman*, M. Yilmaz

Department of Chemistry, Faculty of Science and Arts, Kocaeli University, 41380, Kocaeli, Turkey

Received July 1, 2018; Accepted October 1, 2018

In this study, we focused on *in vitro* salt stress on peroxidase (POD) enzyme activity change of *Amsonia orientalis*. The plant was subjected to 25, 50, 75, 100, 125 and 150 mM NaCl salinity for 30 days. Change of POD activity was observed by spectrophotometric and activity staining assays. Our findings indicated that POD activity didn't dramatically change especially when plant was exposed to high salinity. The specific activity of POD of non-stressed plant was calculated as 0.74 (U/mg), while the highest specific activity was seen at 50 mM NaCl and the lowest specific activity at 150 mM NaCl as 0.87 (U/mg) and 0.54 (U/mg), respectively. For further analysis of salt stress effect on POD activity, the enzyme was purified from non-stressed and 50 mM salt-stressed *A. orientalis*. Similar purification profiles were observed for non-stressed and 50 mM salt-stressed plant at 4.570-fold purification with 8% yield and at 4.10-fold purification with 7% yield. The molecular weights of purified enzymes from both extracts were determined by electrophoretic methods as 59 kDa. These results suggest that POD is a strong defensive enzyme against salinity due to non-change of its activity especially in 50 mM NaCl by monitoring POD activity in crude and purified extracts.

Keywords: Peroxidase (POD), *Amsonia orientalis*, Salt stress, Purification

INTRODUCTION

Salinity is an abiotic stress that inhibits biological and physiological parameters of plants. Salinity stress alters general metabolic processes and enzymatic activities and leads to molecular damage to important metabolic pathways of plants like photosynthesis by causing increased production of reactive oxygen species [1]. Reactive oxygen species (ROS: singlet oxygen (O_2), superoxide radical (O_2^-), hydrogen peroxide (H_2O_2) and hydroxyl radical (HO^\cdot)) are regarded as the main sources of damage to cells under biotic and abiotic stresses [2]. Toxicity effect of reactive oxygen species is highly efficient on antioxidant defense systems, including both nonenzymic (ascorbate, glutathione, alpha-tocopherol) and enzymic (catalase (CAT), ascorbate peroxidase (APX), superoxide dismutase (SOD) peroxidases (POD)) constituents in plant cells [3]. Antioxidant enzymes, which act as detoxifiers due to their ROS scavenging activities, are important defensive biomolecules of plants. Peroxidase (POD: EC 1.11.1.7) [4], which converts H_2O_2 to water, is an important antioxidant enzyme involved in oxidative protection. POD, an iron heme protein, catalyzes the reduction of H_2O_2 with a concurrent oxidation of the substrate, mostly located in the cell wall and involved in oxidation of phenol compounds in the synthesis of lignin [5]. *Amsonia orientalis* Decne. (syn. *Rhazya orientalis* (Decne.) A. DC.) which

belongs to Apocynaceae family, is commonly known as "Blue star" with its profuse pale-blue flowers. It is a medicinal and ornamental plant having natural distribution only in northwest Turkey and northeast Greece [6]. Within the Bern Convention (1979) [7], the European Council placed the plant in the list of the plant species that must be conserved on European scale. Also, the plant is listed in the category of "Critically Endangered" (CR) in the "Red Data Book of Turkish Plants" [8]. This data, by themselves, bring doubts about the plant's ability of resistance to several stress factors. Thus, samples from Balıkesir population of the plant were taken to *ex situ* conservation to protect the plant from stress factors [9] and the plant's genetic diversity among the remaining populations was determined [10]. Also, as a conservation strategy, *in vitro* studies were conducted and mass production of the plant was achieved [11,12]. Yet, it is not clear that the decrease in the number of individuals or in the distribution area of the plant is caused by any environmental stress factors. Therefore, it is thought that understanding of stress-related plant reactions would shed light on the plant's ability to survive in case of exposure to such stresses. For such purposes, *in vitro* plant studies provide reliable data by using controlled, non-season-dependent and repeatable experiments. In this study, we focused on the investigation of the

* To whom all correspondence should be sent:
E-mail: yavci@kocaeli.edu.tr,
yonca.avciduman@gmail.com

peroxidase enzyme activity of *A. orientalis* under *in vitro* salinity stress, and the purification of the plant peroxidase in order to assess the reliability of activity data and finally to understand the plant's defensive ability and mechanism to response to salinity stress, and to develop more efficient conservation strategies.

MATERIALS AND METHODS

Plant material and disinfection

Healthy shoots, 10 cm in length, were collected from 8-year-old field-grown individuals of *Amsonia orientalis* before flowering in May 2013 and all leaves were cut off. The shoots were washed under tap water for 15 min, and then cut into 1-2 cm long segments that had at least one node (single node explants). Explants were disinfected by dipping in 70% ethyl alcohol (EtOH) for 2 min and then in 1% (v/v) sodium hypochlorite (NaOCl) for 12 min. Disinfected explants were rinsed with sterilized water three times in order to remove NaOCl residues. Excess water on the explants was taken by sterile filter papers before inoculations.

Culture establishment, explant preparation and in vitro salt treatment

Disinfected single node explants were inoculated vertically in culture vessels containing 40 mL of Murashige and Skoog's (1962) medium (MS), [10], supplemented with 1.0 mg l⁻¹ BAP. At the end of the incubation period, following the excision of emerged shoots from explants and cutting them into single node explants, these were sub-cultured on the same fresh medium. Through repeating this process, subcultures were regularly obtained on the same medium at 30 d intervals until a desired number of single node explants was reached. Single node explants were then transferred to a fresh MS medium containing 0, 25, 50, 75, 100, 125 and 150 mM NaCl and incubated for 30 d under the same conditions.

Culture medium and conditions

All variants of MS medium were supplemented with 30 g l⁻¹ of sucrose and 7 g l⁻¹ of plant agar. The pH of the plant culture media was adjusted to 5.7 with 1 N NaOH or 1 N HCl prior to autoclaving. Disinfection treatments and inoculations were carried out aseptically in a laminar air flow cabinet. Cultures were maintained at a temperature of 23±1°C in a plant growth chamber with a 16/8 h light/dark photoperiod under an illumination of 80 μmol m⁻² s⁻¹ photosynthetic photon flux density provided by cool-white fluorescent lights.

Preparation of crude extract

Non-treated (2.92 g) and 25, 50, 75, 100, 125 and 150 mM salt-stressed plants (1.5, 2.08, 1.57, 2.85, 1.54 and 2.63 g, respectively) were homogenized with a mortar in a 20-fold extraction buffer of 50 mM sodium phosphate (pH 7.0). The homogenate was filtered and then centrifuged at 14000 g for 15 min at +4 °C (Sigma 4-16 K). The supernatant was collected and used as crude extract for analysis of POD activity. Protein concentration was determined according to Bradford method with bovine serum albumin as standard [13].

Determination of POD activity

POD activity was determined using the pyrogallol oxidation method [14] in a 2 mL reaction mixture containing 50 mM potassium phosphate buffer (pH 7.0), 10 mM pyrogallol, 100 μL suitably diluted enzyme and 5 mM H₂O₂. The increase in absorbance was recorded at 425 nm within 5 min after enzyme extract was added and the reaction was stopped with 1mL of 2.5 N H₂SO₄. Enzyme activity was determined using the extinction coefficient at 425 of 2640 M⁻¹cm⁻¹ for pyrogallol [15], where one unit of enzyme activity corresponds to the formation of one milligram of purpurogallin per 5 min [16].

SDS-PAGE and activity staining analysis of antioxidant enzymes

The SDS-PAGE was carried out using Bio-Rad Mini-Protean system with 5% stacking and 12% separating gels prepared according to Laemli *et al.* [17]. Sample proteins were dissolved in loading buffer containing a reducing agent and heated to 95 °C for 7 min. SeeBlue® Plus2 Pre-stained Protein Standard (LC5925) was used as molecular weight marker. Electrophoresis was carried out for 10 min at 300 V, followed by 2-3 h run at 400 V. Gels were stained using silver stain [18] and photographed. Electrophoretic analysis of POD was also performed by non-denaturing 12% separating and 5% stacking gels at 4 °C, 100 V for 10 min, then at 120 V for 60 min using Biorad mini protean II electrophoresis system. POD was stained according to the following method: gel activity was detected using incubating gels in 10 mM pyrogallol and 5 mM H₂O₂ in 50 mM pH 7 phosphate buffer at room temperature until appearance of the orange-brown bands, measured against achromatic background.

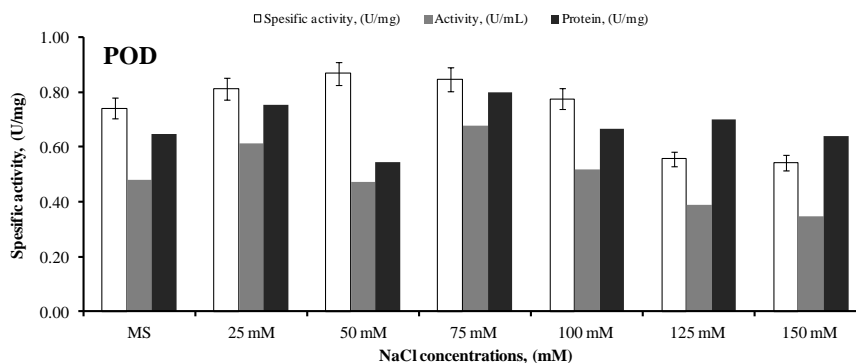


Fig. 1. Effect of increasing NaCl concentration on POD specific activity, activity and total protein amount of *A. orientalis*. Values are the mean \pm SE for three observations. Vertical bars indicate mean \pm SE of three replicates.

Purification of peroxidase from non-treated and 50 mM salt-stressed *A. orientalis*

Separation of POD from other proteins in the supernatant was achieved by a three-step procedure including ammonium sulfate precipitation, anion exchange and gel filtration chromatography. The crude enzyme extract was brought to 90% saturation with ammonium sulfate under continuous stirring. After 7 h, the solution was centrifuged at 14000 g for 15 min. The precipitate was dissolved in a minimum volume of 50 mM phosphate buffer (pH 7.0) and dialyzed overnight in the same buffer. The concentrated dialysate was loaded on a DEAE-Sephacryl column (2 \times 30 cm) previously equilibrated with 100 mM NaCl in 50 mM phosphate buffer (pH 7.0) and as eluted at 0.5 mL/min with the same buffer. The fractions were monitored for protein amount and POD activity. POD active fractions were then pooled and concentrated. Concentration was processed in a 5 kDa cut-off membrane (OMEGA membrane disc, OM005025) with Millipore stirred cell (10 mL working volume and 25 mm diameter).

Partially purified and concentrated POD enzyme (1.5 mL) obtained by ion exchange chromatography was subjected to gel filtration chromatography using Sephacryl S-200 column (GE Healthcare, Uppsala, Sweden). The glass column with an internal diameter of 1 cm was packed to the height of 30 cm. Sample was loaded onto the column previously equilibrated with 50 mM phosphate buffer (pH 7.0) and was eluted at 0.2 mL/min with the same buffer. 2 mL fractions were collected and analyzed for protein content and enzyme activity.

RESULTS AND DISCUSSION

Effect of salt stress on POD activity

According to former reports *A. orientalis* prefers sandy-loamy soils with no salt, slightly alkaline, mid-calcareous, poor in organic material, very rich

in iron and magnesium [9]. In this study, we investigated the effect of salt stress on the antioxidant enzyme POD. The change of enzyme activity is given in Fig. 1.

When compared to control; increasing NaCl concentrations didn't change the POD activity until 150 mM NaCl, but according to protein profile (Fig. 1) the lowest protein content was observed at 50 mM NaCl-stressed plant. The specific activity of an enzyme is the activity of an enzyme per mg of total protein (expressed in U/mg). It is the amount of product formed by an enzyme in a given time interval under given conditions per mg of total proteins. Compared to control, the specific activity increased to 109%, 117%, 114% and 105% at the 25mM, 50 mM, 75 mM and 100 mM NaCl concentrations, respectively. But at the high salt concentrations (125 mM and 150 mM) the specific activity of peroxidase decreased to 75%. The highest specific activity was observed at the 50 mM NaCl concentration. Peroxidases are not only having an important effect on the decomposition of H₂O₂ but also on lignification, plant growth, salt and heavy metal stress [19,20]. The highest specific activity for POD at 50 mM NaCl indicated the highest decomposition capacity of H₂O₂. 50 mM NaCl concentration might be considered as threshold salt concentration for the plant to protect itself against salt stress. Decreasing of specific activity of peroxidase at the increasing NaCl concentrations might be an indicator of reduced defense ability to salinity of *A. orientalis*. The increased or unchanged antioxidant enzyme activity under salt stress may be related to the tolerance to salt stress [21]. In tolerant plant species, POD activity was found to be higher, enabling plants to protect themselves against the oxidative stress whereas such activity was not observed in sensitive plants [22]. In this study, the POD activity remained unchanged in *A. orientalis*. However, specific activity of POD in *A. orientalis* explants

increased at 50 mM NaCl, then decreased at higher salt concentrations (Fig. 1), so 50 mM NaCl treatment indicated that POD might play a role in *A. orientalis* defense against salt. Induced POD activity by salt stress increased for cotton [22], alfalfa [19], *Jatropica curcas* L. [20], but decreased in *Cucumis sativus* L. [23] and remained constant under rising NaCl levels was reported [22].

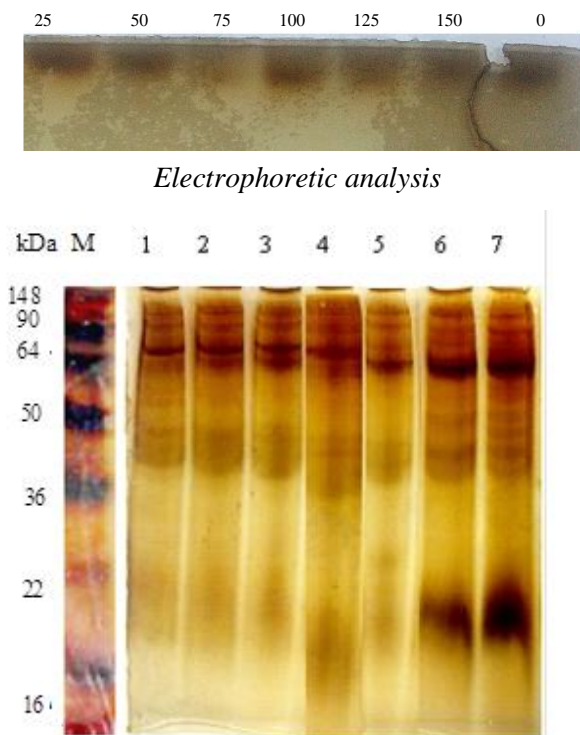


Fig. 2. (A) Staining of POD activity on Native PAGE. Each well was loaded with 15 μ g protein. Numbers on the gels indicate the NaCl concentrations. (B) SDS-PAGE analysis with silver staining of total protein of NaCl treated *A. orientalis*. Lanes M, C, 1, 2, 3, 4, 5, 6, 7 from left to right represent marker and proteins extracted from control, 25, 50, 75, 100, 125 and 150 mM NaCl-treated plants. For each lane, 15 μ g protein was loaded.

POD activity of *A.orientalis* under salt stress was also determined by activity staining. Although more than one POD isoenzyme was reported [24], for this plant single POD isoenzyme was visualized on the gel (Fig. 2A). Intensities of POD activity on gel were not different for both salt-treated and non-treated plant. This result was also supported by spectrophotometric analysis of POD activity suggesting that there was no dramatic decrease in enzyme activity in response to increasing NaCl concentrations. This would contribute to the defense mechanism of *A.orientalis* against higher salt treatments.

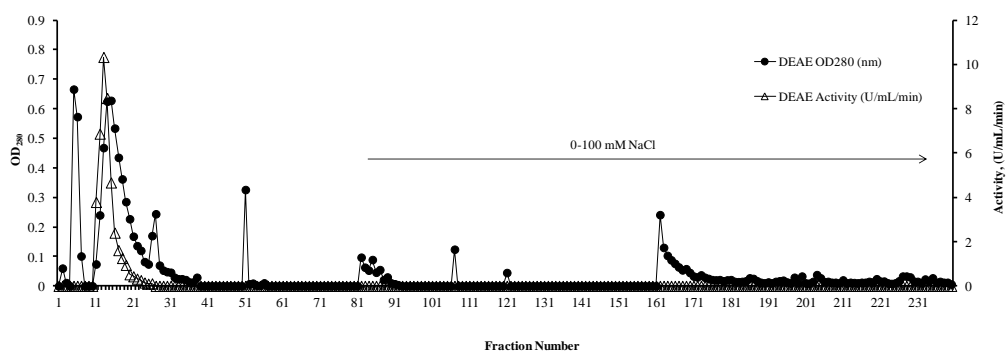
Amounts of total proteins in non-treated and salt-treated extracts of *A. orientalis* were analyzed by SDS-PAGE (Fig. 2B). As visualized from SDS-PAGE intensity, 59 kDa molecular weight protein decreased in amount as a result of 100 mM, 125 mM and 150 mM NaCl treatments (Fig. 2B). Intensity of decrease was dependent on NaCl concentration. But it was also found that the sharpness of the 64 kDa protein band increased at 100 mM, 125 mM and 150 mM NaCl treatment and seemed to be proportional to the NaCl concentration. Moreover, the highest NaCl concentrations (125 mM and 150 mM) exhibited prominently increased protein bands of 19 kDa. These results indicate that a plant grown under salt stress shows either induction (64 and 19 kDa) or repression (81 kDa) in the synthesis of some polypeptides.

Purification of peroxidase from non-stressed and 50 mM salt-stressed A. orientalis

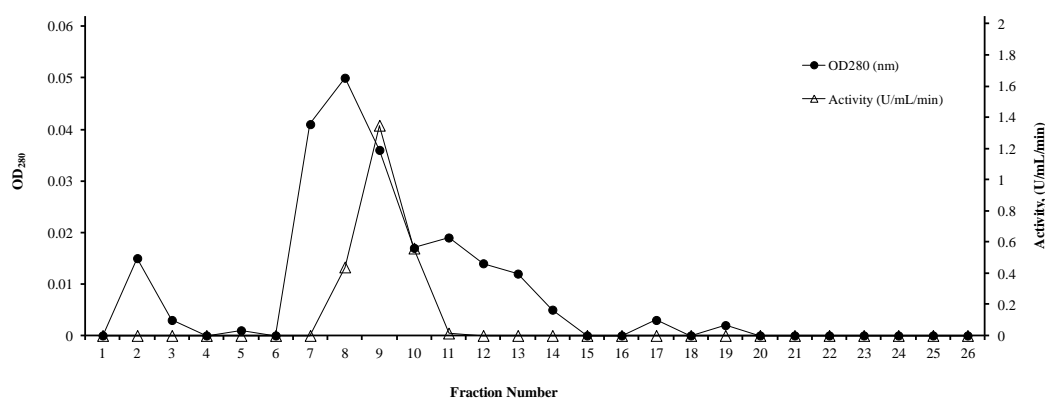
Peroxidases have broad industrial applications, especially in medicine, food and water treatment [25]. There are various reports about purification of peroxidase from different plants using chromatographic techniques [25-27]. As the highest specific activity was observed at 50 mM NaCl-treated *A. orientalis*, we purified peroxidase from 50 mM NaCl salinity and control plant using three simple steps including ammonium sulfate precipitation, anion exchange chromatography with DEAE-sepharose and gel permeation chromatography on Sephacryl-S 200. The purification profile is summarized in Table 1. 4.57-fold and 4.00-fold purification with 8% and 7% yield was achieved for control and 50 mM salt-stressed *A.orientalis*, respectively.

The percent ammonium sulfate was obtained as experimental effect of saturation (30-90%) on the first step of purification process. All fractions were assayed for peroxidase activity and nearly all peroxidase was observed in dialyzed 90% ammonium sulfate saturation while peroxidase activity of supernatant of this fraction equalled zero. Concentrated enzyme with 90% ammonium sulfate saturation was loaded on a DEAE-sepharose column. After anion exchange chromatography, peroxidase was purified 3.57- and 2-fold with 42% and 19% yield for control and 50 mM salt-stressed *A.orientalis*, respectively. This small increase for the number of purifications is probably due to a large amount of proteins non-bound on column material (Fig. 3A). The pooled and concentrated fractions of this step were loaded onto Sephacryl S-200 column for further purification (Fig. 3B). The final purification and yield of peroxidase increased

Y. Duman, M. Yilmaz: Investigation of *in vitro* salt stress on peroxidase enzyme of *Amsonia orientalis* and ... to 4.6 and 8%, 4.1 and 7% for control and 50 mM salt stressed *A. orientalis*, respectively.



(A)



(B)

Fig. 3. (A) Typical elution profile of DEAE fractions of *A. orientalis*. Elution was achieved at a flow rate of 0.5 mL/min with 3-mL fractions. Fractions 1-80 were pooled with 50 mM phosphate buffer (pH 7.0), 81-160 were pooled with 50 mM phosphate buffer (pH 7.0) + 50 mM NaCl, and 161-240 were pooled with 50 mM phosphate buffer (pH 7.0) + 100 mM NaCl. (B) Gel permeation column fractions. The column was equilibrated with 50 mM phosphate buffer (pH 7.0), at a flow rate of 0.2 mL/min and with 2-mL fractions.

Table 1. Purification profile of non-stressed and 50 mM salt-stressed *A. orientalis*

Sample	Volume (ml)	Activity (U)	Protein cont. (mg)	S.A (U/mg)	Purif. Fold	Act. Rec. (%)
Crude extract of non-stressed <i>A. orientalis</i> explant	20.0	95.80	13.00	7.37	1.00	100.00
(NH ₄) ₂ SO ₄ precipitation	4.7	84.38	8.02	10.52	1.43	88.10
DEAE column	7.5	40.00	1.52	26.32	3.57	42.00
Sephacryl S-200 column	6.0	8.09	0.24	33.71	4.57	8.45
Crude extract of 50 mM salt stressed <i>A. Orientalis</i>	20.0	100.76	4.57	22.03	1.00	100.00
(NH ₄) ₂ SO ₄ precipitation	4.8	65.40	2.06	31.77	1.44	64.91
DEAE column	6.9	19.22	0.44	44.08	2.00	19.07
Sephacryl S-200 column	5.0	6.74	0.07	90.28	4.10	6.69

SDS-PAGE (Fig 4) results showed that these steps were sufficient for purification of enzyme, because all contaminated proteins in the crude extract and pooled fractions of DEAE-sepharose column were not observed in the final enzyme extract. Similar steps were performed by Yadav *et al.* [20] for purification of peroxidase from banana stem juice and Tzika and Sotiorudos [28] from olives.

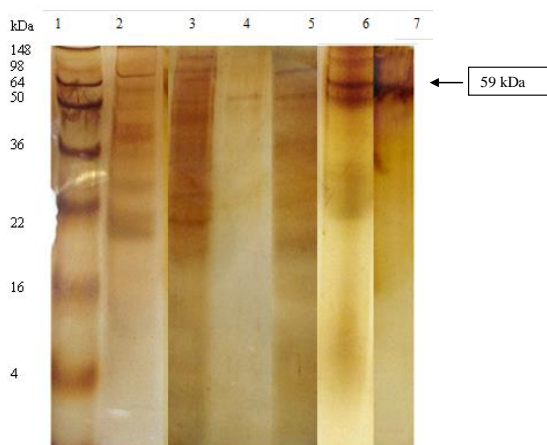


Fig. 4. Silver staining of SDS-PAGE gel. Electrophoresis was carried out at 100 mV for 10 min and at 120 mV for 120 min on 12% polyacrylamide gel system. For 1, 2, 3, 4, 5, 6 and 7 lanes; 15 µg protein; for 6 and 7 lanes 60 µg protein was applied. Lane 1: protein molecular mass marker; lane 2: crude extract of 50 mM NaCl -treated plant; lane 3: crude extract of control plant, lane 4: pooled DEAE fractions of control, lane 5: pooled DEAE fractions of 50 mM NaCl stressed enzyme, lane 6: purified and 4-fold concentrated 50 mM NaCl -treated plant, lane 7: purified and 4-fold concentrated control plant.

In spite of their higher purification number (8.37 and 52), the yield of purified enzyme was nearly 10 and 25 times lower (0.73% and 0.29%) than our results. Purification of recombinant plant peroxidase from *Pichia pastoris* was achieved by Spadiut *et al.* [27] and they reported 4.0 fold purification of the enzyme with 50% yield by anion exchange chromatography and 2.0 fold with 100% yield by size exclusion chromatography. Besides, same steps were carried out by Thogsook and Barrett [29] for purification of peroxidase from broccoli; according to their results these steps were not sufficient for the purified enzyme. But in our study peroxidase was purified with a single band on SDS-PAGE (Fig. 4). Molecular weight of peroxidase from *A.orientalis* was 59 kDa as determined by the SDS-PAGE (Fig. 4). Peroxidase was purified with TPP method by our group and this result is in good agreement with the previously finding of Yuzugullu *et al.* [30]. Peroxidases with

various molecular weight have been reported in the range of 30-150 kDa. 86 kDa and 79 kDa peroxidase from *Pseudomonas* sp. and *Leptogium saturninum* were reported [26,31].

The purification of peroxidase from *A. orientalis* with relatively higher yield was introduced first in the current study, which may contribute to further industrial applications following its proper cultivation and reintegration in its natural habitats. Also, planned *ex situ* conservation studies on the plant would make us include a detailed salinity test of the soils.

Acknowledgements: This work was supported by the Scientific and Technological Research Council of Turkey (TÜBİTAK). Grant No: 113Z609. We would like to thanks to Dr. Yonca Yuzugullu Karakus, Dr. Arda Acemi and Professor Dr. Fazıl Özen contributed some of the experiments in the study and for providing the plant. A part of this work was presented at the "4th International Conference on New Trends in Chemistry", to be held at St. Petersburg dates between 11 – 13th of May 2018.

Conflict of interest: The authors declare that there are no conflicts of interest.

REFERENCES

1. J. K. Zhu, *Trends Plant Sci.*, **6**(2), 66, (2001).
2. N. Candan, L. Tarhan, *Plant Sci.*, **163**, 769, (2003).
3. O. Blokhina, E. Virolainen, K. V. Fagerstedt, *Ann. Bot.* **91**,179, (2003).
4. L. D. Gara, M. C. Pinto, F. Tommasi, *Plant Phys. Biochem.* **41**, 863, (2003).
5. B. K. Singh, S. R. Sharma, B. Singh, *Scientia Horticulturae*, **124**, 9, (2010).
6. T. G. Tutin, V. H. Heywood, N. A. Burges, D. M. Moore DM, D. H. Valentine DH, S. M. Walters SM, D. A. Webb DA, *Flora Europaea*. Cambridge University Press, Cambridge, (1968).
7. Bern Convention 1979 Convention on the Conservation of European wildlife and Natural Habitats. Appendix II, Bern/Berne, **19**, IX, (1979).
8. T. Ekim, M. Koyuncu, M. Vural, H. Duman, Z. Aytaç, N. Adıgüzel, Red Data Book of Turkish Plants, 2000.
9. F. Özen, *J. Balikesir University Inst. Sci. Tech.*, **8**(1), 4, (2006).
10. T. Murashige, F. Skoog, *Physiol. Plantarum* **15**, 473, (1962).
11. A. Acemi, F. Özen, R. Kiran, *Eurasia J. Biosci.*, **6**,105, (2012).
12. A. Acemi, F. Özen, R. Kiran, *Propag. Ornam. Plants*, **13**(1), 25, (2013).
13. M. Bradford, *Anal. Biochem.* **72**, 248, (1976).
14. A. M. Targovnik, O. Cascone, M. V. Miranda, *Sep. Purif. Technol.*, **98**, 199, (2012).

- Y. Duman, M. Yilmaz: Investigation of *in vitro* salt stress on peroxidase enzyme of *Amsonia orientalis* and ...
15. Q. Wang, Z. Yang, L. Wang, M. Ma, B. Xu, *Supplement Materials (ESI) for Chem. Commun.* **1**, (2007).
 16. N. W. Valetti, G. Picó, *Sep. Purif. Technol.*, **119**, 1, (2013).
 17. U. K. Laemmli, *Nature*, **227**(5259), 680, (1970).
 18. H. Blum, H. Beier, H. J. Gross, *Electrophoresis*, **8**, 93, 1987.
 19. W. B. Wang, Y. H. Kim, H. S. Lee, K. Y. Kim, X. P. Deng, S. S. Kwak, *Plant Physiol. Biochem.*, **47**, 570, (2009).
 20. P. Yadav, V. K. Singh, M. Yadav, S. K. Singh, S. Yadava, K. D. S. Yadav, *Indian J. Biochem. Biophys.*, **49**, 42, (2012).
 21. S. Gao, C. Ouyang, S. Wang, Y. Xu, L. Tang, F. Chen, *Plant Soil Environ.*, **54**(9), 374, (2008).
 22. D. A. Meloni, M. A. Oliva, C. A. Martinez, J. Cambraia, *Environ. Exp. Bot.*, **49**, 69, (2003).
 23. S. Shu, L. Y. Yuan, S. R. Guo, J. Sun, Y. H. Yuan, *Plant Physiol. Biochem.*, **63**, 209, (2013).
 24. S. Mittal, N. Kumari, V. Sharma, *Plant Physiol. Biochem.*, **52**, 17, (2012).
 25. C. B. Lavery, M. C. Macinnis, M. J. Macdonald, J. B. Williams, C. A. Spencer, A. A. Burke, D. J. G. Irwin, G. B. D'Cunha, *J. Agric. Food Chem.*, **58**, 8471, (2010).
 26. D. Kalyan, S. Phugare, U. Snedbalkar, J. Jadhav, *Ann. Microbiol.*, **61**, 483, (2011).
 27. O. Spadiut, L. Rosetti, C. Dietzsch, C. Herwig, *Protein Express. Purif.*, **86**, 89 (2012).
 28. E. D. Tzika, T. G. Sotiroidis, V. Papadimitriou, A. Xenakis, *Eur. Food Res. Technol.*, **228**, 487, (2009).
 29. T. Thongsook, D. M. Barrett, *J. Agric. Food. Chem.*, **53**, 3206, (2005).
 30. Y. Y. Karakus, A. Acemi, S. Işık, Y. Duman, *Sep. Sci. Tech.*, **53** (5), 756, (2018).
 31. C. Liers, R. Ullrich, M. Hofrichter, F. V. Minibayeva, R. P. Beckett, *Fungal Genet. Biol.*, **48**, 1139, (2011).

ИЗСЛЕДВАНЕ НА *IN VITRO* СОЛЕВИЯ СТРЕС ВЪРХУ ПЕРОКСИДАЗНИЯ ЕНЗИМ НА *AMSONIA ORIENTALIS* И ПРЕЧИСТВАНЕТО НА ПЕРОКСИДАЗА ОТ НЕСТРЕСИРАНИ И СТРЕСИРАНИ СЪС СОЛ РАСТЕНИЯ

Й. Думан*, М. Йълмаз

Катедра по химия, Факултет по науки и изкуства, Университет Коджаели, 41380, Коджаели, Турция

Постъпила на 1 юли, 2018 г.; приета на 1 октомври, 2018 г.

(Резюме)

В това изследване се фокусирахме върху влиянието на *in vitro* солевия стрес върху промяната на ензимната активност на пероксидазата (POD) на *Amsonia orientalis*. Растението беше подложено на 25, 50, 75, 100, 125 и 150 mM соленаост (NaCl) за 30 дни. Промяната на активността на POD беше проследена спектрофотометрично чрез оцветяване на активността. Нашите изследвания показват, че активността на POD не се променя драстично, особено когато растението е изложено на висока соленаост. Специфичната активност на POD на нетретирано растение е изчислена като 0.74 (U/mg), докато най-високата специфична активност се наблюдава при 50 mM NaCl, а най-ниската специфична активност при 150 mM NaCl като 0.87 (U/mg) и 0.54 (U/mg). За по-нататъшен анализ на влиянието на солевия стрес върху активността на POD, ензимът от нетретиран и третиран с 50 mM NaCl *A. orientalis* беше пречистен. Подобен профил на пречистване беше наблюдаван при нестресирани и стресирани с 50 mM NaCl растения, като 4.57-кратно пречистване дава 8% добив, а 4.10-кратно пречистване - 7% добив. Молекулното тегло на пречистените ензими от двата екстракта беше определен чрез електрофоретични методи като 59 kDa. Тези резултати показват, че POD е силен защитен ензим срещу соленаост, което се дължи на непроменената му активност, по-специално при 50 mM NaCl, при наблюдение на активността на POD в суров и пречистен екстракт.

Inhibition effect of polyacrylic acid and its mixture with potassium iodide on mild steel corrosion in acid solution

I. Dehri*, G. Sigircik, A. Sari, M. Erbil

Çukurova University, Faculty of Science and Letter, Chemistry Department, Adana, Turkey

Received July 1, 2018; Accepted October 1, 2018

The synergistic inhibition effect of polyacrylic acid and iodide ions was studied against mild steel corrosion in 0.5 M HCl solution. Potentiodynamic and electrochemical impedance spectroscopy measurements were realized in order to examine the corrosion process. In addition, the effect of long exposure period on inhibition efficiency was investigated. Surface morphology of steel was investigated by scanning electron microscopy technique. The obtained consequences revealed that mixture of polyacrylic acid and potassium iodide exhibited enhanced inhibition efficiency for mild steel corrosion because of synergistic effect.

Keywords: Synergistic effect, acid solution, corrosion inhibitor

INTRODUCTION

Mild steel and its alloys are widely used in industrial applications for lots of purposes such as construction materials, storage tanks and pipelines, etc. These metallic substances are in general exposed to hydrochloric and sulphuric acid solutions for pickling, cleaning and descaling processes in industries [1-5]. Various efforts have been made to better protect metals against corrosion in industrial processes. Organic corrosion inhibitors are some of the most suitable agents for prevention metals from corrosive species due to their strong adsorptive interaction with the metal surface. The molecular structure of inhibitor molecules plays a decisive role on their adsorption ability. In particular, heteroatoms like sulphur, nitrogen, phosphorus and oxygen, π -electrons and electronegative functional groups display high adsorption capacity for organic molecules [6-10]. A protective adsorption layer is formed since inhibitor molecules adhere to the metal surface. Besides, some properties of organic corrosion inhibitors such as low cost, environmental friendliness and good inhibition efficiency in aqueous corrosive solution are generally expected [11,12]. Synergistic effect offers a successful way to enhance inhibition efficiency on metal against corrosion. It is well known that inhibition efficiency could be increased with the addition of halide ions. The synergistic inhibition effect of halide ions is in the order: $I^- > Br^- > Cl^-$. The high synergistic effect of the iodide ion is related to its low electronegativity, large ionic radius and high hydrophobicity [13-16].

The aim of this study is to investigate the inhibition efficiency of polyacrylic acid with potassium iodide for mild steel corrosion in 0.5 M

HCl solution. Electrochemical impedance spectroscopy and potentiodynamic measurements were utilized. The change of inhibition efficiency with immersion time was also studied *via* electrochemical impedance spectroscopy measurements. The surface was examined by scanning electron microscopy. The results show that the inhibition efficiency increased in the presence of iodide ions.

EXPERIMENTAL

Mild steel cylindrical rods with 0.5 cm² immersed surface area were used. The working surface area was abraded mechanically with SiC paper to 1200 grit finish, then degreased with 1:1 ethanol/water mixture and washed with distilled water. Finally, mild steel electrodes were dried at room temperature. Polyacrylic acid (PA) was used within the range of 3%, 5% and 10% without and with addition of 1.0 mM KI in 0.5 M HCl acid solution. The corrosive aqueous solution was obtained by dilution of analytical grade 37% HCl with distilled water. The molecular structure of polyacrylic acid is given in Fig. 1.

Electrochemical measurements were performed in a conventional three-electrode system. A mild steel working electrode was used. The auxiliary electrode was a platinum sheet and Ag/AgCl (3 M KCl) electrode was used as the reference. The electrochemical impedance spectroscopy (EIS) measurements were carried out at instantaneous open circuit potential, in the frequency range of 10 mHz - 100 kHz and amplitude was 5 mV. The potentiodynamic polarization measurements were performed for cathodic (from open circuit potential (E_{ocp}) to -1.0 V) and anodic (from open circuit

* To whom all correspondence should be sent:
E-mail: idehri@cu.edu.tr

I. Dehri et al.: Inhibition effect of polyacrylic acid and its mixture with potassium iodide on mild steel corrosion ... potential (E_{ocp}) to 0.0 V) current with a scan rate of 1 mV/s. The surface morphology of the mild steel samples in HCl solution without and with 10% PA (in the absence and presence of 1.0 mM KI) were examined by scanning electron microscopy (SEM) after 5 days immersion period.

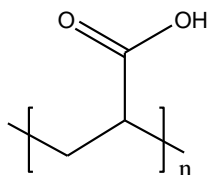


Figure 1. The molecular structure of polyacrylic acid.

RESULTS AND DISCUSSION

Potentiodynamic polarization measurements

Potentiodynamic polarization measurements were applied in order to study the corrosion inhibition process. The potentiodynamic measurement results of mild steel in 0.5 M HCl solution in the absence and presence of PA at different concentrations are given in Fig. 2. It is seen from the figure that cathodic current values were lower for PA-containing acid solution. Besides, the cathodic current values decreased regularly with the increase of inhibitor concentration. This situation was related to the good interaction between metal surface and inhibitor molecules. Thus, in cathodic side, the rate of hydrogen evolution reaction decreased due to adsorption of PA molecules on the metal surface. Addition of PA molecules to the corrosive solution led to a significant decrease of the anodic current values, too. Thus, anodic current values were even much lower for 3% PA-containing acid solution. This situation could be attributed to the significant adsorption property of PA with electronegative oxygen atoms and $-OH$ groups. Aliphatic chain

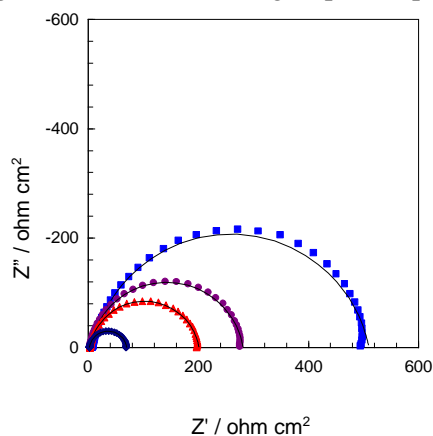


Figure 3. The EIS results of mild steel in 0.5 M HCl solution (\blacklozenge) and containing 3% (\blacktriangle), 5% (\bullet), 10% (\blacksquare) PA. (solid lines show fitted results)

also offers a hydrophobicity characteristic against the attack of corrosive solution by forming a protective film on the metal surface.

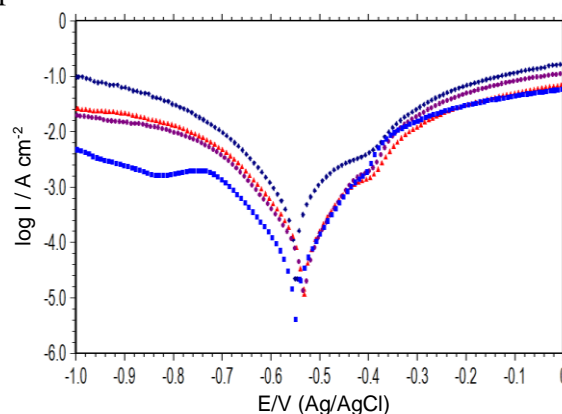
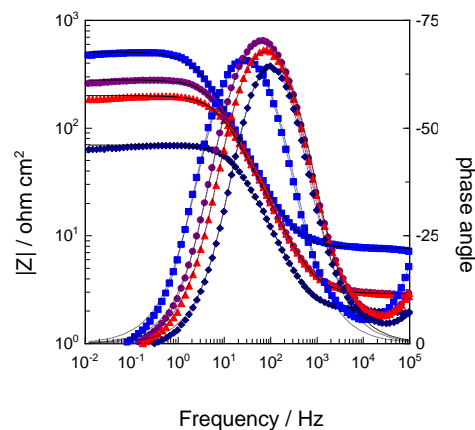


Figure 2. The potentiodynamic polarization curves of mild steel in 0.5 M HCl solution (\blacklozenge) and containing 3% (\blacktriangle), 5% (\bullet), 10% (\blacksquare) PA.

Electrochemical impedance spectroscopy measurements

EIS measurements were carried out to investigate the inhibitor effect of PA in 0.5 M HCl solution in the absence and presence of KI on mild steel corrosion. In Fig. 3, Nyquist and Bode plots are given. Single capacitive loop was observed for all Nyquist plots. This shows that the corrosion of mild steel is mostly controlled by the rate of charge transfer process in 0.5 M HCl solution [17]. The Nyquist plot is applied to determine polarization resistance (R_p) value which includes charge transfer resistance (R_{ct}) and diffuse layer resistance (R_d). As can be clearly seen from the Nyquist plots, the R_p values increased with increasing inhibitor concentration. As a result, the corrosion rate of mild steel decreased. It is also seen that only one time constant is observed in the Bode plots of mild steel in 0.5 M HCl solution without and with different PA concentration.



In Fig. 4a, the electrical equivalent circuit applied to model the mild steel/solution interface is depicted. The used equivalent contains CPE, R_s and R_p . In here, CPE is the constant phase element, R_s and R_p are solution and polarization resistance, respectively.

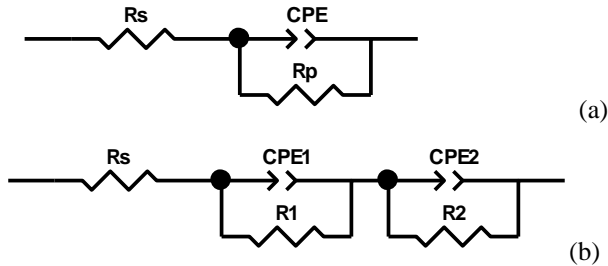


Figure 4. The equivalent circuit used to fit the EIS results without and with PA (a), after 48h and more immersion time with PA in presence of KI (b).

The impedance of the CPE is explained by equation (1), where Y_o is a proportionality coefficient, $j^2 = -1$ is the imaginary number, w is the angular frequency and n is the phase shift. The n value is related to the deviation from ideal capacitance behaviour. Thus, CPE does not have the equal unit with the capacitance ($F\text{ cm}^{-2}$ or $s\ \Omega^{-1}\text{ cm}^{-2}$). Dimension of CPE is given with $s^n\ \Omega^{-1}\text{ cm}^{-2}$, so the unit correction was utilized as defined by Mansfeld and Hsu [18].

$$Z_{CPE} = [Y_o(jw)^n]^{-1} \quad (1)$$

The inhibition efficiency (η) was determined from the polarization resistance by the help of the equation (2) where R_p and R_p' are the polarization resistances in the absence and presence of inhibitor molecules, respectively. The parameters calculated from EIS results are listed in Table 1.

$$\eta\% = \left(\frac{R_p' - R_p}{R_p'} \right) \times 100 \quad (2)$$

The polarization resistance value was determined as $67.5\ \Omega\text{ cm}^2$ for the condition without inhibitor. These R_p values increased with the addition of inhibitor molecules in the HCl solution. This is a result of the protective adsorption layer formed between PA molecules and steel surface. It is seen from Table 1 that the obtained R_p values of mild steel have increased with increasing inhibitor concentration. The polarization resistance value was determined as $502.0\ \Omega\text{ cm}^2$ and inhibition efficiency was calculated as 86.6% for 10% PA.

Besides, the CPE values which are related to open surface area decreased with addition of PA. It follows from these results that the corrosion rate has gradually decreased because of adsorption capacity of PA molecules on steel surface.

Effect of KI addition

Inhibitor molecules are responsible for reducing the corrosion rate by forming an adsorption layer on the metal surface. This situation is strongly related to their interaction capability with the metal surface. Adsorption ability of an inhibitor molecule has crucial importance on inhibition efficiency. The protective adsorption layer is formed as long as inhibitor molecules take place on the metal surface. Synergistic effect offers a successful way to enhance inhibition efficiency on the metal against corrosion. Adsorption of organic molecules could be improved with halide ions *via* forming intermediate bridges between positively charged inhibitor molecules and metal surface. Thus, inhibition efficiency could be increased with the addition of halide ions, especially iodide ions, to the acidic medium [15,19].

EIS method was used to study the synergistic effect of iodide ions on inhibition efficiency in 0.5 M HCl solution. Both Nyquist and Bode plots are given in Fig. 5. Nyquist plots have the similar appearance with iodide-free condition. However, the diameter of the capacitive loop increased gradually with increasing concentration of PA in the presence of iodide ions. Therefore, the iodide ions enhanced the inhibition efficiency of PA at all concentrations. Such occurrences have been observed in lots of studies in the literature [20,21]. The parameters calculated from EIS results for 1.0 mM KI containing various concentrations of PA in 0.5 M HCl solution are listed in Table 1, too. The polarization resistance value was determined as $750.0\ \Omega\text{ cm}^2$ and inhibition efficiency was calculated as 91.0% for 10% PA in the presence of 1.0 mM KI. Furthermore, smaller CPE values were obtained compared with those in the absence of iodide. This result is an evidence for a synergism between the iodide ions and PA molecules. As a result, the corrosion current has significantly decreased due to the strong adsorption behaviour of PA and KI molecules on the steel surface.

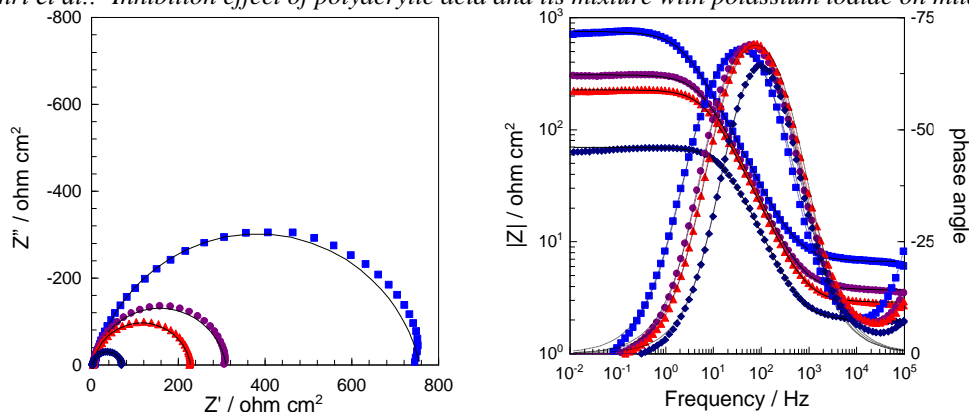


Figure 5. The EIS results of mild steel in 0.5 M HCl solution (♦) and containing 3% (▲), 5% (●), 10% (■) PA in the presence of 1.0 mM KI. (solid lines show fitted results)

Table 1. Electrochemical parameters obtained from EIS results.

	C_{inh} (%)	R_p ($\Omega\text{ cm}^2$)	CPE Y_0 ($\times 10^6\text{ s}^n\Omega^{-1}\text{ cm}^{-2}$)	n	C_{dl} ($\times 10^6\text{ s}\Omega^{-1}\text{ cm}^{-2}$)	$\eta\%$
Blank	-	67.5	225.4	0.92	157.2	-
PA	3	198.0	155.3	0.90	104.9	65.9
	5	278.0	150.1	0.90	105.4	75.7
	10	502.0	164.7	0.88	118.1	86.6
PA+ 1.0 mM KI	3	224.9	145.6	0.90	100.3	70.0
	5	305.9	134.9	0.90	94.7	77.9
	10	750.0	131.1	0.86	91.3	91.0

Effect of immersion time

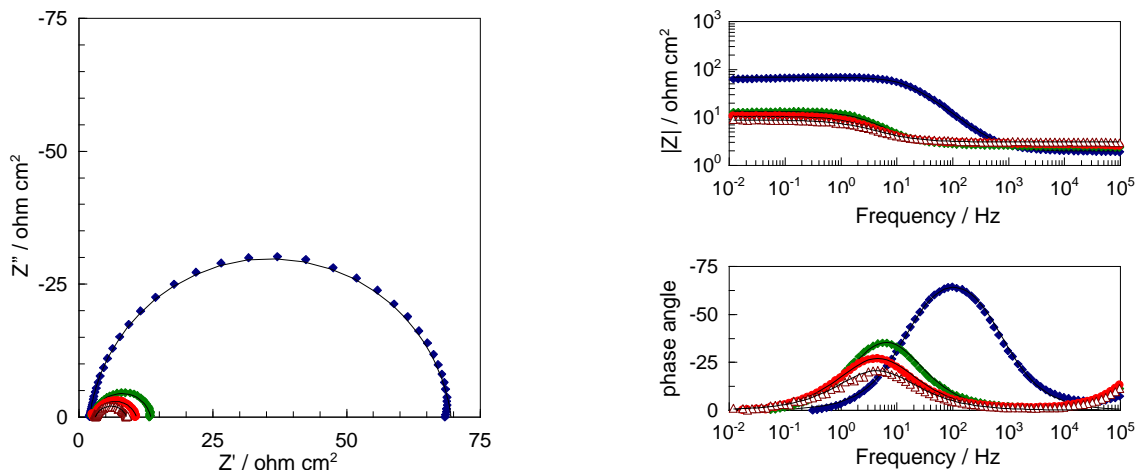


Figure 6. The EIS results of mild steel in 0.5 M HCl solution at different immersion time: 1h (♦), 48h (◆), 72h (●), 96h (Δ).

The effect of exposure time on the inhibition efficiency was also investigated by EIS. The Nyquist and Bode plots of mild steel in 0.5 M HCl at different immersion times are shown in Fig. 6. One capacitive loop was observed for all Nyquist plots at different exposure times. After 48h immersion time, polarization resistance value significantly decreased. This case could be

explained with the fact that there is no opportunity for the formation of a protective layer on the metal surface in this acidic medium. The polarization resistance value was determined as $10.9\ \Omega\text{ cm}^2$ after 48h. Moreover, due to this reason, the polarization resistance values tend to gradually decrease with further increasing of the immersion period. The EIS measurement results of mild steel

in 0.5 M HCl solution containing 10% PA in the absence and presence of 1.0 mM KI at different immersion times are given in Figs. 7 and 8, respectively. As it is seen from Fig. 7, the polarization resistance values are still high enough due to the adsorption of PA on the metal surface at a long exposure time. These R_p values decreased because of the stronger dissolution of metal compared with the first hour of immersion. However, high inhibition efficiency (98.4%) was calculated after 96h. Together Nyquist and Bode plots for mild steel in 0.5 M HCl solution containing 10% PA with 1.0 mM KI at different exposure period are depicted in Fig. 8. As it is expected from these Nyquist plots the obtained diameters of the capacitive loops were higher than iodide free form for all concentrations. Besides, the polarization resistances of mild steel remain almost stable with the further immersion time. This

situation is attributed to improved adsorption ability of inhibitor molecules via iodide ions which offer synergistic effect [22]. As a result, electrified interface altered since steel surface was covered strongly by PA molecules and iodide ions. The used electrical equivalent circuit was shown in Fig. 4b. In this equivalent circuit, CPE1 and CPE2 represent the film capacitance and double layer capacitance. R_p value is the sum of R1 and R2 which are related to every capacitive loop.

The obtained R_p and inhibition efficiency values at different exposure time were given in Table 2. The polarization resistance values were determined as $367.1 \Omega \text{ cm}^2$ and $676.8 \Omega \text{ cm}^2$ without and with iodide ions after 96h. The inhibition efficiencies were calculated as 98.4% and 99.1% in the absence and presence of iodide ions, respectively after 96h immersion time.

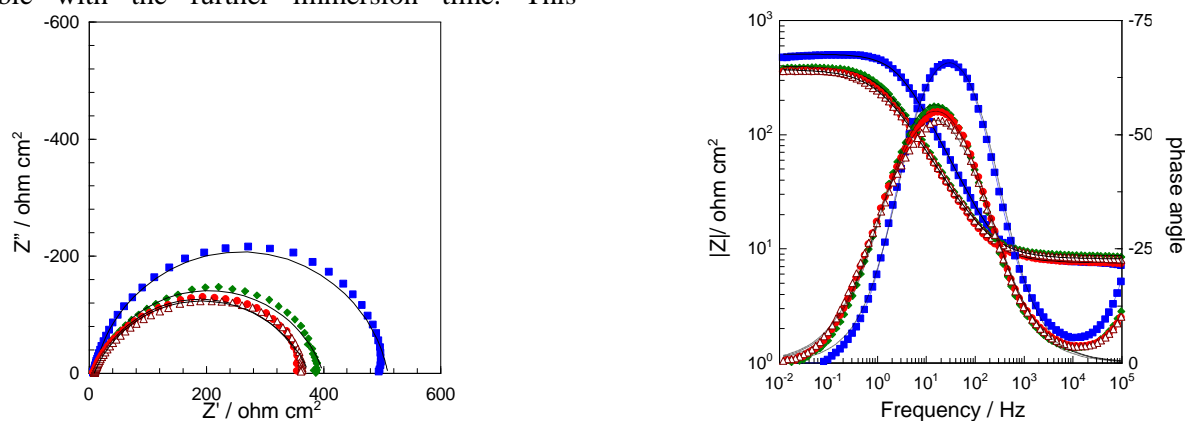


Figure 7. The EIS results of mild steel in 0.5 M HCl solution containing 10% PA at different immersion time: 1h (■), 48h (◆), 72h (●), 96h (△).

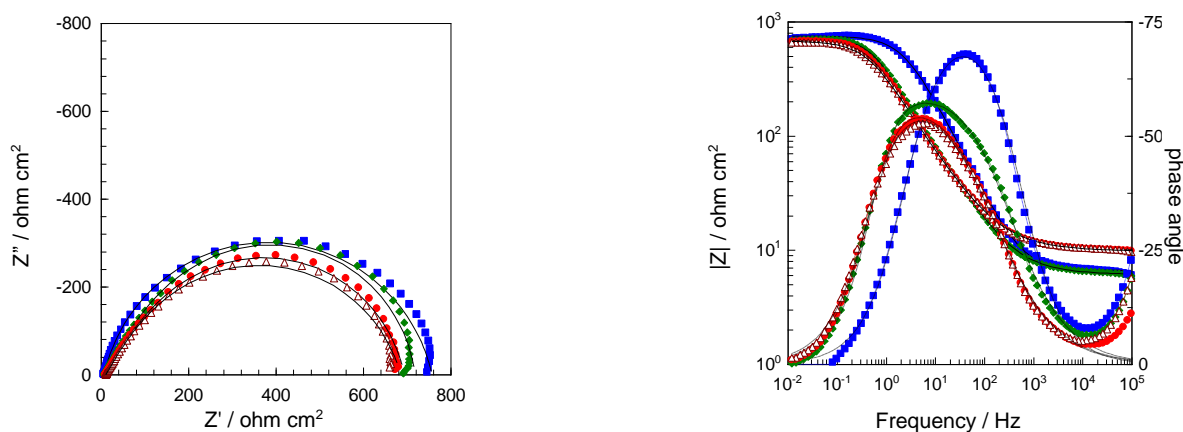


Figure 8. The EIS results of mild steel in 0.5 M HCl solution containing 10% PA in presence of 1.0 mM KI at different immersion time: 1h (■), 48h (◆), 72h (●), 96h (△).

Table 2. R_p values obtained from EIS results and calculated $\eta\%$ at different exposure time.

Immersion time	R_p (Ω cm ²)		$\eta\%$	R_p (Ω cm ²)		$\eta\%$
	blank	10% PA		10% PA+ 1.0 mM KI		
1h	67.5	502.0	86.6	750.0	91.0	
48h	10.9	390.9	97.2	713.1	98.5	
72h	7.9	363.9	97.8	684.8	98.8	
96h	5.8	367.1	98.4	676.8	99.1	

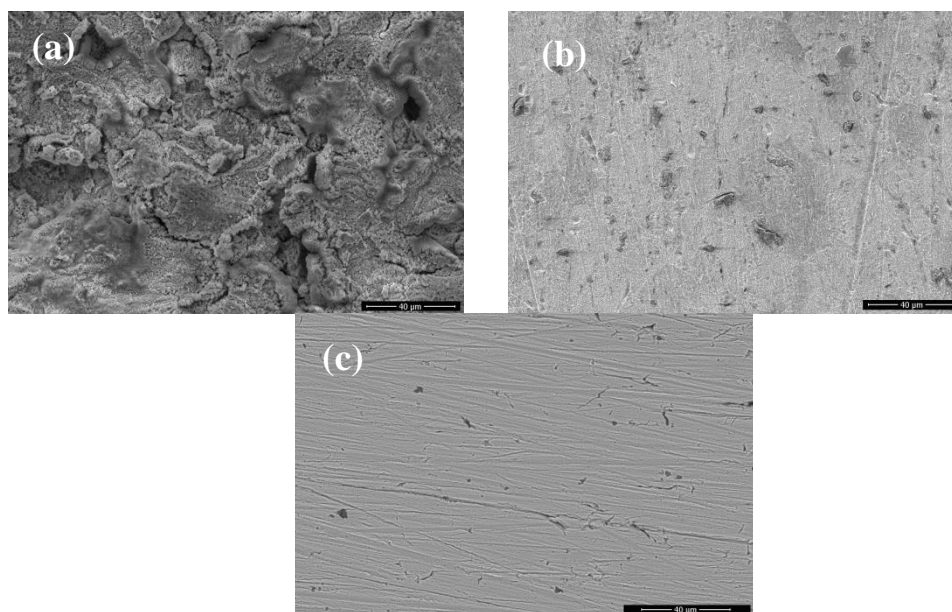


Figure 9. The SEM images of mild steel in 0.5 M HCl solution (a), with 10% PA (b) and with 10% PA in the presence of 1.0 mM KI (c) after 5 days immersion time.

Scanning electron microscopy studies

To observe the appearance of the metal surface is a practical way to have information about the role of inhibitor molecules on the corrosion process. The SEM images of mild steel in 0.5 M HCl solution after 5 days of exposure are given in Fig. 9a. The metal surface is strongly damaged and contains holes and porous structures. This is an expected result for bare metal in acidic environment because of the open surface area for corrosive species. The SEM images of mild steel in 0.5 M HCl solution containing 10% PA without and with 1.0 mM KI after 5 days immersion time are depicted in Figs. 9b and c. Steel surface is more homogeneous with less damage in the presence of PA. Smoother and much less damaged surface was obtained in the presence of iodide. These results also support the synergistic effect of iodide ions added to the inhibitor on corrosion process.

CONCLUSIONS

The potentiodynamic polarization measurement results showed that both anodic and cathodic current values which are related with metal dissolution and hydrogen evolution reactions were reduced in the presence of PA. EIS measurement results revealed that polarization resistance values increased with increasing inhibitor concentration in the absence and presence of iodide ions. Moreover, inhibition efficiencies increased for all PA concentrations in the presence of 1.0 mM KI through synergism. Thus, the corrosion rate decreased due to enhanced adsorption of inhibitor *via* iodide ions on the steel surface. Immersion time results revealed that polyacrylic acid with potassium iodide exhibited better inhibition efficiency even for a long exposure period. Thus, iodide ions provided strong interaction between mild steel and inhibitor molecules. Furthermore, SEM images showed that the addition of iodide ions synergistically improved the formation of adsorptive layer on the steel surface. Mild steel

I. Dehri et al.: Inhibition effect of polyacrylic acid and its mixture with potassium iodide on mild steel corrosion ... surface has smoother appearance even after 5 days exposure time.

Acknowledgements: This research was supported by the Çukurova University Scientific Research Project Coordination Unit (Project Number: FBA-2017-5008).

REFERENCES

1. P. Mourya, S. Banerjee, M. M. Singh, Corrosion inhibition of mild steel in acidic solution by *Tagetes erecta* (Marigold flower) extract as a green inhibitor, *Corrosion Science*, **85**, 352 (2014).
2. R. Yıldız, T. Doğan, İ. Dehri, Evaluation of corrosion inhibition of mild steel in 0.1 M HCl by 4-amino-3-hydroxynaphthalene-1-sulphonic acid, *Corrosion Science*, **85**, 215 (2014),
3. H. M. Abd El-Lateef, Experimental and computational investigation on the corrosion inhibition characteristics of mild steel by some novel synthesized imines in hydrochloric acid solutions, *Corrosion Science*, **92**, 104 (2015).
4. C.B. Pradeep Kumar, K.N. Mohana, Corrosion inhibition efficiency and adsorption characteristics of some Schiff bases at mild steel/hydrochloric acid interface, *Journal of the Taiwan Institute of Chemical Engineers*, **45**, 1031 (2014).
5. L. Feng, S. Zhang, Y. Qiang, S. Xu, B. Tan, S. Chen, The synergistic corrosion inhibition study of different chain lengths ionic liquids as green inhibitors for X70 steel in acidic medium, *Materials Chemistry and Physics*, **215**, 229 (2018).
6. M. Abd El-Raouf, E.A. Khamis, M.T.H. Abou Kana, N.A. Negm, Electrochemical and quantum chemical evaluation of new bis (coumarins) derivatives as corrosion inhibitors for carbon steel corrosion in 0.5 M H₂SO₄, *Journal of Molecular Liquids*, **255**, 341 (2018).
7. M. Mobin, S. Zehra, M. Parveen, L-Cysteine as corrosion inhibitor for mild steel in 1M HCl and synergistic effect of anionic, cationic and non-ionic surfactants, *Journal of Molecular Liquids*, **216**, 598 (2016).
8. X. Li, X. Xie, S. Deng, G. Du, Two phenylpyrimidine derivatives as new corrosion inhibitors for cold rolled steel in hydrochloric acid solution, *Corrosion Science*, **87**, 27 (2014).
9. V.V. Torres, V.A. Rayol, M. Magalhães, G.M. Viana, L.C.S. Aguiar, S.P. Machado, H. Orofino, E. D'Elia, Study of thioureas derivatives synthesized from a green route as corrosion inhibitors for mild steel in HCl solution, *Corrosion Science*, **79**, 108 (2014).
10. M. Faustin, A. Maciuk, P. Salvin, C. Roos, M. Lebrini, Corrosion inhibition of C38 steel by alkaloids extract of *Geissospermum laeve* in 1 M hydrochloric acid: Electrochemical and phytochemical studies, *Corrosion Science*, **92**, 287 (2015).
11. L.L. Liao, S. Mo, J.L. Lei, H.Q. Luo, N.B. Li, Application of a cosmetic additive as an eco-friendly inhibitor for mild steel corrosion in HCl solution, *Journal of Colloid and Interface Science*, **474**, 68 (2016).
12. X. Ma, X. Jiang, S. Xia, M. Shan, X. Li, L. Yua, Q. Tang, New corrosion inhibitor acrylamide methyl ether for mild steel in 1 M HCl, *Applied Surface Science*, **371**, 248 (2016).
13. A.Y. Musa, A.B. Mohamad, A.A.H. Kadhum, M.S. Takriff, L.T. Tien, Synergistic effect of potassium iodide with phthalazone on the corrosion inhibition of mild steel in 1.0 M HCl, *Corrosion Science*, **53**, 3672 (2011).
14. S.A. Umoren, M.M. Solomon, Effect of halide ions on the corrosion inhibition efficiency of different organic species - A review, *Journal of Industrial and Engineering Chemistry*, **21**, 81 (2015).
15. B. Qian, J. Wang, M. Zheng, B. Hou, Synergistic effect of polyaspartic acid and iodide ion on corrosion inhibition of mild steel in H₂SO₄, *Corrosion Science*, **75**, 184 (2013).
16. M.K. Pavithra, T.V. Venkatesha, K. Vathsala, K.O. Nayana, Synergistic effect of halide ions on improving corrosion inhibition behaviour of benzisothiazole-3-piperazine hydrochloride on mild steel in 0.5 M H₂SO₄ medium, *Corrosion Science*, **52**, 3811 (2010).
17. G. Sığırcık, D. Yıldırım, T. Tüken, Synthesis and inhibitory effect of N,N'-bis(1-phenylethanol) ethylenediamine against steel corrosion in HCl Media, *Corrosion Science*, **120**, 184 (2017).
18. C.H. Hsu, F. Mansfeld, Technical note: concerning the conversion of the constant phase element parameter Y_o into a capacitance, *Corrosion Science*, **57**, 747 (2001).
19. M. Özcan, R. Solmaz, G. Kardaş, İ. Dehri, Adsorption properties of barbiturates as green corrosion inhibitors on mild steel in phosphoric acid, *Colloids and Surfaces A: Physicochem. Eng. Aspects*, **325**, 57 (2008).
20. H. Vashisht, I. Bahadur, S. Kumar, M.S. Goyal, G. Kaur, G. Singh, L. Katata-Serub, E.E. Ebenso, Synergistic interactions between tetra butyl phosphonium hydroxide and iodide ions on the mild steel surface for corrosion inhibition in acidic medium, *Journal of Molecular Liquids*, **224**, 19 (2016).
21. S. Hu, A. Guo, Y. Geng, X. Jia, Sh. Sun, J. Zhang, Synergistic effect of 2-oleyl-1-oleylamidoethyl imidazoline ammonium methylsulfate and halide ions on the inhibition of mild steel in HCl, *Materials Chemistry and Physics*, **134**, 54 (2012).
22. A.A. Farag, T.A. Ali, The enhancing of 2-pyrazinecarboxamide inhibition effect on the acid corrosion of carbon steel in presence of iodide ions, *Journal of Industrial and Engineering Chemistry*, **21**, 627 (2015).

ИНХИБИРАЩ ЕФЕКТ НА ПОЛИАКРИЛОВА КИСЕЛИНА И СМЕСТА Й С КАЛИЕВ ЙОДИД ВЪРХУ КОРОЗИЯТА НА МЕКА СТОМАНА В КИСЕЛ РАЗТВОР

И. Дехри*, Г. Сигирчик, А. Сари, М. Ербил

Университет Чукурова, Научен факултет, Департамент по химия, Адана, Турция

Постъпила на 1 юли, 2018 г.; приета на 1 октомври, 2018 г.

(Резюме)

Изследван е синергичният инхибиращ ефект на полиакрилова киселина и йодидни йони върху корозията на мека стомана в разтвор на 0.5 М HCl. Корозионният процес е изследван с помощта на потенциодинамични и електрохимично импедансни спектроскопски измервания. Изследвано е и влиянието на дълъг период на експозиция върху ефективността на инхибицията. Повърхностната морфология на стоманата е изследвана чрез сканираща електронна микроскопия. От получените резултати следва, че сместа от полиакрилова киселина и калиев йодид проявява повишена инхибиционна ефективност върху корозията на мека стомана поради синергичен ефект.

Instructions about Preparation of Manuscripts

General remarks: Manuscripts are submitted in English by e-mail. The text must be typed on A4 format paper using Times New Roman font size 11, normal character spacing. The manuscript should not exceed 15 pages (about 3500 words), including photographs, tables, drawings, formulae, etc. Authors are requested to use margins of 2 cm on all sides.

Manuscripts should be subdivided into labelled sections, e.g. **Introduction, Experimental, Results and Discussion, etc.** The **title page** comprises headline, author's names and affiliations, abstract and key words. Attention is drawn to the following:

a) **The title** of the manuscript should reflect concisely the purpose and findings of the work. Abbreviations, symbols, chemical formulas, references and footnotes should be avoided. If indispensable, abbreviations and formulas should be given in parentheses immediately after the respective full form.

b) **The author's** first and middle name initials and family name in full should be given, followed by the address (or addresses) of the contributing laboratory (laboratories). **The affiliation** of the author(s) should be listed in detail by numbers (no abbreviations!). The author to whom correspondence and/or inquiries should be sent should be indicated by asterisk (*) with e-mail address.

The abstract should be self-explanatory and intelligible without any references to the text and containing not more than 250 words. It should be followed by key words (not more than six).

References should be numbered sequentially in the order, in which they are cited in the text. The numbers in the text should be enclosed in brackets [2], [5, 6], [9–12], etc., set on the text line. References are to be listed in numerical order on a separate sheet. All references are to be given in Latin letters. The names of the authors are given without inversion. Titles of journals must be abbreviated according to Chemical Abstracts and given in italics, the volume is typed in bold, the initial page is given and the year in parentheses. Attention is drawn to the following conventions: a) The names of all authors of a certain publication should be given. The use of "*et al.*" in the list of references is not acceptable. b) Only the initials of the first and middle names should be given. In the manuscripts, the reference to author(s) of cited works should be made without giving initials, e.g. "Bush and Smith [7] pioneered...". If the reference carries the names of three or more authors it should be quoted as "Bush *et al.* [7]", if Bush is the first author, or as "Bush and co-workers [7]", if Bush is the senior author.

Footnotes should be reduced to a minimum. Each footnote should be typed double-spaced at the bottom of the page, on which its subject is first mentioned. **Tables** are numbered with Arabic numerals on the left-hand top. Each table should be referred to in the text. Column headings should be as short as possible but they must define units unambiguously. The units are to be separated from the preceding symbols by a comma or brackets. Note: The following format should be used when figures, equations, etc. are referred to the text (followed by the respective numbers): Fig., Eqns., Table, Scheme.

Schemes and figures. Each manuscript should contain or be accompanied by the respective illustrative material as well as by the respective figure captions in a separate file (sheet). As far as presentation of units is concerned, SI units are to be used. However, some non-SI units are also acceptable, such as °C, ml, l, etc. The author(s) name(s), the title of the manuscript, the number of drawings, photographs, diagrams, etc., should be written in black pencil on the back of the illustrative material (hard copies) in accordance with the list enclosed. Avoid using more than 6 (12 for reviews, respectively) figures in the manuscript. Since most of the illustrative materials are to be presented as 8-cm wide pictures, attention should be paid that all axis titles, numerals, legend(s) and texts are legible.

The authors are required to submit the text with a list of three individuals and their e-mail addresses that can be considered by the Editors as potential reviewers. Please, note that the reviewers should be outside the authors' own institution or organization. The Editorial Board of the journal is not obliged to accept these proposals.

The authors are asked to submit **the final text** (after the manuscript has been accepted for publication) in electronic form by e-mail. The main text, list of references, tables and figure captions should be saved in separate files (as *.rtf or *.doc) with clearly identifiable file names. It is essential that the name and version of the word-processing program and the format of the text files is clearly indicated. It is recommended that the pictures are presented in *.tif, *.jpg, *.cdr or *.bmp format.

The equations are written using “Equation Editor” and chemical reaction schemes are written using ISIS Draw or ChemDraw programme.

EXAMPLES FOR PRESENTATION OF REFERENCES

REFERENCES

1. D. S. Newsome, *Catal. Rev.–Sci. Eng.*, **21**, 275 (1980).
2. C.-H. Lin, C.-Y. Hsu, *J. Chem. Soc. Chem. Commun.*, 1479 (1992).
3. R. G. Parr, W. Yang, *Density Functional Theory of Atoms and Molecules*, Oxford Univ. Press, New York, 1989.
4. V. Ponec, G. C. Bond, *Catalysis by Metals and Alloys (Stud. Surf. Sci. Catal., vol. 95)*, Elsevier, Amsterdam, 1995.
5. G. Kadinov, S. Todorova, A. Palazov, in: *New Frontiers in Catalysis (Proc. 10th Int. Congr. Catal., Budapest, (1992)*, L. Gucci, F. Solymosi, P. Tetenyi (eds.), Akademiai Kiado, Budapest, 1993, Part C, p. 2817.
6. G. L. C. Maire, F. Garin, in: *Catalysis. Science and Technology*, J. R. Anderson, M. Boudart (eds), vol. 6, SpringerVerlag, Berlin, 1984, p. 161.
7. D. Pocknell, *GB Patent 2 207 355* (1949).
8. G. Angelov, PhD Thesis, UCTM, Sofia, 2001, pp. 121-126.
- 9 JCPDS International Center for Diffraction Data, Power Diffraction File, Swarthmore, PA, 1991.
10. CA **127**, 184 762q (1998).
11. P. Hou, H. Wise, *J. Catal.*, in press.
12. M. Sinev, private communication.
13. <http://www.chemweb.com/alchem/articles/1051611477211.html>.

Texts with references which do not match these requirements will not be considered for publication!!!

CONTENTS

Preface.....	4
D. Sakar Dasdan, G. Tosun, Y. Karahan, An investigation of the pH effect on the particle size and zeta potentials of poly (ethylene glycol) and poly ethylene-block-poly(ethylene glycol) with various molecular weights.....	5
S. Senol, E. Akyol, Controlled release of donepezil hydrochloride from PEG-DA hydrogels.....	12
F. Noyan Tekeli, D. Sakar Dasdan, G. Karakus, Particle size prediction of copolymer-drug conjugate using partial least squares regression.....	18
G. Serdaroglu, N. Uludag, An entry to the synthesis of the uleine-type alkaloids by Fischer indole synthesis reactions: the FT-IR, NMR spectroscopy and computational study of the substituted carbazole compound.....	25
R. Khattak, M. Sufaid Khan, I. Imam Naqvi, Mechanism of the electron-exchange reactions between mixed ligand Fe(III) complexes and cyano complex of Fe(II).....	38
B. Eren, Y. Yalcin Gurkan, Possible reaction pathways of the acetamiprid molecule according to the DFT calculation method.....	45
Y. Duman, M. Yilmaz, Investigation of <i>in-vitro</i> salt stress on peroxidase enzyme of <i>Amsonia Orientalis</i> and purification of peroxidase from non-stressed and salt-stressed plants.....	53
İ. Dehri, G. Siğircik, A. Sari, M. Erbil, Inhibition effect of polyacrylic acid and its mixture with potassium iodide on mild steel corrosion in acid solution.....	60
<i>Instructions for authors</i>	68

СЪДЪРЖАНИЕ

Предговор.....	4
Д. Сакар Дашдан, Г. Тосун, Я. Карахан, Изследване влиянието на рН върху размера на частиците и зета потенциала на полиетиленгликол и полиетилен-блок-полиетиленгликол с различно молекулно тегло.....	11
С. Сенол, Е. Акьол, Контролирано освобождаване на донепезил хидрохлорид от PEG-DA хидрогелове.....	17
Ф. Ноян Текели, Д. Сакар Дашдан, Г. Каракуш, Предсказване на размера на частиците на конюгат полимер-лекарство с използване на регресия на частични най-малки квадрати.....	24
Г. Сердароглу, Н. Улудаг, Относно синтеза на алкалоиди от улеинов тип чрез Фишера реакция на индолов синтез: FT-IR, NMR спектроскопско и изчислително изследване на заместено карбазолово съединение.....	37
Р. Хатак, М. Суфаид Хан, И. Имам Накви, Механизъм на реакциите на обмен на електрони между смесени лигандни комплекси на Fe(III) и циано комплекс на Fe(II).....	44
Б. Ерен, Я. Ялджин Гуркан, Възможни реакционни пътища на молекулата на ацетамиприд по DFT изчислителния метод.....	52
Й. Думан, М. Йълмаз, Изследване на <i>in vitro</i> солевия стрес върху пероксидазния ензим на <i>Amsonia Orientalis</i> и пречистването на пероксидаза от нестресирани и стресирани със сол растения.....	59
И. Дехри, Г. Сигирчик, А. Сари, М. Ербил, Инхибиращ ефект на полиакрилова киселина и сместа ѝ с калиев йодид върху корозията на мека стомана в кисел разтвор.....	67